Fall 11-10-2020

Mucosal Immune System of African Lungfish

Ryan D. Heimroth
University of New Mexico - Main Campus

Ryan D. Heimroth
candidate

Biology
Department

This dissertation is approved, and is acceptable in quality and form for publication:

Approved by the Dissertation Committee:

Dr. Irene Salinas, Chairperson

Dr. Eric Y. Denkers

Dr. Christopher A. Johnston

Dr. Chris T. Amemiya

Mucosal Immune System of African Lungfish

By

Ryan D. Heimroth

B.S., Biology, Stonehill College, 2015

DISSERTATION

Submitted in Partial Fulfillment
of the Requirements for the Degree of
Doctor of Philosophy

Ph.D. in Biology

Center for Evolutionary and Theoretical Immunology
Biology Department
The University of New Mexico
Albuquerque, New Mexico

December 2020

DEDICATION

For my family and friends, for their unconditional love and support throughout this endeavor.

ACKNOWLEDGEMENTS

I'd like to thank my advisor, Dr. Irene Salinas for the opportunity she provided me in order to pursue this degree and giving me the chance to further my career in science. I look forward to seeing all the continuing amazing things that your lab will do in comparative immunology.

Thank you to my committee members, Dr. Eric Y. Denkers, Dr. Chris A. Johnston and Dr. Chris T. Amemiya. Thank you, Eric and Chris J., for the thoughtful discussion on my work and helping guide me through the early years of my graduate degree. Thank you, Chris A. for the wonderful collaborations we've worked on and that great discussion at ISDCI.

Thank you to Dr. Gregory Maniero, my first mentor in science and research. I blame all of this work and late nights on you and Dr. Irvin Pan at Stonehill. Without your guidance I would have never been introduced to the joys and terrors of research in the field of comparative immunology, or ever have muttered the phrase, "that's it, I'm becoming a plumber." You are the one who encouraged me to pursue a graduate degree and have kept encouraging me since my days at Stonehill. And finally, you are the one who convinced me to apply to work with Dr. Cooper by threatening to "hit me with a fish" if I didn't. I couldn't have asked for a better friend and mentor. Thank you for this and a lot more that isn't written here.

Thank you to my lab and office mates throughout the years: Jacob Gillis, John Walent, and Daniel Lukason from Stonehill College. You were my first lab mates and helped me learn how to have fun in the lab and enjoy late nights running hemolytic assays and PCRs while listening to everything from Christmas music in May to Elton John to A Day to Remember. Without your guy's motivation and drive, that spark I have for wanting to be the best in what I do would've never been lit. From UNM: Aurora L. Kraus, Ryan M. Brown, Dr. Ali Sepahi, Dr.

Elisa Casadei, Pankoj Kumar Das, Amir Mani, Linda Salazar, Mariah Sanchez, Gabriela Ruano, Dr. Susana Magadan, and Mariella Cisco. We shared some of the highs and low of research at UNM together and I thank you for all of your support and guidance. I wish you all continued success and happiness.

My utmost gratitude to my close friends near and far for keeping me sane through these last five years in the desert. Especially, Aurora and Luke for always looking out for me and making sure I would get out and away from my laptop to enjoy the outdoors. Also, Aurora and Ryan Brown for always being willing to go have a beer and talk about projects and find a solution. Whether it was conceptually based or coding, I wouldn't have been able to do it without you guys. Sean Cappiello, thanks bud for our 4-5 hour long phone conversations every few weeks to help me relax and reminisce about all the crazy things we've done through the years.

Love and thanks to my family, who without I wouldn't be the person I am today. My siblings Jamie and Kristen for all of the encouragement and support. To my Mom, Dad, and Grandparents thank you for your continued support and all of phone conversations keeping me up to date on what's happening on the island and the constant never-ending encouragement and love.

Mucosal Immune System of African Lungfish

By

Ryan D. Heimroth

B.S., Stonehill College, 2015

Ph.D., Biology, University of New Mexico, 2020

ABSTRACT

Conquering land was an apex moment in the evolution of vertebrates. Physiologically, the first vertebrates to transition to life on land had to adapt in order to survive in an oxygen-rich environment where gravity forces and limited water prevailed. These changes involved drastic alterations of the integument, new gas exchange structures, skeletal modifications and waste excretion among others. Several extant vertebrates including anurans and lungfish, survive droughts by undergoing aestivation. African lungfish (*Protopterus sp.*) are the extant relative to all tetrapods, and therefore hold a key phylogenetic position. Unfavorable environmental conditions trigger lungfish to aestivate. Aestivation is a process of metabolic torpor wherein the fish will encase itself in a mucus cocoon and not move until favorable environmental conditions (food and water) are reintroduced. Aestivation can be reproduced in laboratory settings and, thus, lungfish can be used as a model to investigate the transition from aquatic to terrestrial life. Once in their cocoon, lungfish are immobile and therefore cannot escape pathogens present in the external environment. Moreover, metabolic torpor means limited energy to fight infection. Clearly, aestivation poses a challenge to the vertebrate immune system as we know it and lungfish must have evolved unique solutions to overcome such challenges. The goal of this dissertation is to characterize the unique innovations of the mucosal immune system of lungfish in water and land by using “omics” as well as cell, molecular and immunological approaches.

The findings presented here reveal drastic adaptations in the immune system of free-swimming lungfish that serve them during the aestivating phase. Additionally, the lungfish cocoon appears as an outer body living tissue that traps bacteria during life on land. Combined, this body of work reveals previously unknown mechanisms by which vertebrates overcome the problem of fighting pathogens during metabolic torpor.

TABLE OF CONTENTS

Chapter 1: Introduction

Comparative Immunology

The field of Comparative Immunology dates back to the days of Élie Metchnikoff and Paul Ehrlich in the late 1800s who discovered the basis of cellular and humoral immunity, respectively (Metchnikoff, 1905). Though, a very young field of science in comparison to others, Comparative Immunology has been increasingly growing at exponential rates. In 1976, the International Society of Developmental and Comparative Immunology (ISDCI) was founded, solidifying the field as a formal discipline. Comparative Immunologists investigate the diversity of immune systems in the tree of life using non-traditional model organisms and novel experimental techniques. This budding field addresses the evolution and development of one of the most important challenges for living organisms: the detection and elimination of danger.

Comparative Immunologists can illuminate how the immune system has evolved over time and identify unique innovations in certain branches of the tree of life. Convergent evolution has allowed for key immune processes to arise in different taxa, underscoring the idea that there is not one solution to the problem of danger detection. Collectively, this field of study encourages the discovery of many interesting biological processes that allowed for the survival and diversification of life on earth and that can also bring novel insights into human health and disease.

Sarcopterygii

Lungfish Biology:

Lungfish have genetically been shown to be the extant relative to tetrapods and belong to the clade Sarcopterygii or lobe-finned fishes, subclass Dipnoi (Jordan and Speidel, 1931; Zardoya and Meyer, 1996; Brinkmann et al., 2004; Amemiya et al., 2013). The divergence

between lungfish and tetrapods is believed to have occurred 382-388 MYA (Brinkman et al., 2004; Hallström and Janke, 2009). There are three extant genera of lungfish; *Neoceratodus forsteri* in Australia, *Lepidosiren paradoxa* in South America, and *Protopterus* in Africa with four species; *P. aethiopicus, P. amphibious, P. annectens,* and *P. dolloi*. Lungfish have very large genomes, with *P. dolloi* being tetraploid and *P. annectens, P. aethiopicus and P. amphibious* being diploid (Vrvoort, 1980; Gregory, 2005). Compared to humans that have 3.5 pg/cell of DNA, lungfish have 40 to over 100 pg/cell (Biscotti et al., 2016). It is not fully understood when the divergence of the *Protopterus sp.* took place, but it has been proposed that *P. dolloi* diverged 20MYA before the other species of the *Protopterus* genus (Zhang et al., 2014).

Lungfish are interesting vertebrates because they display bimodal gas exchange through both gills and lungs (Maina and Maloity, 1985). Lungfish have both internal and external gills with the external gills receding and disappearing as they mature. Unlike coelacanths and ray-finned fish, the gills of lungfish are greatly reduced and in the case of the South American lungfish are lacking secondary lamellae entirely (de Moraes et al., 2005). Lungfish possess paired lungs that are symmetrical, extending the length of the body cavity and consist of an endodermal lung wall encased by a mesothelium covered pleural membrane (Hsia et al., 2013). With these physiological adaptations, lungfish are able to survive in both in aquatic and terrestrial environments.

Every dry season, African lungfish undergo a physiological process called aestivation. Aestivation is a state of metabolic torpor characterized by decreased oxygen consumption, the slowing in heart rate and the complete dependence on air breathing. These adaptations are critical for prolonged survival in areas that are subject to extreme environmental conditions

(Smith, 1930; Fishman et al., 1986). During the dry seasons, as water evaporates from the rivers and food becomes scarce, lungfish detect these environmental cues and turn them into internal signals. This causes the production of copious amounts of mucus that, once dried, encases the lungfish in a hardened cocoon and induces behavioral, physiological, and biochemical changes in preparation of aestivation.

Early histological studies showed drastic remodeling in many vital organs of the lungfish in response to terrestrialization. In "free-swimming" lungfish, the integument consists of a thick epidermis made up of living epidermal cells intermixed with goblet cells and other secretory cells. Adjacent to the basal membrane, abundant chromatophores responsible for skin pigmentation are observed. Upon aestivation, the epidermis becomes thinner, epithelial cells flatten and goblet cells become exhausted. Additionally, an increased in granulocytes can be observed in the dermis and epidermis (Sturla et al., 2002; Schaffeld et al., 2005; Heimroth et al., 2018). Changes in other organs including the gut (Icardo et al., 2010), the lungs and gills (Maina, 1987; Garofalo et al., 2014), the kidneys (Ojeda et al. 2006), and the brain (Chew and Hiong, 2014) have also been described in aestivating lungfish (Sturla et al., 2002). Overall, aestivation results in conservation of energy and moisture that prevents desiccation (Delaney et al., 1974; Sturla et al., 2002).

Lungfish have also given insight into limb regeneration through a genetic mechanism similar to that of tetrapods. *De novo* transcriptome assembly and differential gene expression analysis has revealed significant similarities between lungfish and salamander limb regeneration, which included strong downregulation of muscle proteins and upregulation of oncogenes, and developmental genes (Nogueira et al., 2016). More recent transcriptomic analysis has shown that similar to salamanders, lungfish tail regeneration occurs through the formation of a proliferative

blastema which results in the restoration of the original structures including skeleton, muscle and spinal cord (Verissimo et al., 2020). Overall previous research in lungfish biology has shown that this organism can answer many questions in immunology, tissue regeneration and evolutionary biology that are still unknown.

The immune system of Protopterus sp.

Anatomically, the immune system of lungfish is remarkably different from that of other ectotherms. Lungfish have a unique intestine (similar to that of cartilaginous fish) consisting of a thick spiral valve with a pyloric fold that separates the foregut and the midgut. The spiral valve begins with a deep prepyloric groove that contains the prepyloric spleen, with a separate post-pyloric spleen that is embedded within the spiral valve (Rafin and Wingstrand, 1981). These pre- and post-pyloric spleens are essential secondary immune structures providing protection for the lungfish. Unlike ray-finned fish, lungfish lack a head kidney, but they possess a thymus similar to that of tetrapods (Mohammad et al., 2007). Overall, they have a very unique lymphoid anatomy that likely has evolved to serve their unique lifestyle.

Early studies revealed that lungfish have unusually large deposits of granulocytes. In 1931, Jordan and Speidel described in detail the abundance and morphology of white blood cells in lungfish. Unlike other vertebrates, lungfish have a great variability of granulocytes located in large tissue reservoirs found in the gut, gonads and kidney walls. These granulocytes were suggested to play an important role in the aestivation and possibly being the key towards the lungfishes' ability to survive the physiological change to life on land (Jordan and Speidel, 1931; Ribeiro et al., 2007).

Interestingly, lungfish appear to have primordial mucosa associated lymphoid tissues (O-MALT). In 2015, O-MALT were described in the nasal cavity and gut of *Protopterus sp*. These

lymphoid aggregates (LAs) were characterized as clusters of lymphocytes in mucosal surfaces. Unlike O-MALT in tetrapods, LAs are primarily composed of T cells with little to no compartmentalization. In response to bacterial infection, the cellular density in lungfish LAs is reduced compared to free-swimming fish. Numbers of LAs do not change due to infection but their size does increase. Importantly, no signs of somatic hypermutation were observed in the LAs of infected lungfish. Given that O-MALT is not present in bony fish, Chapter 2 of this dissertation aims to elucidate the molecular mechanisms behind the development and organization of vertebrate O-MALT including LAs in lungfish.

Lungfish, just as other gnathostomes, have an innate and an adaptive immune system. The adaptive immune system of jawed vertebrates from cartilaginous fish to mammals has been defined by the presence of lymphocytes expressing MHC and recombination activating gene- (RAG)- dependent antigen receptors (Flajnik, 2002). Yet, the lungfish immune system remains largely uncharacterized, in part due to the lack of a sequenced genome and the fact that lungfish cannot be bred in captivity. To date, the development of B and T cells in primary lymphoid tissues of lungfish remains unknown. Recent studies reported the diversity of Ig genes in two African lungfish species. Lungfish have a unique set of Igs containing subclasses such IgM1-3, IgW1-2, IgN1-3, and only found in *P. annectens* IgQ (Zhang et al., 2014). Lungfish express a J chain that is structurally similar to that of tetrapods allowing for the generation of polymeric Igs at mucosal barriers. Interestingly, gut epithelial cells express J chain in lungfish suggesting novel functions for this molecule within Dipnoi (Tacchi et al., 2013). Lungfish TCRs have not been described in detail, but preliminary data from our laboratory has shown higher diversity of TCR CDR3s in systemic lymphoid tissues compared to the skin (not published). Lungfish O-MALT

contain both B and T cells in a 26.5% to 32.7% ratio, respectively and upon infection, this proportion changes to 36.2% IgH^+ cells and 60% $CD3^+$ cells (Tacchi et al., 2015).

Overall, the lungfish immune system appears to have many innovations not found in other vertebrate taxa. The goal of this dissertation is to apply cutting-edge genomics, proteomics and immunological tools to the investigation of the lungfish immune system. In order to uncover the unique immunological innovations that allow lungfish to live in both water and land and survive extreme environmental conditions for long periods of time.

Significance

The body of work of this dissertation is presented in four main chapters. Chapter one is a general introduction to the biology of African lungfish and vertebrate terrestrialization. Chapter two, published in "*The Journal of Immunology*", focuses on the re-investigation of the development and formation of secondary lymphoid tissues in representative jawed vertebrate species. This chapter revisits the tumor necrosis factor superfamily (TNFs) hypothesis and their role in the formation and compartmentalization of secondary lymphoid tissue. Using next-generation sequencing, we determine that there are novel genes and biological processes other than TNFs that influence the development and organization of secondary lymphoid tissues at mucosal surfaces, largely indicating convergent evolution.

Chapter three was published in the journal "*Frontiers in Immunology*" and focuses on the proteomic characterization of the terrestrialized mucus cocoon of African lungfish. We hypothesized that terrestrialization would result in a change in the proteomic mucus composition in the skin and, specifically, in an increased metabolic investment towards production of immune molecules that will help protect the lungfish against invading pathogens and novel land stressors. In this chapter we show that there is a defined remodeling of the integument during

terrestrialization, making the skin resemble tetrapod skin. Moreover, we observed increased numbers of granulocytes in the epidermis of terrestrialized animals compared to controls. The protein composition of free-swimming mucus, terrestrialized soluble gill mucus and terrestrialized hardened mucus cocoon are all unique from each other, with an increase in immune related proteins found in both the gill and skin mucus of terrestrialized animals. Specifically, we detect an increase in abundance of proteins with antimicrobial activity in the terrestrialized skin mucus. We also find differences in the immunoglobulins (Igs) present in each sample. Whereas no Igs are detectable in the terrestrialized gill mucus, IgW1 long form (IgW1L) and IgM1 are found in the control mucus, and IgW1L, IgM1 and IgM2 in the terrestrialized skin mucus. These findings suggest that adaptation to life on land also imposed drastic changes in microbial pressures in the lungfish skin. Thus, in response to terrestrialization, lungfish secrete unique suites of innate and adaptive immune molecules in the skin that likely allow the colonization of beneficial microbes but defend themselves from invading pathogens. Overall, this chapter reveals immunological changes in the skin mucus composition of lungfish that may favor survival on land.

Chapter 4 utilizes a wide array of laboratory techniques to deeply investigate the physiological and immunological changes that take place in the African lungfish in order to cope with the stressors of terrestrialization and will be submitted after my defense. This chapter reinforces what has previously been shown in Chapter 3: the process of aestivation causes drastic changes in the integument in African lungfish (Jordan and Speidel, 1931; Sturla et al., 2002; Heimroth et al., 2018). We report that the terrestrialized mucus cocoon is not just an inert physical barrier that protects lungfish against desiccation, but rather a living organ that has distinct structures and protects lungfish against invading pathogens. Using transcriptomics

analyses, we show that the skin of terrestrializing lungfish has a global proinflammatory state that results in recruitment of granulocytes. Once in the skin, lungfish granulocytes are very effective producers of extracellular traps (ETs). ETs are one of the most ancient and conserved mechanisms of innate immunity present from plants to mammals (Abi Abdallah et al., 2012; Guimarães-Costa et al., 2012; Biermann et al., 2016; Lázaro-Díez et al., 2017) yet their presence in lungfish had never been described. ETs consist of expelled DNA containing histones, myeloperoxidase, neutrophil elastase and antimicrobial peptides used as a net that captures invading pathogens (Estúa-Acosta et al., 2019). In support of the essential role for ETosis in lungfish terrestrialization, depletion of extracellular DNA *in vivo* results in bacterial invasion, signs of edema, skin lesions and septicemia. Overall, this chapter shows that mucosal inflammation is a hallmark of lungfish skin during terrestrialization and that granulocytes and ETosis are essential for successful terrestrialization.

This dissertation demonstrates how traditional approaches along with current molecular and "omics" techniques in a non-model organism can address long-standing questions in biodiversity, evolution and immunology. The work here presented is accessible to all scientists interested in comparative immunology, evolutionary biology and the general public alike. All next-generation sequencing datasets and proteomic datasets have been made publicly available online, as to provide a potential resource for investigators of evolutionary immunology in discovering the unknown. We have also shared plasma samples, DNA samples and histology samples with many scientists from around the globe.

I want to greatly stress to those interested in the mysteries of the evolution of the immune system to consider non-model organisms to address the many questions that remain in this field.

Only by investigating non-model organisms can we unveil the secrets of the immune systems and the success of life on earth.

References:

1. Abi Abdallah, D. S, and E. Y. Denkers. 2012. Neutrophils cast extracellular traps in response to protozoan parasites. *Front. Immunol.* 3(382): 1-6.

2. Amemiya, C.T., Alföldi, J., Lee, A.P., Fan, S., Philippe, H., MacCallum, I., Braasch, I., Manousaki, T., Schneider, I., and N. Rohner. 2013. The African coelacanth genome provides insights into tetrapod evolution. *Nature*. 496: 311–316.

3. Biermann, M. H. C., Podolska, M. J., Knopf, J., Reinwald, C., Weidner, D., Maueröder, C., Hahn, J., Kienhöfer, D., Barras, A., Boukerroub, R., Szunerits, S., Bilyy, R., Hoffmann, M., Zhao, Y., Schett, G., Herrmann, M., and L. E. Munoz. 2016. Oxidative burst-dependent NETosis is implicated in the resolution of necrosis-associated sterile inflammation. *Front. Immunol.* 7(557): 1-13.

4. Biscotti, M.A, Gerdol, M., Canapa, A., Forconi, M., Olmo, E., Pallavicini, A., Barucca, M., and M. Schartl. 2016. The lungfish transcriptome: a glimpse into molecular evolution events at the transition from water to land. *Sci. Reports.* 6(21571): 1-12.

5. Brinkmann, H., Venkatesh, B., Brenner, S., and A. Meyer. 2004. Nuclear protein-coding genes support lungfish and not the coelacanth as the closest living relatives of land vertebrates. *Proc Natl Acad Sci*. 101: 4900–4905.

6. Chew, S. F., and K. Hiong. 2014. Aestivation and brain of the African lungfish *Protopterus annectens. Temperature.* 1(2): 82-83.

7. de Moraes, M. F. P. G., Hõller, S., da Costa, O. T. E., Glass, M.L., Fernandes, M. N., and S. F. Perry. 2005. Morphometric comparison of the respiratory organs in the South American lungfish Lepidosiren paradoxa (Dipnoi). *Physiol. Biochem. Zool*. 78:546–559.

8. Delaney, R. G., Lahiri, S., and A. P. Fishman. 1974. Aestivation of the African lungfish protoperus aethiopicus: cardiovascular and respiratory functions. *J. Exp. Biol.* 61: 111- 128.

9. Estúa-Acosta, G. A., Zamora-Ortiz, R., Buentell-Volanta, B., García-Mejía, M., and Y. Garfias. 2019. *Cells*. 8(9): 1-16.

10. Fishman, A.P., Pack, A., Delaney, R. G., and R. J. Galante. 1986. Estivation in Protopterus. *J. Morphol. Suppl*. 1: 237–248.

11. Flajnik, M. F. 2002. Comparative analyses of immunoglobulin genes: surprises and portents. *Nat. Rev. Immunol.* 2(9): 688-698.

12. Garofalo, F., Amelio, D., Icardo, J. M., Chew, S. F., Tota, B., Cerra, M. C., and Y. K. Ip. 2014. Signal molecule changes in the gills and lungs of the African lungfish Protopterus annectens, during the maintenance and arousal phases of aestivation. *Nitric Oxide.* 44:71-80.

13. Gregory, T. R. 2005. Genome size evolution in animals. The evolution of the genome. Academic Press. 3-87.

14. Guimarães-Costa, A. B., Nascimento, M. T. C., Wardini, A. B., Pinto-da-Silva, L. H., and E. M. Saraiva. 2012. ETosis: A microbicidal mechanism beyond cell death. *J. Parastol. Res.* Article ID 929743: 1-11.

15. Hallström, B.M., and A. Janke. 2009. Gnathostome phylogenomics utilizing lungfish EST sequences. *Mol Biol Evol*. 26:463–471.

16. Heimroth, R. D., Casadei, E., and I. Salinas. 2018. Effects of experimental terrestrialization on the skin mucus proteome of African lungfish (*Protopterus dolloi*). *Front. Immunol.* 9(1259): 1-11.

17. Hsia, C. C. W., Schmitz, A., Lambertz, M., Perry, S. F., and J. N. Maina. 2013. Evolution of air breathing: oxygen homeostasis and the transitions from water to land and sky. *Compr. Physiol.* 3(2): 849-915.

18. Icardo J. M., Wong, W. P., Colvee, E., Loong A. M., and Y. K. IP. 2010. The anatomy of the gastrointestinal tract of the African lungfish, Protopterus annectens. *Anat. Rec.* 293: 1146-1154.

19. Jordan, H. E. and C. C. Speidel. 1931. Blood formation in the African lungfish, under normal conditions and under conditions of prolonged estivation and recovery. *J. Morph.*51(2): 319-371.

20. Lázaro-Díez, M., Chapartegui-González, I., Redondo-Salvo, S., Leigh, C., Merino, D., Segundo D. S., Fernández A., Navas J., Icardo, J. M., Acosta, F., Ocampo-Sosa, A., Martínez- Martínez L., and J. Ramos-Vivas. 2017. Human neutrophils phagocytose and kill Acinetobacter baumannii and A. pittii. *Sci. Rep.* 7(4571): 1-11.

21. Maina, J. N. 1987. The morphology of the lung of the African lungfish, Protopterus aethiopicus. *Cell Tissue Res.* 250: 191-196.

22. Maina, J. N., and G. M. O. Maloity. 1985. The morphometry of the lung of the African lungfish (Protopterus aethiopicus): its structural-functional correlations. *Pro. R. Soc. Lond. B.* 224: 399-420.

23. Metchnikoff, E., 1905. Immunity in Infective Disease. Cambridge University Press, Cambridge.

24. Mohammad, M. G., Chilmonczyk, S., Birch, D., Aladaileh, S., Raftos, D., and J. Joss. 2007. Anatomy and cytology of the thymus in juvenile Australian lungfish, *Neoceratodus forsteri. J. Anat.* 211(6): 784 -797.

25. Nogueira, A. F., Costa, C. M., Lorena, J., Moreira, R. N., Frota-Lima, G. N., Furtado, C., Robinson, M., Amemiya, C. T., Darnet, S., and I. Schneider. 2016. Tetrapod limb and sarcopterygian fin regeneration share a core genetic programme. *Nat. Commun*. 7 :13364.

26. Ojeda, J. L., Icardo, J. M., Wong, W. P., and Y. K. Ip. 2006. Microanatomy and ultrastructure of the kidney of the African lungfish Protopterus dolloi. *Anat. Rec.* 288A: 609-625.

27. Rafn, S., and K. G. Wingstrand. 1981. Structure of intestine, pancreas, and spleen of the Australian lungfish, *Neoceratodus forsteri* (Krefft). *Zool Scrip.* 10: 223–239.

28. Ribeiro, M. L. S, DaMatta, R. A., Diniz, J. A. P., de Souza, W., do Nascimento, J. L. M., and T. M. U. de Carvalho. 2007. Blood and inflammatory cells of the lungfish *Lepidosiren paradoxa. Fish Shellfish Immun.* 23: 178-187.

29. Schaffeld, M., Bremer, M., Hunzinger, C., and J. Markl. 2005. Evolution of tissue-specific keratins as deduced from novel cDNA sequences of the lungfish Protopterus aethiopicus. *Eur. J. Cell. Biol*. 84(2-3): 363-377.

30. Smith, H. W. 1930. Metabolism of lungfish Protopterus aethiopicus. *J. Biol. Chem.* 88: 97-130.

31. Sturla, M., Paola, P., Carlo, G., Anegla, M. M., and U. B. Maria. 2002. Effects of induced aestivation in protopterus annectens: a histomorphological study. *J. Exp. Zool.* 292: 26-31.

32. Tacchi, L., Larragoite, E. T., and I. Salinas. 2013. Discovery of J chain in African lungfish (Protopterus dolloi, sarcopterygii) using high throughput transcriptome sequencing: implications in mucosal immunity. *PLOS one.* 8(8): 1-9.

33. Tacchi, L., Larragoite, E. T., Muñoz, P., Amemiya, C. T., and I. Salinas. 2015. African lungfish reveal the evolutionary origins of organized mucosal lymphoid tissue in vertebrates. *Curr. Biol.* 25: 2417-2424.

34. Verissimo, K. M., Perez, L. N., Dragalzew, A. C., Senevirathne, G., Darnet, S., Barroso Mendes, W. R., Ariel Dos Santos Neves, C., Monteiro Dos Santos, E., Nazare de Sousa Moraes, C., Elewa, A., Shubin, N., Fröbisch, N. B., de Freitas Sousa, J., and I. Schneider. 2020. Salamander-like tail regeneration in the West African lungfish. *Proceedings. Biological Sciences.* 287(1935): 20192939.

35. Vervoort A. 1980. Tetraploidy in Protopterus (Dipnoi). *Experientia*. 36: 294–296.

36. Zardoya, R. and A. Meyer. 1996. The complete nucleotide sequence of the mitochondrial genome of the lungfish (*Protopterus dolloi*) supports its phylogenetic position as a close relative of land vertebrates. *Genetics Society of America*. 142: 1249-1263.

37. Zhang, T., Tacchi, L., Wei, Z., Zhao, Y., and I. Salinas. 2014. Intraclass diversification of immunoglobulin heavy chain genes in the African lungfish. *Immunogen.* 66(5): 335-351.

Chapter 2: Molecular Drivers of Lymphocyte Organization in Vertebrate Mucosal Surfaces: Revisiting the TNF Superfamily Hypothesis

Heimroth, R.D., Casadei, E., Salinas, I. 2020. Molecular Drivers of Lymphocyte Organization in Vertebrate Mucosal Surfaces: Revisiting the TNF Superfamily Hypothesis. J. Immunol. 204 (10) 2697-2711

Abstract

The adaptive immune system of all jawed vertebrates relies on the presence of B and T cell lymphocytes that aggregate in specific body sites to form primary and secondary lymphoid structures. Secondary lymphoid organs include organized MALT (O-MALT) such as the tonsils and Peyer patches. O-MALT became progressively organized during vertebrate evolution, and the TNF superfamily of genes has been identified as essential for the formation and maintenance of O-MALT and other secondary and tertiary lymphoid structures in mammals. Yet, the molecular drivers of O-MALT structures found in ectotherms and birds remain essentially unknown. In this study, we provide evidence that TNFSFs, such as lymphotoxins, are likely not a universal mechanism to maintain O-MALT structures in adulthood of teleost fish, sarcopterygian fish, or birds. Although a role for TNFSF2 (TNFα) cannot be ruled out, transcriptomics suggest that maintenance of O-MALT in nonmammalian vertebrates relies on expression of diverse genes with shared biological functions in neuronal signaling. Importantly, we identify that expression of many genes with olfactory function is a unique feature of mammalian Peyer patches but not the O-MALT of birds or ectotherms. These results provide a new view of O-MALT evolution in vertebrates and indicate that different genes with shared biological functions may have driven the formation of these lymphoid structures by a process of convergent evolution.

1. Introduction

The development and organization of lymphoid tissues was a vital step in the evolution of the vertebrate immune system (1–3). Lymphoid organs can be classified into primary and secondary lymphoid organs (SLOs). Primary lymphoid organs are sites of lymphogenesis where lymphocyte progenitor cells differentiate into B and T lymphocytes. These sites include the bone

marrow and the thymus in mammals, the thymus and bursa of Fabricius in birds and the thymus and head kidney in teleosts. SLOs are sites where immune cells interact with each other and immune responses are activated against foreign Ags. SLOs, such as the spleen, lymph nodes (LNs), and MALT, are therefore the birthplace of effective adaptive immune responses. SLO formation is genetically programmed, whereas tertiary lymphoid structures (TLS) are considered ectopic lymphoid accumulations that appear during adulthood in response to environmental stimuli (4).

MALT are immune inductive sites located at mucosal barriers that provide increased protection at areas of high pathogen encounter, allowing for efficient Ag trapping and rapid activation of the adaptive immune response. MALT includes diffuse MALT and organized MALT (O-MALT). Diffuse MALT consists of immune cells scattered throughout the epithelium acting as sentinels against invading pathogens and is present in all vertebrates from agnathans to mammals. O-MALT are composed of clusters of lymphocytes and can be found in both ectotherms and endotherms. Similar to other SLOs, the O-MALT of endotherms is segregated into B and T cell zones, it contains follicular dendritic cells (FDCs) and the germinal center (GC) reaction allows for affinity maturation of the adaptive immune response via se- lection of high-affinity B cell clones. In ectotherms, however, little to modest affinity maturation can be detected, and SLOs do not have well-defined B and T cell zones (except for the spleen).

The evolutionary origins of O-MALT have long been a subject of debate among evolutionary immunologists. O-MALT was thought to have emerged in anuran amphibians as primitive lymphoid aggregates (LAs), but in 2015, primitive O-MALT structures were found in the gut and nasopharyngeal tissue of African lungfish (Sarcopterygii) (5) revealing that O-MALT is an innovation that predates the emergence of tetrapods. Lungfish LAs are thought to be SLOs

because they were present in similar anatomical locations in all animals examined, and tertiary lymphoid organs (TLOs) coined as inducible LAs appeared in response to infection (5). Lungfish LAs share features with previously described LA in ectotherms because no compartmentalization into B and T cell zones or GCs were identified. Importantly, lungfish LAs are mostly composed of T cells and, to a lesser extent, B cells. Additionally, no evidence for somatic hypermutation was evident in lungfish Las, and therefore, the function of these structures remains enigmatic.

Although bona fide LAs are not present in teleost fish, a unique O-MALT–like structure known as interbranchial lymphoid tissue (ILT) has been reported in the gill arch of salmonids. The presence of ILT in Atlantic salmon is intriguing because no other lymphoid structures appear to be present in association with other teleost mucosal barriers such as the gastrointestinal tract. Similar to lungfish LAs and in contrast to mammalian SLOs, salmonid ILT mostly consists of diverse T cell clusters, shows high expression of CCL19, no expression of RAG-1, no B and T cell areas, and no GC formation (5–10). This is not surprising because GC reactions as defined in endotherms do not appear to occur in teleosts. Although salmon ILT is not present in yolksac larvae and first appears in juveniles (10), it is thought to be an SLO (10) and not a TLO because its localization and structure is similar in all individuals. In support, during infection, ILT decreases in size (8) rather than displaying the classical emergence of lymphocyte clusters at sites of inflammation associated with TLOs.

O-MALT evolution is also complex within endotherms. Birds, such as turkeys and chickens, do not possess LNs but do possess a pharyngeal tonsil, cecal tonsils (CT), and other O-MALT structures in their gastrointestinal tract that have a high level of organization, with FDCs that form part of the GCs (11–13). In birds, CT, similar to Peyer patches (PPs), develop during embryogenesis and therefore are present at birth (14). Despite the apparent similarity with

mammalian SLOs, birds continue to surprise evolutionary immunologists because of the extensive reductionism of the immune gene repertoire in their genomes (12).

TNF superfamily (TNFSF) members play broad biological roles in cell proliferation, differentiation, inflammation, regulation of affinity maturation, and cell death (15–17). Additionally, TNFSF members are known for their importance in lymphoid tissue organogenesis and maintenance. Using several mouse knock-out models (18–21), eight TNFSF members appear to be required for O-MALT formation, organization, maintenance, and function in mammals (15). Interestingly, TNFSF2 is found in all gnathostomes and some invertebrates (22), and lymphotoxins arose as a result of a gene the duplication process, as evidenced by the tandem arrangement in the human and mouse genomes and their high amino acid identity (23). Whereas knockout models of lymphotoxins and lymphotoxin receptors unequivocally indicate absence of organized SLOs (18, 24–26), TNFSF2/TNFRSF1A/1B knockout mice show very diverse phenotypes with respect to PP organogenesis (20, 21, 26–29).

In support to the TNFSF role in lymphoid development, several studies have suggested a progressive expansion of TNFSFs during vertebrate evolution, potentially explaining the progressive organization of lymphoid structures found from bony fish to mammals (5, 30). However, there are also lines of evidence against the TNFSF hypothesis. First, amphibians express TNFSF1 (LTA) and TNFSF3 (LTB); yet, their SLOs do not have GCs, and only modest levels of affinity maturation are observed (2, 31). Second, birds lack some TNFSFs that are vital for lymphocytic organization in mammals, such as TNFSF1 and TNFSF3 (13, 32) as well as other TNFSFs, such as TNFSF13 (APRIL) and TNFSF12 (TWEAK) (17). Thus, it appears that the function of lymphotoxins in amphibians is not the same as in mammals and that birds must use other mechanisms to generate and maintain O-MALT structures. Combined, these lines of

evidence suggest that the molecular drivers of lymphocyte organization may be different in different vertebrate groups.

We hypothesize, in this study, that given the diversity of O-MALT structures and their different degrees of lymphocytic organization observed in vertebrates, these structures arose by convergent evolution creating lymphocytic aggregations of similar form but potentially different functions. As a consequence, whereas TNFSF may be essential for mammalian O-MALT formation and maintenance, alternative molecular drivers may be responsible for these processes in other vertebrate groups. To test this hypothesis, we use a comparative phylogenetic approach by performing RNA sequencing (RNA-Seq) of different O-MALT structures obtained from mammals, birds, sarcopterygian fish (lungfish), and bony fish, as well as in-depth analyses of TNFSF expression in the O-MALT in these four vertebrate groups. Our results support the notion that the TNFSF hypothesis likely does not explain the diversity of O-MALT structures present in vertebrates and provide a new model in which the molecular drivers of O-MALT formation may require molecules involved in neuronal signaling.

2. Materials and methods

2.1 Animals

Juvenile *Protopterus dolloi* (slender lungfish) (0.5 kg) were obtained from ExoticFishShop.com (https://exoticfishshop.net/) and maintained in 10- gallon aquarium tanks with dechlorinated water and a sand/gravel substrate, at a temperature of 27–29℃. Fish were acclimated to laboratory conditions for a minimum of 3 wk before being used for RNA-Seq. During this acclimation period, they were fed frozen earthworms once a day every third day. Feeding was terminated 48 h before the start of the experiment. A female preadult rainbow trout (200 g) was obtained from the Lisboa Springs Hatchery (Pecos, NM). A C57BL/6 adult female

mouse (8–16 wk old) from The Jackson Laboratory (Bar Harbor, ME) was maintained at the Animal Research Facility of the University of New Mexico School of Medicine. Lungfish and trout were sacrificed with a lethal dose of Tricaine- S (MS-222; Thermo Fisher Scientific) with 200 mg/l water for 30 and 3 min, respectively. All animals used for this study were sampled between 9 and 11 AM. Each RNA-Seq library was prepared from tissues from one individual. All animal studies were reviewed and approved by the Office of Animal Care Compliance at the University of New Mexico (16-200384- MC, mouse protocol number 16-200497-HSC) and the United States Department of Agriculture, Beltsville Agriculture Research Center turkey protocol (number 17-008).

2.2 Tissue sampling

Lungfish nasal LAs were dissected as explained in (5). Adult rainbow trout ILT was dissected by scraping the lymphoid tissue located at the base of the gill arches. The trailing edge of the ILT was not included in the ILT tissue sample. Sterilely dissected mouse inguinal LNs and mouse PPs were generously donated by the Dr. J. Cannon Lab at the University of New Mexico School of Medicine. The turkey CT and turkey cecum from a 32-wk-old adult female turkey were provided by Dr. K. Krasnec at the United States Department of Agriculture. An adult Australian lungfish fin snip sample was kindly donated by Dr. M. Forstner. All samples were placed in RNAlater (Invitrogen, Thermo Fisher Scientific, Waltham, MA) and stored at -80℃ until processing.

2.3 Histology

For light microscopy, tissue samples from trout ILT, lungfish LA, turkey CT, and mouse PPs were fixed in 4% paraformaldehyde overnight, transferred to 70% ethanol, and embedded in paraffin (n = 3, except for turkey, n = 2). Samples were sectioned at a thickness of 5 mm,

dewaxed in xylene, and stained using H&E for general morphological analysis. A total of six sections per sample were observed, and images were acquired with a Nikon Eclipse Ti-S Inverted Microscope and NIS-Elements Advanced Research Software (Version 4.20.02).

2.4 RNA-Seq and assembly

RNA from all tissues was extracted using TRIzol (Ambion, Life Technologies, Carlsbad, CA). Turbo DNAse (Invitrogen, Thermo Fisher Scientific) was used to remove any genomic DNA contamination in the RNA. Illumina libraries were constructed using Kapa mRNA HyperPrep Kits (Roche Sequencing, Pleasanton, CA) and sequenced on an Illumina NextSeq 500 System platform at the University of New Mexico Molecular Biology Core Facility. Each library was generated with tissue from one individual. Sequence Read Archive (SRA) databases from the National Center for Biotechnology Information (NCBI) for trout muscle (DRR046645), turkey muscle (SRR478418), and mouse skin (SRR6884615) were downloaded as non-mucosal lymphoid tissue controls. The sratoolkit.2.9.0 fastq-dump was used to convert the SRAs into paired fastq files (33). The quality of the paired-end reads from our Illumina run and the SRAs were assessed using FastQC (34) and poor-quality reads were trimmed out using Trimmomattic set to default parameters (35). The trimmed reads were then assembled into de novo transcriptomes using Trinity (36, 37). The success of the assembly was assessed by realigning our raw fastq reads to the corresponding transcriptome using BWA (38) and samtools (39).

2.5 Data mining and TNFSF phylogenetic analysis

Published genomes for the representative species listed in Supplemental Table I were searched for TNFSF members in NCBI and Ensembl (40). To search for gene expression patterns in O-MALT from mouse, turkey, lungfish, and rainbow trout, TNFSF and TNFRSF protein sequences were downloaded from NCBI and used as queries for TBLASTN searches in

our de novo–assembled transcriptomes (Supplemental Table II). A summary of transcriptome quality metrics is shown in Supplemental Table II. The resulting nucleotide sequences from these searches were used as queries for BLASTX searches in NCBI using hits with an E-value lower than or equal to $1x10^{-5}$. Only the top hit for each search was used unless the top hit was an uncharacterized sequence, in which case the second hit, if characterized, was used. To ensure the detection of all distant TNF homologs, profile hidden Markov modeling (HMM) was implemented. To do this, our de novo transcriptomes were translated into protein data- bases with the longest open reading frame for each sequence using TransDecoder-5.0.0 (37) set with a minimum length of 100 aa. Raw HMM profiles for TNF (PF00229) and TNFR (PF00020) were downloaded from Pfam (41) and used in HMMER (http://hmmer.org/) to search our translated transcriptomes. Sequence alignments for TNFSF1, TNFSF2, and TNFRSF3 for all vertebrate classes were conducted using MAFFT, a multiple sequence alignment program (42). Selected TNF sequences were used to construct phylogenetic trees for ligands and receptors, respectively. Neighbor-joining phylogenetic trees were constructed using the Poisson correction with a bootstrap value of 1000 in MEGA X, as previously explained in (43) (Supplemental Figs. 1, 2).

To compare all the genes expressed in the generated transcriptomes, we first used DIAMOND (44) with the UniProt database (45). Resulting UniProt accession numbers from each transcriptome were then compared in Venny2.1 (46), and the common and unique accession numbers were used for gene ontology and KEGG pathway analysis using the DAVID bioinformatics database (47). Scatterplots identifying significant KEGG pathways (p , 0.05) were created in R (48).

2.6 Data availability

The datasets generated and/or analyzed during the current study are available in the NCBI under https://www.ncbi.nlm.nih.gov/bioproject/ PRJNA486850 (see Supplemental Table II). Lungfish TNF sequences were submitted to NCBI GenBank (African lungfish TNFSF accession numbers MK935171-MK935184, African lungfish TNFRSF accession numbers MK965520-MK965537, and South American TNFSF accession numbers MN536217-MN536233.

3. Results

3.1 Histological analysis of MALTs

As previously reported, histological examination of O-MALT in mice, turkey, African lungfish, and rainbow trout revealed the presence of poorly organized O-MALT in ectotherms, whereas highly organized O-MALT structures can be found in mice and turkeys (Fig. 1). Lungfish LAs have previously been reported to have a diameter between 300 and 350 mm (5). ILT was first dis- covered in salmon as lymphocytic accumulations at the base of each gill arch as well as a trailing edge to the distal end of the gill filament (9), and we also identified these structures in adult rainbow trout gill. Turkey CT and mouse PP have similar mean diameters of ~300 mm and, as previously reported, both of these structures showed a high degree of histological organization with defined compartmentalization into B and T cell zones (49, 50). Lungfish LA, as previously described (5), showed no compartmentalization, and it was composed of random clustering of lymphocytes with no distinct zones. Although we did not attempt to identify B and T cell zones in trout ILT in this study, these are not present in salmon ILT (9) or any other bony fish SLOs studied to date but are present in the spleen of cartilaginous fish (51).

3.2 Analysis of TNFSF and TNFRSF in vertebrate genomes

Bioinformatic analyses were performed among the major vertebrate classes to identify all TNFSF and TNFRSF genes with a focus on TNFSFs previously described as key factors in lymphoid tissue formation in mammals (Fig. 2A). Tacchi et al. (5) reported the presence of 18 TNF ligands and 27 TNFR in humans, 13 TNF ligands and nine TNFR in teleost, 14 TNF ligands and 15 TNFR in the coelacanth, and 13 TNF ligands and 14 TNFR in African lung- fish. To revisit the TNFSF theory, we expanded our searches to include newly available genomes/transcriptomes for all vertebrate classes (Supplemental Table I). BLAST searches revealed the presence of 14 TNFSF ligands and 25 TNFSF receptors in teleost genomes. BALM was found in the newly sequenced teleost genomes, along with receptors TNFRSF1B, TNFRSF4, TNFRSF6B, TNFRSF7 (CD27), TNFRSF8, TNFRSF9, TNFRSF10B, TNFRSF11A, TNFRSF11B, TNFRSF12A, TNFRSF13B, TNFRSF14, TNFRSF18, TNFRSF19, and TNFRSF25 (Tables I, II). In coelacanth, BLAST searches did not reveal the presence of any new ligands but identified 10 more TNFR: TNFRSF1B, TNFRSF4, TNFRSF7, TNFRSF10B, TNFRSF11B, TNFRSF13B, TNFRSF17, TNFRSF18, TNFRSF25, and TNFRSF27. Searching all new African lungfish transcriptomes revealed the expression of ligands TNFSF9, TNFSF11, and BALM as well as receptors TNFRSF1B, TNFRSF8, TNFRSF12A, TNFRSF13C, and EDAR. In South American lungfish, our transcriptomes showed the expression of 10 ligands and 18 receptors. Amphibian and reptile genomes showed the expression of 12 ligands and 21 receptors and 16 ligands and 24 receptors, respectively. The presence of 12 ligands and 27 receptors was detected in the bird genomes searched. As previously reported, TNFSF1, TNFSF3, and TNFRSF3 (LTBR) were absent from bird genomes (13) (Tables I, II). Finally, our searches confirmed all previously reported TNFSF molecules in human.

Because of the low sequence similarity between TNFSF molecules (52, 53), to identify distant TNFSF homologs we performed additional structural searches using HMM using the TNF homology domain (THD). HMM analyses revealed the presence of three more TNFR (TNFRSF4, TNFRSF8, and TNFRSF13C) in South Ameri- can lungfish not found through BLAST searches. In African lung- fish, HMM searches identified the presence of one additional ligand, TNFSF9, and three additional receptors, TNFRSF EDAR, TNFRSF8, and TNFRSF9. HMM searches in trout, turkey, and mouse transcriptomes did not result in the identification of any novel TNFSFs or TNFRSFs (Tables I, II).

When focusing on the TNFs vital for lymphocyte organization in mice, we found that four of these molecules are evolutionarily conserved from bony fish to mammals, including TNFSF5 (CD40L), TNFRSF1A, TNFRSF5 (CD40), and TNFRSF11A. TNFSF1 and TNFSF3 showed complex evolutionary histories because they are present in the coelacanth but appear to be absent in Australian lungfish. The majority of tetrapods have TNFSF1 and TNFSF3 but they have been lost in Aves (54–56). Our analysis indicates that TNFRSF3 was lost in early tetrapods because it is present in bony fish and lungfish but not in amphibians. TNFRSF3 genes are found in mammals, suggesting deletion of TNFRSF3 in the amphibian lineage (Fig. 2A).

Phylogenetic analysis showed the homology between TNFSFs and TNFRSFs in bony vertebrates. TNFSF ligands mostly grouped within their respective family clade. In particular, within their clade, TNFSF ligands 10, 11, 5, 1, 2, 8, and 12 had bootstrap values higher than 50%. Hence, for these families, the lower sequence divergence may reflect a conservation of function. As expected, in lungfish, TNFSF ligands appeared more closely related to tetrapod TNFSF ligands compared with those of bony fish. TNFSF1 and TNFSF2 ligands shared a bootstrap value of 51%, with no clear separation among their members (Supplemental Fig. 1). As

seen for some TNFSF, the phylogenetic tree for TNFRSFs showed that some receptor families are well conserved with bootstrap values higher than 50%. Specifically, the members of TNFRSF19, 19L, 27, EDAR, 16, 8, 21 and 11A families all appeared well con- served, with no clear separation among teleosts and other vertebrates. The only exception was salmon TNFRSF11A, which was more closely related to salmon and coelacanth TNFRSF5 than to other TNFRSF11A molecules. Interestingly, TNFRSF11B and 6 shared a bootstrap value of 75%, and their members appeared mixed within the two clades. Of particular relevance, we observed that in the majority of the TNFRSF clades, lungfish sequences appeared more closely related to those of teleosts than tetrapod counterparts (Supplemental Fig. 2).

TNFSF2, as predicted, was found in all scanned genomes/ transcriptomes (Fig. 2). As expected, the amino acid alignment of TNFSF2 molecules from representative vertebrate species showed high similarity among them as well as with the TNFSF1 family. Specifically, several conserved amino acids were found in the 10 b-strands domains (A–H) present in human, with the highest degree of conservation observed in domain C (Fig. 3). Interestingly, the amino acid sequence of domain C in birds (*Gallus gallus*) showed several amino acid substitutions that deviate the TNFSF2 sequence considerably from that of mammals, amphibians, and lungfish. The corresponding receptors (TNFRSF1A and TNFRSF1B) were also found in all vertebrate groups, except for amphibians, in which surprisingly, TNFRSF1A is present but TNFRSF1B is missing (Table II).

These results provide a revised view of the complexity of TNFSF evolution in vertebrates and provide further support for the notion that SLOs emerged in each class of vertebrates in novel ways that are not always dependent on TNFSF members such as the lymphotoxin axis.

3.3 Expression of TNFSF and TNFRSF in ectotherm and endotherm O-MALT structures

Because of the lack of published lungfish genomes or transcriptomes obtained from O-MALT, we performed RNA-Seq on O-MALT tissues from mice, turkeys, African lungfish, and rainbow trout (Supplemental Table II). Searching these new transcriptomes indicated a similar expression pattern of TNFSFs as previously shown in Fig. 2A and 2B. Interestingly, we observed the expression of all TNFs vital to lymphoid tissue formation in mammals in the LA of the lungfish. Because a lungfish genome is not available, orthology assignment between lungfish and human TNFSF molecules can only be predicted based on the percentage of amino acid identity (57). Percentage amino acid identity analysis for TNFSF ligand and receptors present in both African lungfish and humans revealed that 17 out of the 32 molecules shared >30% sequence identity supporting orthology (58). Of the eight critical TNFs identified in mammalian studies (15), lungfish TNFSF1, TNFSF5, TNFSF11, and TNFRSF11 have >30% sequence identity with their human counterparts (Table III). The lower sequence identity of the remaining four members raises the question of whether they are involved in lymphoid organ development and organization. To gain some insights into this question, we performed amino acid sequence alignments and motif analyses of vertebrate TNFSF1 and TNFRSF3 molecules. Amino acid alignments for TNFSF1 showed the presence of the conserved THD in all jawed vertebrates. Additionally, this alignment confirmed that teleost TNF-new (TNFN) does not contain the conserved THD for TNFSF1, and therefore, it is not an ortholog of mammalian TNFSF1 (22) (Fig. 4). Similar to tetrapods, lungfish TNFSF1 contained the conserved THD that makes up the typical jelly roll conformation of TNFs (52) and residues vital for binding TNFRSF3 were conserved in mammalian and African lungfish TNFSF1 sequences. In support of this, the percentage identity between human and African lungfish TNFSF1 was above 30% (Table III). Combined, this analysis suggests that lungfish TNFSF1 is an ortholog of mammalian TNFSF1.

Although we did not perform amino acid sequence alignments for TNFSF3, the amino acid identity between lungfish and human TNFSF3 is ~27% (Table III), a value not sufficient to ascertain that the lungfish molecule carries out similar functions to the mammalian counterpart. Phylogenetic analysis showed that all vertebrate TNFSF3 molecules form one clade, whereas TNFSF1 molecules appear to be intermixed with TNFSF2 in a single clade, indicating that they are closely related.

TNFR do not contain a THD, but instead, are composed of short cysteine-rich domains (CRDs), which are essential for the inter- action between TNSRSF3 and the TNFSF1 and TNFSF3 heterodimer (52). Amino acid alignment showed that CRDs are conserved in all the vertebrate TNFRSF3 molecules analyzed (Fig. 5A). The intracellular domain of TNFRSF3 contains both conventional and unconventional TRAF binding domains in coelacanth and tetrapods (59). However, teleost TNFRSF3 molecules, as well as African and South American lungfish TNFRSF3, lack these TRAF binding domains. Instead, teleost and South American lungfish have a bony fish specific conserved TRAF binding motif, whereas the African lungfish does not (Fig. 5B). The lack of a TRAF binding motif suggests that African lungfish TNFRSF3 may not signal the same way as its mammalian counterpart and therefore may have an alternative function. In support, percentage identity analysis of TNFRSF3 sequences aligned in Fig. 5A and 5B show high sequence identity (66.98%) between the human and mouse sequences, whereas the percentage identity between human and African lungfish molecules is only 20.9%, indicating lack of orthology (Fig. 5C). This result supports the phylogenetic analysis findings that showed two separate clades for TNFRSF3, a clade containing teleost, lungfishes, and amphibian molecules and a second clade containing human, mouse, and coelacanth molecules (Supplemental Fig. 2).

As expected, we also noted the absence of TNFSF1, TNFSF3, or TNFRSF3 in turkey CT, as well as absence of TNFSF1 and TNFSF3 expression in rainbow trout, suggesting that alternative molecular mechanisms other than the lymphotoxin axis drive mucosal lymphoid tissue formation in birds and teleost fish. TNFSF2 transcripts were detected in all the O-MALT transcriptomes generated in this study, as well as the receptors TNFRSF1A and TNFRSF1B. Therefore, in the absence of the lymphotoxin axis, TNFSF2 may be driving the clustering of lymphocytes in nonmammalian species.

3.4 Unbiased search of molecular drivers of O-MALT structure in vertebrates

To elucidate previously unidentified molecular drivers and biological pathways involved in O-MALT formation, we compared the transcriptomes generated from four different O-MALT tissues from each representative vertebrate species. We obtained a total of 280,740 transcripts in the mouse PP transcriptome, 164,478 transcripts in the turkey CT transcriptome, 162,353 transcripts in the lungfish LA transcriptome, and 286,901 transcripts in the trout ILT transcriptome. We first removed genes expressed in negative-control tissue (nonlymphoid tissues) transcriptomes from each of the four species. This resulted in a total of 6483 transcripts for the mouse PP, 27,172 transcripts for turkey CT, 6772 transcripts for the lungfish LA, and 13,214 transcripts for the trout ILT. As illustrated by the Venn diagram, we observed few transcripts shared among all four O-MALT transcriptomes (Fig. 6). Turkey CT and trout ILT had the most transcripts in common with 3096 (6.9%), whereas mouse PP and lungfish LA had the lowest percentage of genes in common, with only 263 (0.6%). Turkey CT had the highest number of unique genes, with 20,520 (46%), whereas mouse PP and lungfish LA had a similar percentage of unique genes, with ~4000 (8.7–8.8%) each, and trout ILT had 8300 (18.6%) (Fig. 6).

We next performed gene ontology and KEGG pathway analysis of the respective gene lists that were unique or shared among O-MALTs (Fig. 7). Interestingly, genes unique to mouse PPs were significantly enriched in genes belonging to olfactory transduction (Table IV). These included olfactory receptor (OR) family 8, subfamily B, member 4; OR family 2, subfamily H, member 1; and cyclic nucleotide gated channel b 1 (Table IV). To confirm these findings, we searched previously published SRAs from mouse inguinal LNs. We found that mouse LNs are also enriched in genes belonging to the olfactory transduction pathway, including OR families and cyclic nucleotide gated channels. Interestingly, 14 genes that were unique to lungfish LA were also enriched in the olfactory transduction KEGG pathway (Table IV). Additionally, we found a total of 97 genes that were unique to turkey CT and 20 genes that were unique to trout ILT that were enriched in the neuroactive ligand/receptor pathway. These included glycine receptors, cholinergic receptors, purinergic receptors, thyroid-stimulating hormone receptors, among others (Table V). When looking at genes shared between lungfish LA and turkey CT we found that they shared 12 genes that were enriched in the neuroactive ligand/receptor interaction pathway. Combined, our findings highlight little overlap in the transcriptome of different vertebrate O-MALT structures and unveil unique biological processes that likely drive lymphocyte aggregation in each vertebrate group, such as olfactory-related genes in mammals and sarcopterygian fish and neuronal-derived signals in birds and ectotherms.

4. Discussion

The organization of lymphocytes and other immune cells in discrete lymphoid structures is one of the hallmarks of the immune system of endotherms. This organization is believed to increase cell-Ag interactions, optimize Ag presentation and T cell stimulation, and lead to efficient selection of high-affinity B cell clones during the maturation of the immune response.

SLOs, such as spleen, LNs, and O-MALT, develop during embryogenesis. In contrast, TLSs develop after birth and require chronic inflammation or microbial signals to develop. TLS include the isolated lymphoid follicles in the small intestine, the inducible bronchial-associated lymphoid tissue, and the TLS commonly associated with tumors (5, 60–62).

TNFSFs are vital molecules for the process of lymphoid tissue formation and organization in mammals (63). TNFSF molecules and signaling pathways govern both the formation of SLOs, such as the spleen, LNs, and PPs, as well as FDC, GC, and TLS (61–65). The current model for mammalian LN and PP formation relies on lymphoid tissue inducer (LTi) cells and an initial neuronal-derived signal (66). It has been proposed that retinoic acid released by the vagus nerve induces expression of CXCL13 by mesenchymal cells (66). However, evidence for the neuronal contributions to the initiation of this process are limited because only one previous study introduced this concept and follow-up experimental support is currently lacking. Precursor LTi cells start to cluster and signal through TNFSF11 and TNFRSF11, which initiates the expression of TNFSF1 and TNFSF3 on the precursor LTi cells that then become mature LTi cells. Mature LTi cells also rely on the lymphotoxin axis to initiate the expression of chemokines, adhesion molecules, and cytokines that facilitate the attraction and retention of more hematopoietic cells causing the growth and maintenance of the LN (63, 67–69). Thus, TNFRSF3-mediated signaling in response to the LTa1b2 binding is the main pathway for promoting mammalian lymphoid tissue development. TNFSF1-deficient, TNFSF3-deficient, and TNFRSF3-deficient mice all have similar defects during secondary and tertiary lymphoid organogenesis (70–72), whereas TNFSF2 deficiency results in diverse phenotypes, ranging from altered SLO morphology to no changes in SLO appearance, depending on the mouse model used (20, 21, 26–29). Specific differences in LN and PP organogenesis have, nevertheless, been

reported (63). For instance, mice deficient in TNFRSF1A, a receptor for LTα1β2, lack the formation of PPs but still retain LN development (21). Additionally, unlike LNs, PP formation requires a population of CD11c+ dendritic-like cells that express LTb and the receptor tyrosine kinase RET. Interestingly, RET was previously de- scribed as a neuroregulator (73–75), and innate lymphoid cells (ILCs) ILC3 in the gut express RET and respond to glial- derived neurotrophic factors (76). Additionally, PPs but not LNs are absent or significantly reduced in CXCL13- or CXCR5-deficient animals (77) as well as sharpin-deficient animals (78).

Despite the clear involvement of TNFSF molecules in mammalian SLO and TLS biology, it is still unclear whether TNFSFs also govern O-MALT formation and maintenance in ectotherms and whether these structures serve similar immunological functions to those described in mammals. The evolution of TNFSF and TNFRSF is very complex, and it involved small-scale du- plications as well as large, genome-wide duplications (53). The coevolution of TNFSF and TNFRSF families is characterized by functional convergence, as evidenced by the fact that multiple ligands share the same receptor and that different ligand-receptor interactions can result in the same biological outcome (53). Of interest, Drosophila has one TNF ligand (Eiger) and one TNFR ligand (Wengen) (79), and Drosophila TNFSF molecules are highly expressed in the nervous system (80). We previously reported the expansion in TNFSF genes in African lungfish compared with other ectotherms and proposed that this expansion may explain the presence of O-MALT in lungfish (5). Since that study, new genomes and transcriptomes have become available, allowing us to revisit the TNFSF phylogeny. Additional structural searches also allowed us to refine our approaches that were previously limited to BLAST searches. Thus, in this study we report that TNFSF does not appear to have expanded in sarcopterygian fish because lower numbers of overall TNFSF genes were found in lungfish compared with bony

fish. However, expansion of TNFs within teleosts may not be surprising, given the multiple genome duplication events that have occurred over bony fish evolution (81). *P. dolloi* is also a tetraploid species, and therefore, similar events could have contributed to TNFSF expansions in this lungfish species. Because of the lack of functional experiments at this point, it is unclear whether the TNFSF genes identified in ectotherms encode molecules with homologous functions to their mammalian counterparts, and further work is needed to clarify these questions.

Given the importance of the lymphotoxin axis that was revealed in murine studies, we focused on lymphotoxin sequence analyses in this study. TNFSF1 and TNFSF3 appear to be absent in teleost fish despite the fact that salmonids have ILT in their gills, a structure predominantly composed of T cells that lack the canonical B and T cell areas and GC formation found in endotherms (7, 9). In accord, previous efforts to discern teleost lymphotoxins showed that TNFRSF3 is present in teleosts but TNFSF1 and TNFSF3 are not. Teleost fish have a novel TNF, TNFN, that at first was considered to be the candidate homolog for mammalian lymphotoxins, but a recent study and our amino acid alignment showed that the structure and behavior of TNFN did not relate to either TNFSF1 or TNFSF3 (Fig. 4) (30, 59). Rather, TNFSF14 was found to bind to TNFRSF3, showing that, originally, TNFRSF3 was the receptor for TNFSF14. Recently, single-cell RNA-Seq analysis of RAG2/2 zebrafish revealed the expression of ILC1-, ILC2-, and ILC3-type markers in zebrafish (82). Specifically, an ILC3-like cell subset found in zebrafish shares some transcriptional similarities to the mammalian LTi cells and exclusively expresses *tnfb* (TNFSF2), the ortholog to human LTa and a marker of LTi cells. Interestingly, we detected a partial contig for fish type I TNFSF2 in trout ILT by Illumina sequencing, and therefore, it is possible that TNFSF2 signaling alone is sufficient to drive lymphocytic aggregation in nonmammalian species. Because bony fish have two types of

TNFSF2 (named I and II) (83), further studies are therefore required, for instance, to ascertain a role for each TNFSF2 gene in teleost ILT formation.

Amino acid sequence alignment of TNFRSF3 from jawed vertebrates showed that, whereas the extracellular domains are highly conserved, the transmembrane domain as well as the intracellular domain are not. Thus, the percentage identity at the amino acid level between *Protopterus sp*. TNFRSF3 and human TNFRSF3 is ~20%, a low value that suggests that these two molecules are not orthologs. This finding was further supported by the TNFRSF tree reported in this study (Supplemental Fig. 2). Functionally, our results suggest that TNFRSF3 signaling, as described in mammalian studies, may not occur in lungfish and further studies should investigate the biological function of lungfish TNFRSF3. Similarly, both amphibian and bony fish TNFRSF3 only shared a 20% amino acid identity with human TNFRSF3, indicating that ectotherm TNFRSF3 molecules may lack the signaling capabilities of their mammalian counterparts. Our findings, therefore, indicate that molecular signaling pathways other than the lymphotoxin pathway must be responsible for the formation and maintenance of teleost ILT and lungfish nasal O-MALT structures.

Although birds do not have LNs, they have O-MALT structures, such as CT and pharyngeal tonsils, that are structurally very similar to those found in mammals with FDCs and GCs (84). Mammalian studies have emphasized the importance of signaling through TNFRSF3 for lymphoid tissue formation, but the lack of the lymphotoxin axis in birds has not impeded their ability to form and maintain SLOs with a mammalian-like level of compartmentalization (54). The loss of lymphotoxins in birds is not a rare event. Birds have the unique ability to compensate for losses in numerous immune genes/loci, including the Ig kappa L chain, peroxiredoxin, and other TNFSF members (15, 85–87). Thus, in agreement with previously

published studies (32, 54), we found that bird genomes do not contain TNFSF1, TNFSF3, or TNFRSF3. Furthermore, our comparative transcriptomic data using turkey CT suggests that these structures may be generated by very different pathways in birds and mammals because no common gene expression signatures were found. Because we performed RNA-Seq analysis on O-MALT from adult animals, the gene expression patterns likely captured maintenance rather than organogenesis of this structure. Future studies should evaluate gene expression profiling during embryogenesis of bird SLOs to gain a deeper insight into the genes involved in their early organogenesis.

The interactions between the nervous system and the immune system are complex and bidirectional (88, 89). Along with TNFSFs, neurons have been proposed to produce metabolites such as retinoic acid that could contribute to SLO formation. In addition, a subset of ILC3s are LTi-like cells characterized by the expression of retinoic acid–related orphan receptor g T (RORgt), which are crucial initiators of SLO organogenesis (90). As mentioned earlier, ILC3 also expresses RET and responds to neurotrophic factors, providing additional evidence that neuronal signals may regulate SLO formation. Yet, this hypothesis has not been explored in other vertebrate groups, and experimental evidence is limited at this point. Our findings support a conserved role for neuronal-derived signals in SLO maintenance in adulthood. We found that neuroactive ligand and receptor pathways were enriched in trout, lungfish, turkey, and mouse SLO transcriptomic datasets. Among the genes identified in this pathway, we identified cholinergic receptors, dopamine receptors, g-aminobutyric acid type A receptors, and cholinergic nicotinic receptors. Nicotinic acetylcholine receptors are present within SLOs, which are highly innervated with cholinergic fibers and have been shown to influence lymphocyte development (91). We found expression of five different g-aminobutyric acid type A receptor a genes in

turkey CT but not in other SLO transcriptomes examined. These receptors have been shown to affect a wide variety of immune processes, such as cytokine secretion, cell proliferation, phagocytic activity, and chemotaxis (92). Interestingly, we observed little overlap in the specific genes within this pathway expressed in each SLO, suggesting that neuronal functions rather than specific suites of genes guide SLO maintenance in different species. It is important to note that not all animals sampled in this study were the same age. Whereas African lungfish and trout tissues were obtained from juvenile/preadult stages, mouse and turkey samples were collected from adults. Thus, we cannot rule out that the gene expression patterns found in each SLO depend on the developmental stage as well as immunological and metabolic states at which each animal was sampled. Despite these caveats, we propose, in this study, that neuronal signals may guide the aggregation of T cells and B cells and the maintenance of SLO structures across vertebrates. Further studies are warranted to test this new paradigm.

OR genes are fast evolving genes and the largest gene family in mammalian genomes. In mice, 4% of all genes are olfactory genes, whereas in humans, olfactory genes make 1.4% of the genome (93). Although this expansion of OR genes in mammals is thought to reflect the importance of olfaction in the survival of this vertebrate group, ORs also play vital roles outside of the olfactory system and have widespread expression patterns (94, 95). For instance, OR ectopic expression is thought to be vital for cell-to-cell recognition, cell cycle, and migration in many cell types (96, 97). Additionally, odorant receptors regulate immune cell functions such as T cell migration and T cell accumulation in LNs (98) or chemotaxis of lung macrophages (99). The present study identified that both mammalian PPs, mammalian LNs, and lungfish LAs were significantly enriched in genes belonging to the olfactory transduction pathway. Because the lungfish LA we sampled was a nasal LA, we cannot rule out contamination of olfactory gene

expression from connective tissue surrounding the LA, but contamination issues could not explain OR expression in mouse PPs or LNs. This observation is supported by the fact that ectopic expression of specific OR genes is high in mammalian lymphoid tissues. For instance, OR family 52, subfamily N, member 4 and OR family 56, subfamily B, member 1 expression is highest in human PPs out of 18 tissues measured (100) and OR 2A4 expression is highest in human LNs out of 33 tissues analyzed. Importantly, LTi cells express G protein–coupled receptor 183 (GPR183). This receptor is required for the formation of TLS such as cryptopatches and isolated lymphoid follicles (90). In mice that are deficient in G protein ai2 subunit, PPs regress and colitis is observed, emphasizing the importance of G proteins in the formation and retention of SLO and TLS (101). Expression of OR genes in different subsets of immune cells within SLOs and TLS may allow for fast and specific mechanisms of cell-to-cell communication. Given the complexity, size, and evolutionary rates of the OR gene family in mammals, further work is warranted to define the nature of OR-mediated interactions within mammalian lymphoid structures.

In summary, our findings provide new insights into the molecules that drive the complexity and diversity of lymphocytic aggregates found at mucosal tissues of vertebrates. Exhaustive TNFSF phylogenetic studies indicate that, as suggested by others, this superfamily is not universally used by all vertebrates to achieve O-MALT formation and maintenance. We propose a new paradigm, in which genes with functions in neuroactive ligand and receptor interactions as well as olfactory-related genes may drive O-MALT maintenance in a group-specific manner. Although we do not provide functional evidence for this theory, our transcriptomic analyses suggest that neuronal inputs other than retinoic acid production are required for vertebrate SLO maintenance. Additionally, ectopic expression of olfactory genes

appears to be a unique innovation of mammalian SLOs. Cooperation between olfactory genes and TNFSF members, particularly TNFSF2, may also occur and be critical for the structure and function of O-MALT. Further studies are warranted to confirm these new theories in this study proposed.

5. Acknowledgments

We thank Dr. Martin F. Flajnik for critical review of the manuscript and Dr. Lijing Bu for help with bioinformatics analysis. Dr. Judy Cannon provided mouse tissue samples, Dr. Katina Krasnec provided turkey tissue samples, and Dr. M. Forstner provided Australian lungfish tissue samples. We thank Dr. Amemiya for kindly sharing lungfish RNA-Seq datasets.

6. Figures and Tables

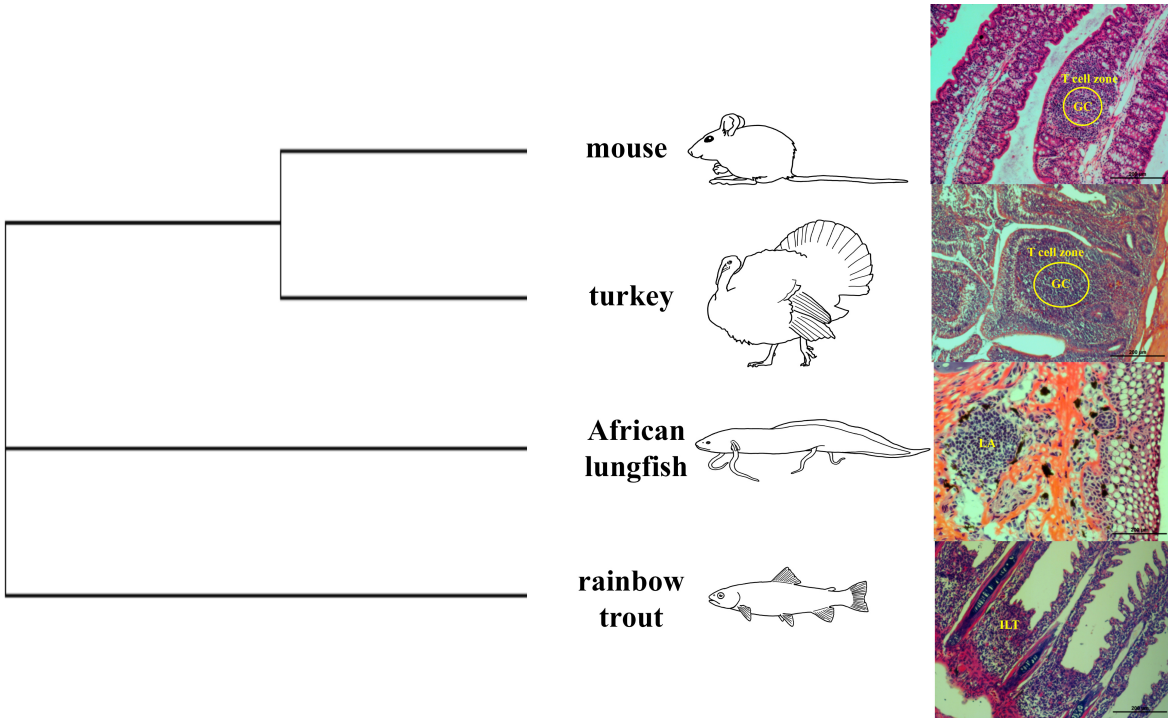

Figure 1. Phylogenetic representation of O-MALT formation in bony jawed vertebrates and light microscopy images of H&E stained sections from the different O-MALT structures used in this study. LA: lymphoid aggregate; GC: germinal center, ILT: interbranchial lymphoid tissue.

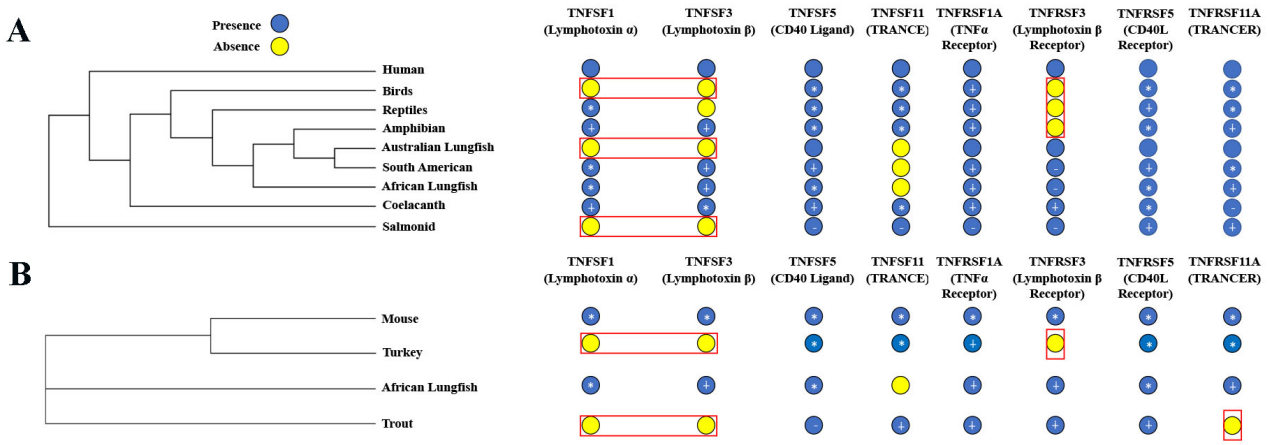

Figure 2. Expression of TNFs vital to secondary lymphoid tissue formation in vertebrates. (A) Expression of TNFs in previously published genomes and transcriptomes. (B) Expression of TNFs in O-MALT sequenced from mouse PP, turkey CT, African lungfish LA, and trout ILT. (*) denotes an amino acid percent identity with human greater or equal to 30%, (+) denotes amino an acid percent identity with human between 30-20%, and (-) denotes amino acid percent identity with human of less than 20%.

Table I. TNFSF ligands present in bony-jawed vertebrates

	TNFSF								
	Teleost	Coelacanth	South American Lungfish	African Lungfish	Amphibian	Reptiles	Bird	Mouse	Human
TNFSF1 (LTA)	−	+	+	+	+	+	−	+	+
TNFSF2 (TNF)	+	+	+	+	+	+	+	+	+
TNFSF3 (LTB)	−	+	+	+	+	−	−	+	+
TNFSF4	−	−	−	−	−	+	+	+	+
TNFSF5 (CD40LG)	+	+	+	+	+	+	+	+	+
TNFSF6 (FASLG)	+	+	+	+	+	+	+	+	+
TNFSF7 (CD70)	−	−	−	−	−	−	−	+	+
TNFSF8	−	+	−	+	−	+	+	+	+
TNFSF9	−	−	+	+[a]	−	+	−	+	+
TNFSF10	+	+	+	+	+	+	+	+	+
TNFSF11	+	+	−	+	+	+	+	+	+
TNFSF12	+	+	−	+	+	+	−	+	+
TNFSF13	+	+	+	+	+	+	−	+	+
TNFSF13B	+	+	+	+	+	+	+	+	+
TNFSF14	+	+	+	+	+	+	+	+	+
TNFSF15	+	+	−	−	−	+	+	+	+
TNFSF18	+	−	−	−	−	+	+	+	+
EDA-A1/EDA-A2	+	+	−	+	+	+	+	+	+
BALM	+	−	−	+	−	−	−	−	−
Ita/TNFN	+	−	−	−	−	−	−	−	−
Total number	14	14	10	15	12	16	12	18	18

Presence and absence of TNF ligands in all vertebrate classes. Only hits with an *E*-value lower than 1×10^{-5} were considered. Note that "presence" does not imply orthology with mammalian counterparts.

[a]Ligands that were not found through BLAST searches but were found using HMM searches. Only hits with an *E*-value lower than 1×10^{-5}were considered.

Table II. TNFRSF members present in bony-jawed vertebrates

	TNFRSF								
	Teleost	Coelacanth	South American Lungfish	African Lungfish	Amphibian	Reptile	Bird	Mouse	Human
TNFRSF1A	+	+	+	+	+	+	+	+	+
TNFRSF1B	+	+	+	+[a]	−	+	+	+	+
TNFRSF3 (LTBR)	+	+	+	+	+	−	−	+	+
TNFRSF4	+	+	+[a]	−	+	+	+	+	+
TNFRSF5 (CD40)	+	+	+	+	+	+	+	+	+
TNFRSF6 (FAS)	+	+	+	+	+	+	+	+	+
TNFRSF6B	+	+	−	−	+	+	+	+	+
TNFRSF7 (CD27)	+	+	−	+	−	−	+	+	+
TNFRSF8	+	−	+[a]	+[a]	+	+	+	+	+
TNFRSF9	+	+	+	+	+	+	+	+	+
TNFRSF10A	+	+	+	+	+	+	+	+	+
TNFRSF10B	+	+	+	−	+	+	+	+	+
TNFRSF10C	−	−	+	−	−	−	+	+	+
TNFRSF10D	−	−	−	−	−	−	−	−	+
TNFRSF11A	+	+	+	+	+	+	+	+	+
TNFRSF11B	+	+	+	+	+	+	+	+	+
TNFRSF12A	+	−	−	+[a]	+	+	+	+	+
TNFRSF13B	+	+	+	+	−	+	+	+	+
TNFRSF13C	−	−	+[a]	−	−	+	+	+	+
TNFRSF14	+	+	+	+	+	+	+	+	+
TNFRSF16 (NGFR)	+	+	−	+	+	+	+	+	+
TNFRSF17	+	+	+	+	+	+	+	+	+
TNFRSF18	+	+	−	−	−	+	+	+	+
TNFRSF19	+	+	−	−	+	+	+	+	+
TNFRSF19L (RELT)	+	+	−	−	+	−	+	+	+
TNFRSF21	+	+	+	+	+	+	+	+	+
EDAR	+	+	−	+[a]	+	+	+	+	+
TNFRSF25	+	+	−	−	−	+	+	+	+
TNFRSF27 (EDA2R)	−	+	−	−	+	+	+	+	+
Total number	25	24	18	18	21	24	27	28	29

Presence or absence of TNFRSF molecules in different vertebrate groups. BLAST and reverse-BLAST searches were performed using available transcriptomes and genomes from the main vertebrate groups. Only hits with an *E*-value lower than 1×10^{-5} were considered. Note that presence does not imply orthology with mammalian counterparts. TNFR superfamily members present in bony-jawed vertebrates.

[a]Sequences only found through HMM and not found through blasting the created transcriptomes.

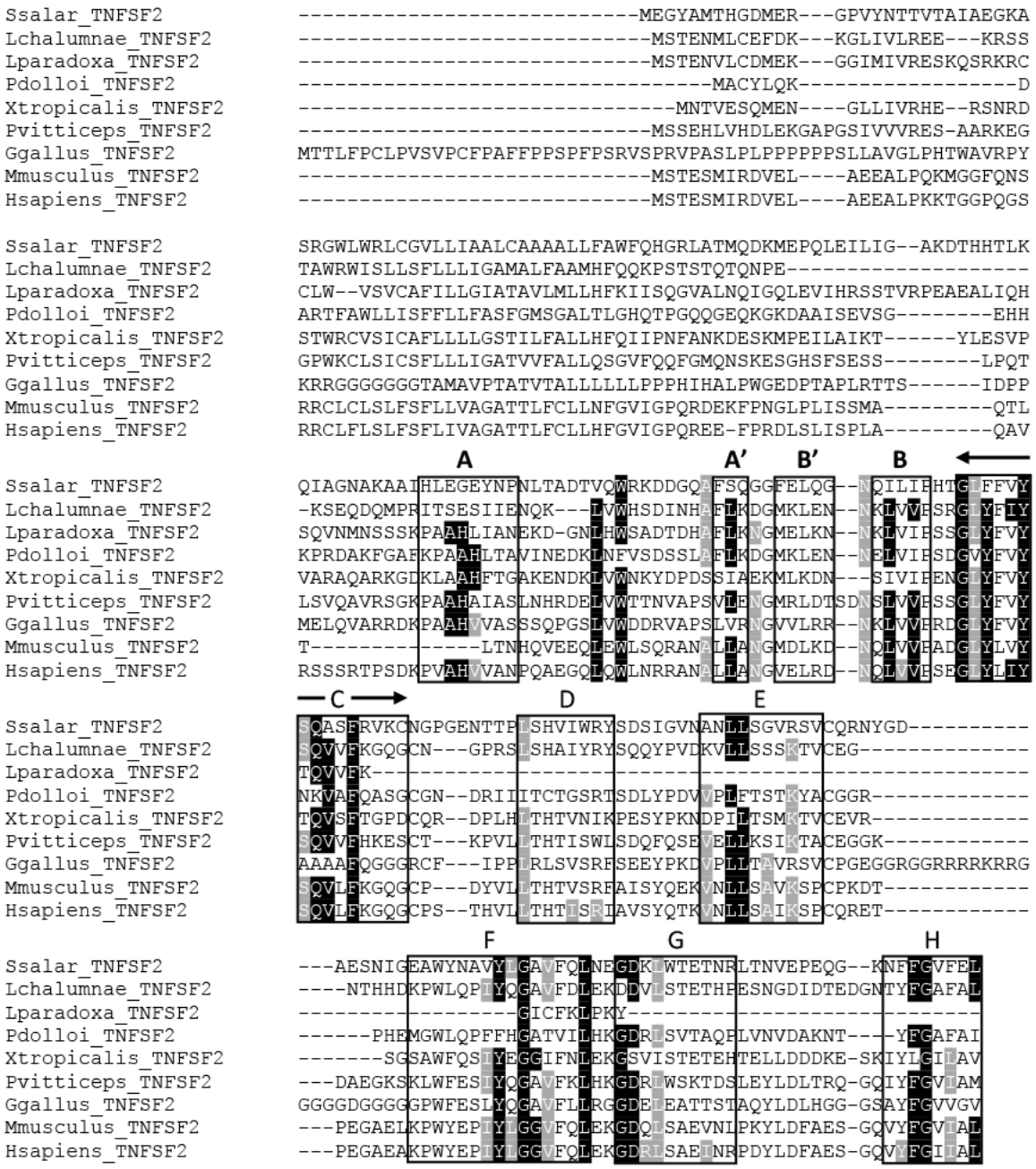

Figure 3. TNFSF2 amino acid alignment. Boxes indicate amino acids that make up the b strand of the typical jelly roll fold for TNF family members. Highlighted in black are conserved amino acids in the THD. Black shading denotes the most conserved amino acids and gray denotes partially conserved amino acids. The black arrows are used to show the entire conserved domain when it did not fit on the same line. Bold letters denote a distinct subunit that makes up TNFSF2.

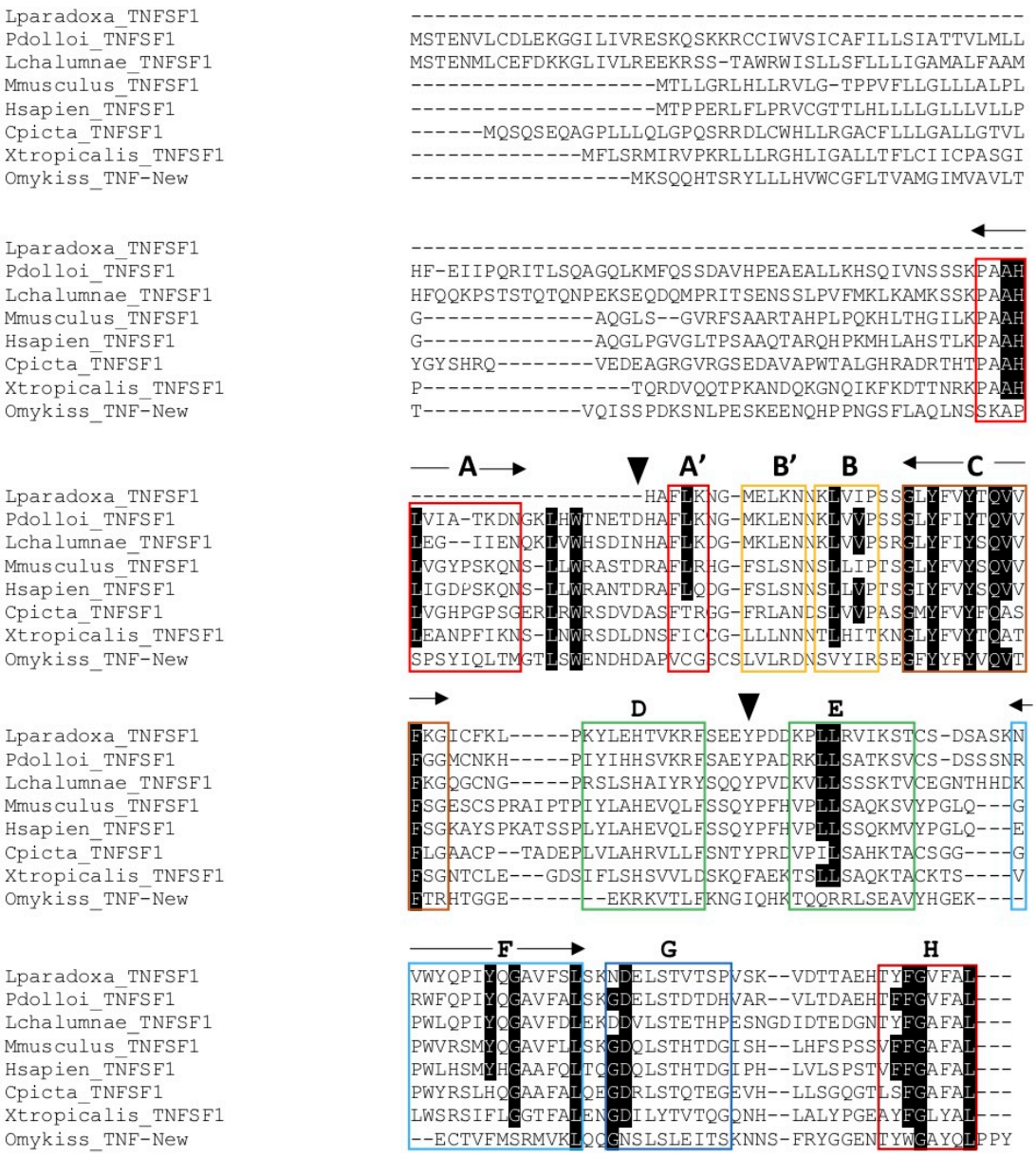

Figure 4. TNFSF1 amino acid alignment. Boxes indicate amino acids that make up the b strand of the typical jelly roll fold for TNF family members. Highlighted in black are conserved amino acids in the THD. The black arrows are used to show the entire conserved domain when it did not fit on the same line. The black arrowheads denoted important amino acids that bind to TNFRSF3. Each bold letter denotes a distinct subunit that makes up TNFSF1.

Table III. Percentage identity of TNFs between African lungfish and humans

Protein	Percentage Identity between *Protopterus* and Human
TNFSF1	**30.24**
TNFSF2	22.97
TNFSF3	27.63
TNFSF5	**32.95**
TNFSF6	**46.95**
TNFSF8	22.07
TNFSF9	19.57
TNFSF10	**39.15**
TNFSF11	**39.17**
TNFSF12	**48.05**
TNFSF13	27.80
TNFSF13B	**41.88**
TNFSF14	**37.31**
EDA	**81.92**
TNFRSF1A	26.84
TNFRSF1B	25.64
TNFRSF3	20.09
TNFRSF5	**30.69**
TNFRSF6	29.25
TNFRSF7	18.52
TNFRSF8	**30.71**
TNFRSF9	**29.80**
TNFRSF10A	19.51
TNFRSF11A	25.32
TNFRSF11B	**34.52**
TNFRSF12A	13.95
TNFRSF13B	**32.00**
TNFRSF14	27.92
TNFRSF16	**50.47**
TNFRSF17	24.32
TNFRSF21	**44.44**
EDAR	**64.79**

Percentage identity of TNF ligand and receptor sequences shared in humans and African lungfish, bold indicates higher percentage identity between lungfish and human sequences.

A

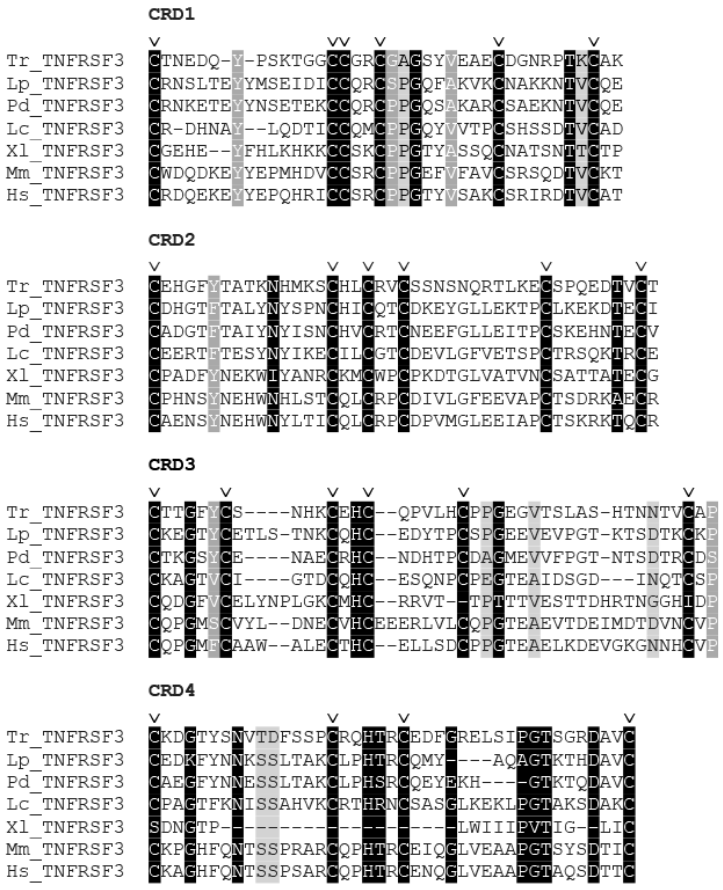

B

C

	1	2	3	4	5	6	7
1.Hsapiens_TNFRSF3	100.000	66.988	20.915	21.865	20.092	25.747	18.692
2.Mmusculus_TNFRSF3	66.988	100.000	18.627	20.900	20.241	22.169	20.000
3.Xlaevis_TNFRSF3	20.915	18.627	100.000	14.379	18.301	16.340	17.647
4Trubripes_TNFRSF3	21.865	20.900	14.379	100.000	21.865	20.257	20.257
5.Protopterus_TNFRSF	20.092	20.241	18.301	21.865	100.000	22.171	50.234
6.Lchalumnae_TNFRSF3	25.747	22.169	16.340	20.257	22.171	100.000	17.991
7.Lparadoxa_TNFRSF3	18.692	20.000	17.647	20.257	50.234	17.991	100.000

Figure 5. Comparison of TNFRSF3 amino acid sequences among jawed vertebrates. (A) Extracellular domain of TNFRSF3, with triangles indicating extracellular CRD and residues required for ligand binding in mammals. (B) Alignment of TNFRSF3 intracellular domain. First box indicates unconventional TRAF binding motif, second box indicates conventional TRAF binding motif, and third box indicates a reported bony fish specific conserved TRAF binding motif. (C) Amino acid sequence identity of TNFRSF3 molecules aligned in (A) and (B), darker shades of gray indicate higher percentage identity. The amino acids shaded in black, dark gray, and light gray denote conserved amino acids going from most conserved to least conserved across vertebrate lineage, respectively. The "v" above certain columns indicates the conserved cysteines that denote the TNFRSF motif.

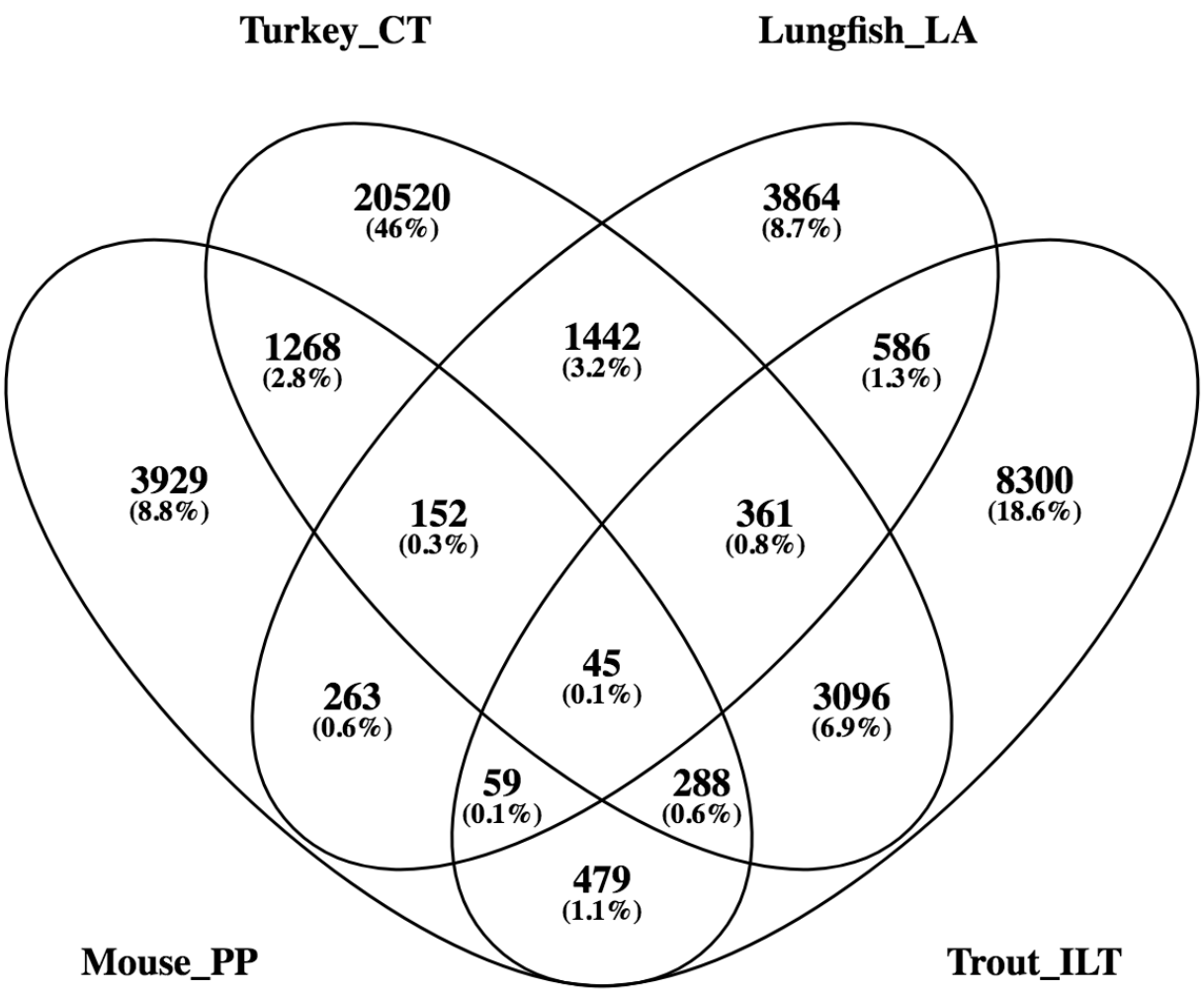

Figure 6. Venn diagram of genes shared between different O-MALT transcriptomes generated in this study. Analysis was performed after removing genes found in control (non–O-MALT) tissues for each corresponding species.

Unique Mouse PP

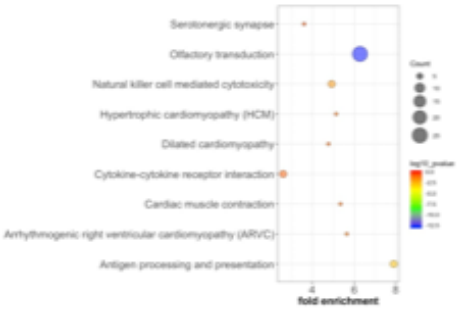

Unique Turkey CT

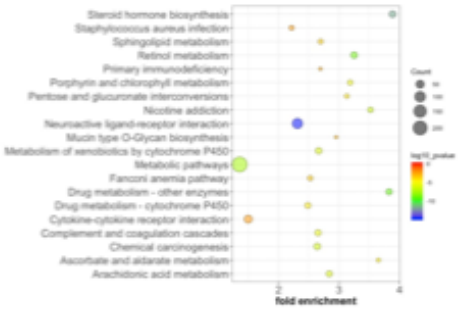

Unique Lungfish LA

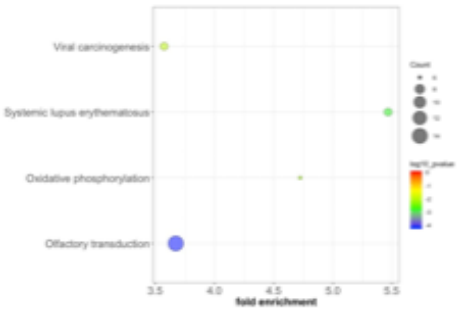

Unique Trout ILT

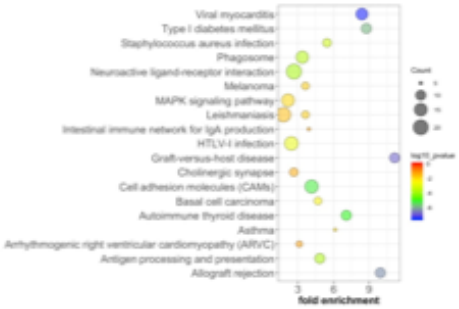

Common to Turkey CT and Trout ILT

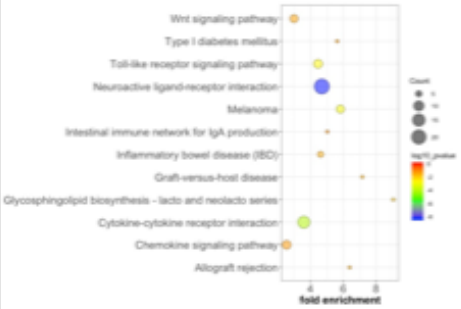

Common to Turkey CT and Lungfish LA

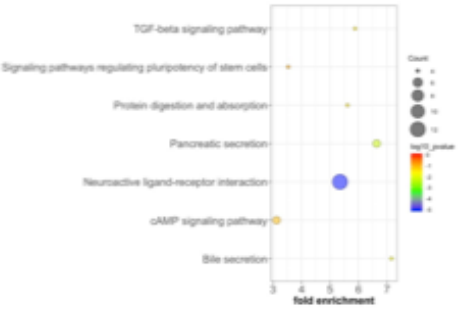

Common to Mouse PP and Turkey CT

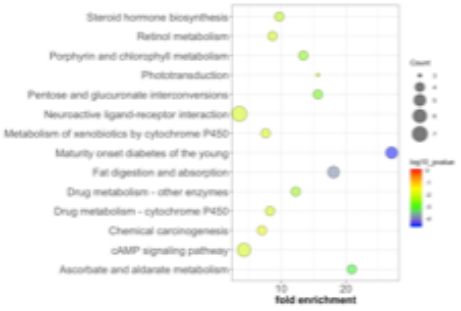

Common to Mouse PP and Lungfish LA

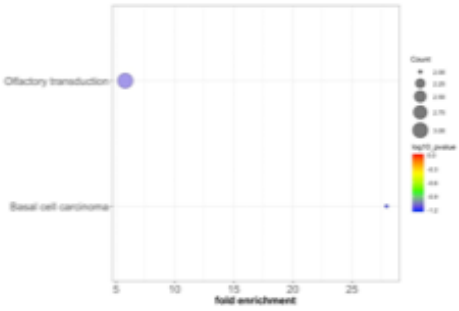

Figure 7. Significantly enriched KEGG pathways from O-MALT transcriptomic data after removing genes expressed in corresponding negative control (non–O-MALT) transcriptomes for each species.

Table IV. KEGG pathway analysis: enriched genes for the olfactory transduction pathway

Mouse PP	Lungfish LA	Mouse PP and Lungfish LA
6M1-16	OR10T2	CNGA3
OR11H4	OR13A1	OR52H1
OR14J1	OR4A16	OR52W1
OR1L4	OR52A1	
OR2G2	OR52A5	
OR2H1	OR52B2	
OR2L13	OR52B4	
OR2L2	OR52I1	
OR2L5	OR52I2	
OR2M4	OR52J3	
OR2M7	OR56A5	
OR2T10	OR5P2	
OR2T12	OR5P3	
OR2T29	OR9G9	
OR2T33		
OR2T5		
OR2T8		
OR4K5		
OR4P4		
OR52E6		
OR5D16		
OR5D18		
OR5L1		
OR5L2		
OR8B4		
OR8J1		

Genes within the olfactory transduction KEGG pathway found to be significantly enriched in lungfish LA and mouse PP transcriptomes.

Table V. KEGG pathway analysis: enriched genes for the neuroactive ligand and receptor interaction pathway

Turkey CT			Trout ILT	Lungfish LA and Turkey CT	Turkey CT and Trout ILT	Mouse PP and Turkey CT
ADORA1	GRIK1	PLG	ADRA2A	CHRM2	ADORA3	CHRM1
ADORA2A	GRIK2	PTGDR	BDKRB2	CHRM4	AVPR1A	CHRM5
ADORA2B	GRIK3	PTGER1	C5AR1	DRD5	AVPR1B	GLP2R
ADRA1B	GRIK4	PTGER2	CCKAR	FSHR	AVPR2	NMUR1
ADRA1D	GRIK5	PTGER3	CHRNA1	GABRR2	C3AR1	NPBWR1
ADRB3	GRIN2A	PTGER4	CHRNA3	GPR35	CTSG	OPRL1
AGTR1	GRIN2B	PTGFR	CHRNA6	GPR83	CYSLTR1	TRHR
APLNR	GRIN2C	PTGIR	CHRNB1	GRIN1	GALR3	
BRS3	GRIN2D	PTH2R	GABBR1	HTR1B	GLRA1	
CALCR	GRIN3A	RXFP1	GABRQ	MC3R	GLRA2	
CALCRL	GRIN3B	RXFP2	GALR1	OPRD1	GLRA3	
CHRFAM7A	GRM5	RXFP4	GALR2	PRLHR	GLRB	
CHRM3	HRH2	S1PR4	GZMA		GPR156	
CHRNA7	HTR1D	SSTR2	HRH3		HTR1A	
CHRNA9	HTR1E	SSTR3	HRH4		HTR4	
DRD1	HTR2C	SSTR4	LTB4R2		HTR5A	
DRD2	HTR6	SSTR5	P2RY11		MC5R	
DRD3	HTR7	TAAR1	P2RY13		NPBWR2	
DRD4	LEPR	TACR1	P2RY14		NPFFR2	
F2	LTB4R	TACR2	PRLR		OXTR	
F2RL2	MC2R	TACR3			PTAFR	
F2RL3	MC4R	TBXA2R			UTS2R	
FPR2	MLNR	TSPO				
FPR3	MTNR1A					
FPRL1	MTNR1B					
FPRL2	NMDAR2C					
GABRA1	NMUR2					
GABRA2	NPFFR1					
GABRA3	NPY1R					
GABRA4	NR2A					
GABRA5	NTSR1					
GABRA6	OPRK1					
GLP1R	OPRM1					
GRIA1	P2RY10					
GRIA2	P2RY6					
GRIA3	P2RY8					
GRIA4	PBR					

Significant genes involved in the neuroactive ligand and receptor interactions KEGG pathway found to be enriched in each *O*-MALT transcriptome or shared by two *O*-MALT transcriptomes.

Published datasets searched for TNF analysis

Organism	Genomes/Transcriptomes	Date Published
Mammals	Human	2001
	Mouse	2002
Aves	Zebra Finch	2010
	Chicken	2004
	Turkey	2011
	Mallard Duck	2013
Reptile	Western Painted Turtle	2013
	American Alligator	2012
	Chinese Alligator	2013
Amphibian	Western Clawed Frog	2010
	North American Bullfrog	2017
	High Himalaya Frog	2015
Sarcopterygii	Coelacanth	2013
	West African Lungfish	2013
	South American Lungfish	2015
Salmonids	Rainbow Trout	2014
	Salmon	2016
	Coho Salmon	2017

Supplementary Table I. Comprehensive list of genomes analyzed for the presence of TNFSF members in this study.

Statistical analysis of assembled transcriptomes

Transcriptome Statistics	Mouse Peyer's patch	Mouse skin	Trout interbranchial lymphoid tissue	Trout Muscle	Turkey cecal tonsil	Turkey muscle	Lungfish lymphoid aggregate	Lungfish skin
Organism	*Mus musculus*	*Mus musculus*	*Oncorhynchus mykiss*	*Oncorhynchus mykiss*	*Meleagris gallopavo*	*Meleagris gallopavo*	*Protopterus dolloi*	*Protopterus dolloi*
Accession Numbers	SRR8114138	SRR6884615	SRR8112130	DRR046645	SRR7771850	SRR478418	SRR7879313	SRR8137461
Raw total sequences	68,691,990	57,486,984	31,379,578	157,592,662	37,217,902	25,983,202	57,607,080	37,794,958
Reads mapped and paired	67,068,330	56,347,246	29,359,424	148,341,764	35,589,842	24,619,708	56,232,156	36,707,530
% Reads mapped and paired	97.64%	98.02%	93.56%	94.13%	95.63%	94.72%	97.61%	97.12%
Reads unmapped	1,278,627	889,825	1,587,745	6,703,289	1,255,693	1,085,299	1,088,166	845,117
n_scaffolds	280,740	246,275	286,901	176,993	164,478	247,098	162,353	128,529
scaf_bp	201,556,902	306,900,459	212,361,256	110,893,564	176,631,903	163,148,464	114,958,573	101,050,590
scaf_N50	38,844	32,520	43,533	36,610	20,275	30,971	21,735	16,845
scaf_L50	1,265	2,778	1,336	882	2,521	1,275	1,398	1,468
scaf_N90	196,215	142,164	198,077	129,778	97,765	175,721	112,489	87,167
scaf_L90	280	425	283	274	349	250	258	295
scaf_max	16,461	35,601	15,868	9,880	18,221	18,940	10,356	47,530
gc_avg	0.46728	0.49312	0.45933	0.47307	0.4534	0.44589	0.39734	0.40296
gc_std	0.07262	0.07403	0.06972	0.0802	0.09034	0.09161	0.05759	0.05204

Supplementary Table II. Statistical analysis of assembled transcriptomes.

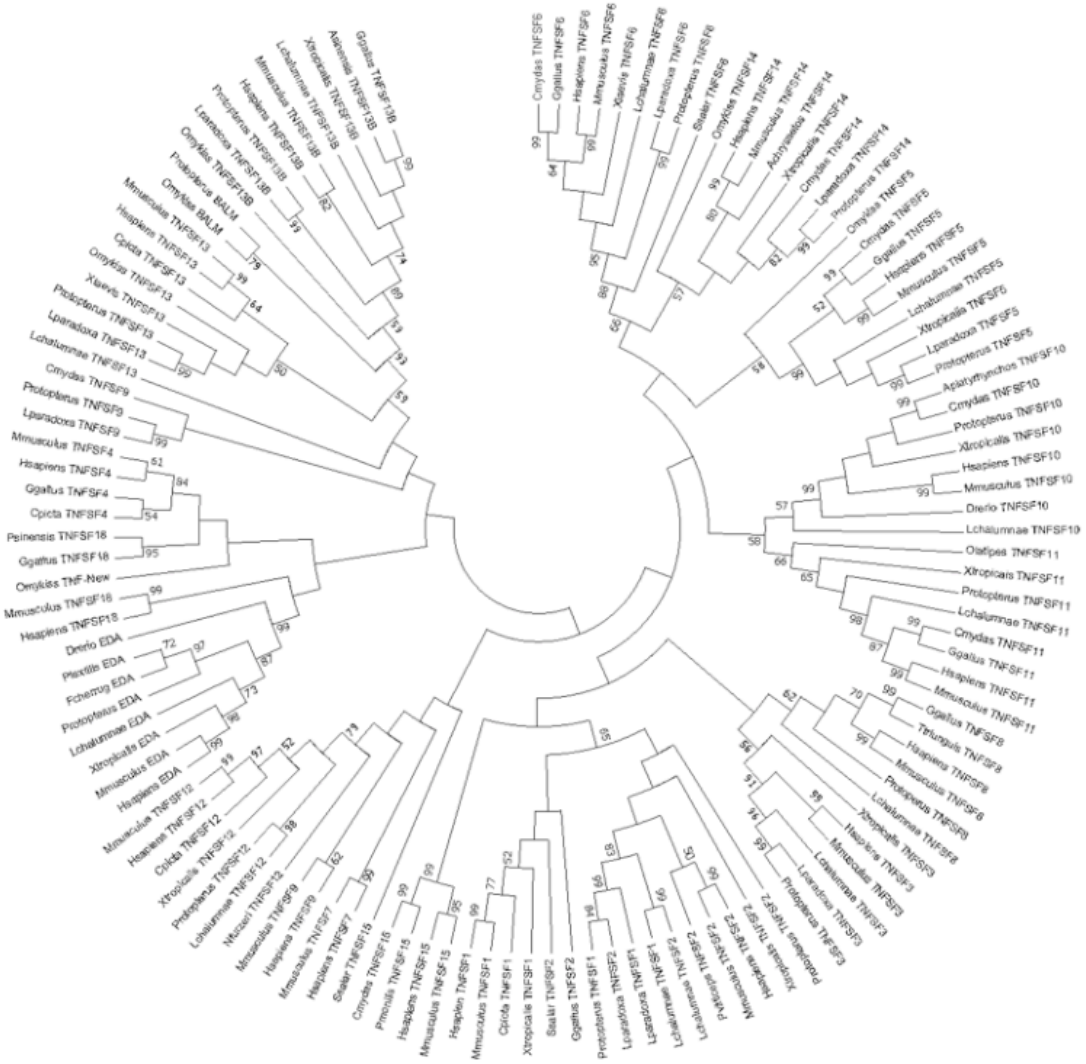

Supplementary Figure 1. Phylogenetic tree showing the evolutionary relationship of vertebrate TNFSF proteins. The analysis was performed on homologous sequences aligned with Muscle using MEGA 10 software (Kumar et al. 2018). The evolutionary distances were computed using a Poisson substitution model and the tree was constructed with the Neighbor-Joining method. Tree was bootstrapped 1000 times. Value lower than 50% were removed from the tree. Note that Lparadoxa TNFSF10, Lchalumnae TNFSF14 and Drerio TNFSF18 are not included in the phylogenetic tree. Species in the tree are abbreviated as follows: Hsapiens: human (Hs); Mmusculus: mouse (Mm); Ggallus: chicken (Gg); Aplatyrhynchos: mallard duck (Ap); Fcherrug: saker falcon (Fc); Pmonilis: band-tailed pigeon (Pm); Asinensis: Chinese alligator (As); Pvitticeps: bearded dragon (Pv); Ttriunguis: turtle; Cmydas: sea turtle (Cm); Psinensis: Chinese soft shelled turle (Ps); Cpicta: painted turtle (Cp); Ptextilis: brown snake (Pt); Achrysaetos: golden eagle (Ac); Xtropicalis: Western clawed frog (Xt); Xlaevis: African clawed frog (Xl); Protopterus: African lungfish; Lchalumnae: coelacanth (Lc); Lparadoxa: South American lungfish (Lp); Omykiss: rainbow trout (Om); Ssalar: salmon (Ss); Drerio: zebrafish (Dr); Olatipes: Japenese rice fish (Ol); Nfurzeri: killifish (Nf).

Supplementary Figure 2. Phylogenetic tree showing the evolutionary relationship of vertebrate TNFRSF proteins. The analysis was performed on homologous sequences aligned with Muscle using MEGA 10 software (Kumar et al. 2018). The evolutionary distances were computed using a Poisson substitution model and the tree was constructed with the Neighbor-Joining method. Tree was bootstrapped 1000 times. Value lower than 50% were removed from the tree. Note that TNFRSF 4, 7, 25, 17 are not included in the phylogenetic tree for clarity purposes. Species in the tree are abbreviated as follows: Hsapiens: human (Hs); Mmusculus: mouse (Mm); Ggallus: chicken (Gg); Scamelus australis: Wild ostrich (Sca); Xtropicalis or Xlaevis: frog (Xt or Xl); Protopterus: African lungfish; Acarolinensins: lizard (Ac); Amississippiensis: alligator (Am); Pbivittatus: python (Pb); Lchalumnae: coelacanth (Lc); Lparadoxa: South American lungfish (Lp); Drerio: zebrafish (Dr); Ssalar: salmon (Ss); Fheteroclitus: mummichog killifish (Fh); Omykiss: rainbow trout (Om).

7. References

1. Neely, H. R., and M. F. Flajnik. 2016. Emergence and evolution of secondary lymphoid organs. Annu. Rev. Cell Dev. Biol. 32: 693–711.

2. Flajnik, M. F. 2018. A cold-blooded view of adaptive immunity. Nat. Rev. Immunol. 18: 438–453.

3. Zapata, A., and C. T. Amemiya. 2000. Phylogeny of lower vertebrates and their immunological structures. Curr. Top. Microbiol. Immunol. 248: 67–107.

4. Ruddle, N. H., and E. M. Akirav. 2009. Secondary lymphoid organs: responding to genetic and environmental cues in ontogeny and the immune response. J. Immunol. 183: 2205–2212.

5. Tacchi, L., E. T. Larragoite, P. Mun˜oz, C. T. Amemiya, and I. Salinas. 2015. African lungfish reveal the evolutionary origins of organized mucosal lymphoid tissue in vertebrates. Curr. Biol. 25: 2417–2424.

6. Bjørgen, H., O. M. Løken, I. B. Aas, P. G. Fjelldal, T. Hansen, L. Austbø, and E. O. Koppang. 2019. Visualization of CCL19-like transcripts in the ILT, thymus and head kidney of Atlantic salmon (Salmo salar L.). Fish Shellfish Immunol. 93: 763–765.

7. Haugarvoll, E., I. Bjerka˚s, B. F. Nowak, I. Hordvik, and E. O. Koppang. 2008. Identification and characterization of a novel intraepithelial lymphoid tissue in the gills of Atlantic salmon. J. Anat. 213: 202–209.

8. Aas,I.B.,L.Austbø,M.Ko¨nig,M.Syed,K.Falk,I.Hordvik,andE.O.Koppang. 2014. Transcriptional characterization of the T cell population within the salmonid interbranchial lymphoid tissue. J. Immunol. 193: 3463–3469.

9. Dalum, A. S., L. Austbø, H. Bjørgen, K. Skjødt, I. Hordvik, T. Hansen, P. G. Fjelldal, C. M. Press, D. J. Griffiths, and E. O. Koppang. 2015. The interbranchial lymphoid tissue of Atlantic Salmon (Salmo salar L) extends as a diffuse mucosal lymphoid tissue throughout the trailing edge of the gill filament. J. Morphol. 276: 1075–1088.

10. Dalum,A.S.,D.J.Griffiths,E.C.Valen,K.S.Amthor,L.Austbø,E.O.Koppang, C. M. Press, and A. Kvellestad. 2016. Morphological and functional development of the interbranchial lymphoid tissue (ILT) in Atlantic salmon (Salmo salar L). Fish Shellfish Immunol. 58: 153–164.

11. Ola´h, I., and B. Glick. 1979. Structure of the germinal centers in the chicken caecal tonsil: light and electron microscopic and autoradiographic studies. Poult. Sci. 58: 195–210.

12. Crole, M. R., and J. T. Soley. 2012. Evidence of a true pharyngeal tonsil in birds: a novel lymphoid organ in Dromaius novaehollandiae and Struthio camelus (Palaeognathae). Front. Zool. 9: 21.

13. Magor, K. E., D. Miranzo Navarro, M. R. Barber, K. Petkau, X. Fleming- Canepa, G. A. Blyth, and A. H. Blaine. 2013. Defense genes missing from the flight division. Dev. Comp. Immunol. 41: 377–388.

14. Kajiwara, E., A. Shigeta, H. Horiuchi, H. Matsuda, and S. Furusawa. 2003. Development of Peyer's patch and cecal tonsil in gut-associated lymphoid tissues in the chicken embryo. J. Vet. Med. Sci. 65: 607–614.

15. Das, S., Y. Sutoh, M. Hirano, Q. Han, J. Li, M. D. Cooper, and B. R. Herrin. 2016. Characterization of lamprey BAFF-like gene: evolutionary implications. J. Immunol. 197: 2695–2703.

16. Fütterer, A., K. Mink, A. Luz, M. H. Kosco-Vilbois, and K. Pfeffer. 1998. The lymphotoxin beta receptor controls organogenesis and affinity maturation in peripheral lymphoid tissues. Immunity 9: 59–70.

17. Pfeffer, K. 2003. Biological functions of tumor necrosis factor cytokines and their receptors. Cytokine Growth Factor Rev. 14: 185–191.

18. De Togni, P., J. Goellner, N. H. Ruddle, P. R. Streeter, A. Fick, S. Mariathasan, S. C. Smith, R. Carlson, L. P. Shornick, J. Strauss-Schoenberger, et al. 1994. Abnormal development of peripheral lymphoid organs in mice deficient in lymphotoxin. Science 264: 703–707.

19. Banks, T. A., B. T. Rouse, M. K. Kerley, P. J. Blair, V. L. Godfrey, N. A. Kuklin, D. M. Bouley, J. Thomas, S. Kanangat, and M. L. Mucenski. 1995. Lymphotoxin- alpha-deficient mice. Effects on secondary lymphoid organ development and humoral immune responsiveness. J. Immunol. 155: 1685–1693.

20. Pasparakis, M., L. Alexopoulou, M. Grell, K. Pfizenmaier, H. Bluethmann, and G. Kollias. 1997. Peyer's patch organogenesis is intact yet formation of B lymphocyte follicles is defective in peripheral lymphoid organs of mice deficient for tumor necrosis factor and its 55-kDa receptor. Proc. Natl. Acad. Sci. USA 94: 6319–6323.

21. Neumann, B., A. Luz, K. Pfeffer, and B. Holzmann. 1996. Defective Peyer's patch organogenesis in mice lacking the 55-kD receptor for tumor necrosis factor. J. Exp. Med. 184: 259–264.

22. Wiens, G. D., and G. W. Glenney. 2011. Origin and evolution of TNF and TNF receptor superfamilies. Dev. Comp. Immunol. 35: 1324–1335.

23. Cuff, C. A., and N. H. Ruddle. 1998. Lymphotoxin. In Encyclopedia of Immunology. P. J. Delves, and I. Roitt, eds. Academic Press, London, p. 1637–1641.

24. Liepinsh, D. J., S. I. Grivennikov, K. D. Klarmann, M. A. Lagarkova, M. S. Drutskaya, S. J. Lockett, L. Tessarollo, M. McAuliffe, J. R. Keller, D. V. Kuprash, and S. A. Nedospasov. 2006. Novel lymphotoxin alpha (LTalpha) knockout mice with unperturbed tumor necrosis factor expression: reassessing LTalpha biological functions. Mol. Cell. Biol. 26: 4214–4225.

25. Ying, X., K. Chan, P. Shenoy, M. Hill, and N. H. Ruddle. 2005. Lymphotoxin plays a crucial role in the development and function of nasal-associated lymphoid tissue through regulation of chemokines and peripheral node addressin. Am. J. Pathol. 166: 135–146.

26. Ruddle, N. H. 2014. Lymphotoxin and TNF: how it all began-a tribute to the travelers. Cytokine Growth Factor Rev. 25: 83–89.

27. Tumanov, A. V., S. I. Grivennikov, A. A. Kruglov, Y. V. Shebzukhov, E. P. Koroleva, Y. Piao, C. Y. Cui, D. V. Kuprash, and S. A. Nedospasov. 2010. Cellular source and molecular form of TNF specify its distinct functions in organization of secondary lymphoid organs. Blood 116: 3456–3464.

28. Körner, H., D. S. Riminton, D. H. Strickland, F. A. Lemckert, J. D. Pollard, and J. D. Sedgwick. 1997. Critical points of tumor necrosis factor action in central nervous system autoimmune inflammation defined by gene targeting. J. Exp. Med. 186: 1585–1590.

29. Kuprash, D. V., A. V. Tumanov, D. J. Liepinsh, E. P. Koroleva, M. S. Drutskaya, A. A. Kruglov, A. N. Shakhov, E. Southon, W. J. Murphy, L. Tessarollo, et al. 2005. Novel tumor necrosis factor-knockout mice that lack Peyer's patches. Eur. J. Immunol. 35: 1592–1600.

30. Glenney, G. W., and G. D. Wiens. 2007. Early diversification of the TNF superfamily in teleosts: genomic characterization and expression analysis. J. Immunol. 178: 7955–7973.

31. Hofmann, J., M. Greter, L. Du Pasquier, and B. Becher. 2010. B-cells need a proper house, whereas T-cells are happy in a cave: the dependence of lymphocytes on secondary lymphoid tissues during evolution. Trends Immunol. 31: 144–153.

32. Kaiser, P. 2012. The long view: a bright past, a brighter future? Forty years of chicken immunology pre- and post-genome. Avian Pathol. 41: 511–518.

33. Sequence Read Archive Submissions Staff. 2011. Understanding SRA search results. In SRA Knowledge Base. National Center for Biotechnology Information (US), Bethesda, MD. Available at: https://www.ncbi.nlm.nih.gov/books/ NBK56913/. Accessed: October 10, 2018.

34. Andrews, S. 2010. FastQC: a quality control tool for high throughput sequence data. Available at: http://www.bioinformatics.babraham.ac.uk/projects/fastqc. Accessed: October 10, 2018.

35. Bolger, A. M., M. Lohse, and B. Usadel. 2014. Trimmomatic: a flexible trimmer for Illumina sequence data. Bioinformatics 30: 2114–2120.

36. Grabherr, M. G., B. J. Haas, M. Yassour, J. Z. Levin, D. A. Thompson, I. Amit, X. Adiconis, L. Fan, R. Raychowdhury, Q. Zeng, et al. 2011. Full-length transcriptome assembly from RNA-seq data without a reference genome. Nat. Biotechnol. 29: 644–652.

37. Haas, B. J., A. Papanicolaou, M. Yassour, M. Grabherr, P. D. Blood, J. Bowden, M. B. Couger, D. Eccles, B. Li, M. Lieber, et al. 2013. De novo transcript sequence reconstruction from RNA-seq using the Trinity platform for reference generation and analysis. Nat. Protoc. 8: 1494–1512.

38. Li, H., and R. Durbin. 2009. Fast and accurate short read alignment with Burrows-Wheeler transform. Bioinformatics 25: 1754–1760.

39. Li, H., B. Handsaker, A. Wysoker, T. Fennell, J. Ruan, N. Homer, G. Marth, G. Abecasis, and R. Durbin, 1000 Genome Project Data Processing Subgroup. 2009. The sequence alignment/map format and SAMtools. Bioinformatics 25: 2078–2079.

40. Zerbino, D. R., P. Achuthan, W. Akanni, M. R. Amode, D. Barrell, J. Bhai, K. Billis, C. Cummins, A. Gall, C. G. Giro´n, et al. 2018. Ensembl 2018. Nucleic Acids Res. 46: D754–D761.

41. Finn, R. D., P. Coggill, R. Y. Eberhardt, S. R. Eddy, J. Mistry, A. L. Mitchell, S. C. Potter, M. Punta, M. Qureshi, A. Sangrador-Vegas, et al. 2016. The Pfam protein families database: towards a more sustainable future. Nucleic Acids Res. 44: D279–D285.

42. Katoh, K., and D. M. Standley. 2013. MAFFT multiple sequence alignment software version 7: improvements in performance and usability. Mol. Biol. Evol. 30: 772–780.

43. Kumar, S., G. Stecher, M. Li, C. Knyaz, and K. Tamura. 2018. MEGA X: molecular evolutionary genetics analysis across computing platforms. Mol. Biol. Evol. 35: 1547–1549.

44. Buchfink, B., C. Xie, and D. H. Huson. 2015. Fast and sensitive protein alignment using DIAMOND. Nat. Methods 12: 59–60.

45. Chen, C., H. Huang, and C. H. Wu. 2017. Protein bioinformatics databases and resources. Methods Mol. Biol. 1558: 3–39.

46. Oliveros, J. C. 2015. Venny. An interactive tool for comparing lists with Venn's diagrams. Available at: http://bioinfogp.cnb.csic.es/tools/venny/index.html. Accessed: March 12, 2018.

47. Huang D., W., B. T. Sherman, and R. A. Lempicki. 2009. Systematic and integrative analysis of large gene lists using DAVID bioinformatics resources. Nat. Protoc. 4: 44–57.

48. R Core Team. 2017. R: A Language and Environment for Statistical Computing. R Foundation for Statistical Computing, Vienna, Austria. Available at: https:// www.R-project.org/. Accessed: February 12, 2017.

49. Jung, C., J. P. Hugot, and F. Barreau. 2010. Peyer's patches: the immune sensors of the intestine. Int. J. Inflamm. 2010: 823710.

50. Rezaian, M., and S. Hamedi. 2007. Histological study of the caecal tonsil in the cecum of 4- 6 months of age white leghorn chicks. Am. J. Anim. Vet. Sci. 2: 50–54.

51. Rumfelt, L. L., E. C. McKinney, E. Taylor, and M. F. Flajnik. 2002. The development of primary and secondary lymphoid tissues in the nurse shark Ginglymostoma cirratum: B-cell zones precede dendritic cell immigration and T-cell zone formation during ontogeny of the spleen. Scand. J. Immunol. 56: 130–148.

52. Bodmer, J. L., P. Schneider, and J. Tschopp. 2002. The molecular architecture of the TNF superfamily. Trends Biochem. Sci. 27: 19–26.

53. Collette, Y., A. Gilles, P. Pontarotti, and D. Olive. 2003. A co-evolution perspective of the TNFSF and TNFRSF families in the immune system. Trends Immunol. 24: 387–394.

54. Kaiser, P., T. Y. Poh, L. Rothwell, S. Avery, S. Balu, U. S. Pathania, S. Hughes, M. Goodchild, S. Morrell, M. Watson, et al. 2005. A genomic analysis of chicken cytokines and chemokines. J. Interferon Cytokine Res. 25: 467–484.

55. Dalloul, R. A., J. A. Long, A. V. Zimin, L. Aslam, K. Beal, P. Blomberg Le Ann, P. Bouffard, D. W. Burt, O. Crasta, R. P. Crooijmans, et al. 2010. Multi- platform next-generation sequencing of the domestic Turkey (Meleagris gallopavo): genome assembly and analysis. PLoS Biol. 8: e1000475.

56. Barreda, D. R., H. R. Neely, and M. F. Flajnik. 2016. Evolution of myeloid cells. Microbiol. Spectr. DOI: 10.1128/microbiolspec.MCHD-0007-2015.

57. van Noort, V., B. Snel, and M. A. Huynen. 2003. Predicting gene function by conserved co-expression. Trends Genet. 19: 238–242.

58. Rost, B. 1999. Twilight zone of protein sequence alignments. Protein Eng. 12:85–94.

59. Maeda, T., H. Suetake, T. Odaka, and T. Miyadai. 2018. Original ligand for LTβR is LIGHT: insight into evolution of the LT/LT βR system. J. Immunol. 201: 202–214.

60. Lorenz, R. G., D. D. Chaplin, K. G. McDonald, J. S. McDonough, and R. D. Newberry. 2003. Isolated lymphoid follicle formation is inducible and dependent upon lymphotoxin-sufficient B lymphocytes, lymphotoxin beta receptor, and TNF receptor I function. J. Immunol. 170: 5475–5482.

61. Drayton, D. L., S. Liao, R. H. Mounzer, and N. H. Ruddle. 2006. Lymphoid organ development: from ontogeny to neogenesis. Nat. Immunol. 7: 344–353.

62. Buckley, C. D., F. Barone, S. Nayar, C. Bénézech, and J. Caamaño. 2015. Stromal cells in chronic inflammation and tertiary lymphoid organ formation. Annu. Rev. Immunol. 33: 715–745.

63. van de Pavert, S. A., and R. E. Mebius. 2010. New insights into the development of lymphoid tissues. Nat. Rev. Immunol. 10: 664–674.

64. Ager, A. 2017. High endothelial venules and other blood vessels: critical regulators of lymphoid organ development and function. Front. Immunol. 8: 45.

65. Finke, D., and J. P. Kraehenbuhl. 2001. Formation of Peyer's patches. Curr. Opin. Genet. Dev. 11: 561–567.

66. van de Pavert, S. A., B. J. Olivier, G. Goverse, M. F. Vondenhoff, M. Greuter, P. Beke, K. Kusser, U. E. Höpken, M. Lipp, K. Niederreither, et al. 2009. Chemokine CXCL13 is essential for lymph node initiation and is induced by retinoic acid and neuronal stimulation. Nat. Immunol. 10: 1193–1199.

67. Hehlgans, T., and K. Pfeffer. 2005. The intriguing biology of the tumour necrosis factor/tumour necrosis factor receptor superfamily: players, rules and the games. Immunology 115: 1–20.

68. Upadhyay, V., and Y. X. Fu. 2014. Lymphotoxin organizes contributions to host defense and metabolic illness from innate lymphoid cells. Cytokine Growth Factor Rev. 25: 227–233.

69. Onder, L., and B. Ludewig. 2018. A fresh view on lymph node organogenesis. Trends Immunol. 39: 775–787.

70. Matsumoto, M., Y. X. Fu, H. Molina, G. Huang, J. Kim, D. A. Thomas, M. H. Nahm, and D. D. Chaplin. 1997. Distinct roles of lymphotoxin a and the type I tumor necrosis factor (TNF) receptor in the establishment of follicular dendritic cells from non-bone marrow-derived cells. J. Exp. Med. 186: 1997– 2004.

71. Mounzer, R. H., O. S. Svendsen, P. Baluk, C. M. Bergman, T. P. Padera, H. Wiig, R. K. Jain, D. M. McDonald, and N. H. Ruddle. 2010. Lymphotoxin- alpha contributes to lymphangiogenesis. Blood 116: 2173–2182.

72. Upadhyay, V., and Y. X. Fu. 2013. Lymphotoxin signaling in immune homeostasis and the control of microorganisms. Nat. Rev. Immunol. 13: 270–279.

73. Sugaya, R., S. Ishimaru, T. Hosoya, K. Saigo, and Y. Emori. 1994. A Drosophila homolog of human proto-oncogene ret transiently expressed in embryonic neuronal precursor cells including neuroblasts and CNS cells. Mech. Dev. 45: 139–145.

74. Soba, P., C. Han, Y. Zheng, D. Perea, I. Miguel-Aliaga, L. Y. Jan, and Y. N. Jan. 2015. The Ret receptor regulates sensory neuron dendrite growth and integrin mediated adhesion. eLife.

75. Perea, D., J. Guiu, B. Hudry, C. Konstantinidou, A. Milona, D. Hadjieconomou, T. Carroll, N. Hoyer, D. Natarajan, J. Kallijärvi, et al. 2017. Ret receptor tyrosine kinase sustains proliferation and tissue maturation in intestinal epithelia. EMBO J. 36: 3029–3045.

76. Ibiza, S., B. García-Cassani, H. Ribeiro, T. Carvalho, L. Almeida, R. Marques, A. M. Misic, C. Bartow-McKenney, D. M. Larson, W. J. Pavan, et al. 2016. Glial-cell-derived neuroregulators control type 3 innate lymphoid cells and gut defence. Nature 535: 440–443.

77. Velaga, S., H. Herbrand, M. Friedrichsen, T. Jiong, M. Dorsch, M. W. Hoffmann, R. Förster, and O. Pabst. 2009. Chemokine receptor CXCR5 supports solitary intestinal lymphoid tissue formation, B cell homing, and induction of intestinal IgA responses. J. Immunol. 182: 2610–2619.

78. Seymour, R., B.-J. Shirley, H. HogenEsch, L. D. Shultz, and J. P. Sundberg. 2013. Loss of function of the mouse sharpin gene results in Peyer's patch regression. PLoS One 8: e55224.

79. Kanda, H., T. Igaki, H. Kanuka, T. Yagi, and M. Miura. 2002. Wengen, a member of the Drosophila tumor necrosis factor receptor superfamily, is required for Eiger signaling. J. Biol. Chem. 277: 28372–28375

80. Igaki, T., H. Kanda, Y. Yamamoto-Goto, H. Kanuka, E. Kuranaga, T. Aigaki, and M. Miura. 2002. Eiger, a TNF superfamily ligand that triggers the Drosophila JNK pathway. EMBO J. 21: 3009-3018.

81. Ravi, V., and B. Venkatesh. 2018. The divergent genomes of teleosts. Annu. Rev. Anim. Biosci. 6: 47-68.

82. Herna ÃÅndez, P. P., P. M. Strzelecka, E. I. Athanasiadis, D. Hall, A. F. Robalo, C. M. Collins, P. Boudinot, J. P. Levraud, and A. Cvejic. 2018. Single-cell transcriptional analysis reveals ILC-like cells in zebrafish. Sci. Immunol. 3: eaau5265.

83. Hong, S., R. Li, Q. Xu, C. J. Secombes, and T. Wang. 2013. Two types of TNF- a exist in teleost fish: phylogeny, expression, and bioactivity analysis of type-II TNF-a3 in rainbow trout Oncorhynchus mykiss. J. Immunol. 191: 5959-5972.

84. Nagy, N., and I. Ola ÃÅh. 2007. Pyloric tonsil as a novel gut-associated lymphoepithelial organ of the chicken. J. Anat. 211: 407-411.

85. Das, S., N. Nikolaidis, J. Klein, and M. Nei. 2008. Evolutionary redefinition of immunoglobulin light chain isotypes in tetrapods using molecular markers. Proc. Natl. Acad. Sci. USA 105: 16647-16652.

86. Das, S., U. Mohamedy, M. Hirano, M. Nei, and N. Nikolaidis. 2010. Analysis of the immunoglobulin light chain genes in zebra finch: evolutionary implications. Mol. Biol. Evol. 27: 113-120.

87. Pirson, M., A. Clippe, and B. Knoops. 2018. The curious case of peroxiredoxin- 5: what its absence in aves can tell us and how it can be used. BMC Evol. Biol. 18: 18.

88. Wrona, D. 2006. Neural-immune interactions: an integrative view of the bidirectional relationship between the brain and immune systems. J. Neuroimmunol. 172: 38-58.

89. Aballay, A. 2013. Role of the nervous system in the control of proteostasis during innate immune activation: insights from C. elegans. *PLoS Pathog.* 9:e1003433.

90. Emgård, J., H. Kammoun, B. García-Cassani, J. Chesné, S. M. Parigi, J. M. Jacob, H. W. Cheng, E. Evren, S. Das, P. Czarnewski, et al. 2018. Oxysterol sensing through the receptor GPR183 promotes the lymphoid-tissue- inducing function of innate lymphoid cells and colonic inflammation. Immunity 48: 120–132.e8.

91. Skok, M., R. Grailhe, F. Agenes, and J. P. Changeux. 2006. The role of nicotinic acetylcholine receptors in lymphocyte development. J. Neuroimmunol. 171: 86–98.

92. Mendu, S. K., A. Bhandage, Z. Jin, and B. Birnir. 2012. Different subtypes of GABA-A receptors are expressed in human, mouse and rat T lymphocytes. PLoS One 7: e42959.

93. Godfrey, P. A., B. Malnic, and L. B. Buck. 2004. The mouse olfactory receptor gene family. Proc. Natl. Acad. Sci. USA 101: 2156–2161.

94. Feldmesser, E., T. Olender, M. Khen, I. Yanai, R. Ophir, and D. Lancet. 2006. Widespread ectopic expression of olfactory receptor genes. BMC Genomics 7:121.

95. Maßberg, D., and H. Hatt. 2018. Human olfactory receptors: novel cellular functions outside of the nose. Physiol. Rev. 98: 1739–1763.

96. Zhang, X., and U. S. Eggert. 2013. Non-traditional roles of G protein-coupled receptors in basic cell biology. Mol. Biosyst. 9: 586–595.

97. Tsai, T., S. Veitinger, I. Peek, D. Busse, J. Eckardt, D. Vladimirova, N. Jovancevic, S. Wojcik, G. Gisselmann, J. Altmüller, et al. 2017. Two olfactory receptors-OR2A4/7 and OR51B5-differentially affect epidermal proliferation and differentiation. Exp. Dermatol. 26: 58–65.

98. Clark, A. A., S. Nurmukhambetova, X. Li, S. D. Munger, and J. R. Lees. 2016. Odorants specifically modulate chemotaxis and tissue retention of CD4+ T cells via cyclic adenosine monophosphate induction. J. Leukoc. Biol. 100: 699–709.

99. Li, J. J., H. L. Tay, M. Plank, A. T. Essilfie, P. M. Hansbro, P. S. Foster, and M. Yang. 2013. Activation of olfactory receptors on mouse pulmonary macrophages promotes monocyte chemotactic protein-1 production. PLoS One 8: e80148.

100. Bastian, F., G. Parmentier, J. Roux, S. Moretti, V. Laudet, and M. Robinson-Rechavi. 2008. Bgee: integrating and comparing heterogeneous transcriptome data among species. Lect. Notes Comput. Sci. 5109: 124–131.

101. Öhman, L., L. Franzen, U. Rudolph, L. Birnbaumer, and E. H. Hörnquist. 2002. Regression of Peyer's patches in G a i2 deficient mice prior to colitis is associated with reduced expression of Bcl-2 and increased apoptosis. Gut 51: 392–397.

Chapter 3. Effects of Experimental Terrestrialization on the Skin Mucus Proteome of African lungfish (Protopterus dolloi)

Heimroth, R.D., Casadei, E., and Salinas, I. 2018. Effects of Experimental Terrestrialization on the Skin Mucus Proteome of African Lungfish (Protopterus dolloi). *Front. Immunol.* 9:1259. doi: 10.3389/fimmu.2018.01259.

Abstract

Animal mucosal barriers constantly interact with the external environment, and this interaction is markedly different in aquatic and terrestrial environments. Transitioning from water to land was a critical step in vertebrate evolution, but the immune adaptations that mucosal barriers such as the skin underwent during that process are essentially unknown. Vertebrate animals such as the African lungfish have a bimodal life, switching from freshwater to terrestrial habitats when environmental conditions are not favorable. African lungfish skin mucus secretions contribute to the terrestrialization process by forming a cocoon that surrounds and protects the lungfish body. The goal of this study was to characterize the skin mucus immunoproteome of African lungfish, *Protopterus dolloi*, before and during the induction phase of terrestrialization as well as the immunoproteome of the gill mucus during the terrestrialization induction phase. Using LC-MS/ MS, we identified a total of 974 proteins using a lungfish Illumina RNA-seq database, 1,256 proteins from previously published lungfish sequence read archive and 880 proteins using a lungfish 454 RNA-seq database for annotation in the three samples analyzed (free-swimming skin mucus, terrestrialized skin mucus, and terrestrialized gill mucus). The terrestrialized skin mucus proteome was enriched in proteins with known antimicrobial functions such as histones and S100 proteins compared to free-swimming skin mucus. In support, gene ontology analyses showed that the terrestrialized skin mucus proteome has predicted functions in processes such as viral process, defense response to Gram-negative bacterium, and tumor necrosis factor-mediated signaling. Importantly, we observed a switch in immunoglobulin heavy chain secretion upon terrestrialization, with IgW1 long form (IgW1L) and IgM1 present in free-swimming skin mucus and IgW1L, IgM1, and IgM2 in terrestrialized skin mucus. Combined, these results indicate an increase in investment in the production of unique immune molecules in

P. dolloi skin mucus in response to terrestrialization that likely better protects lungfish against external aggressors found in land.

1. Introduction

Transitioning to life on land was a fundamental step in the success and diversification of the vertebrate lineage (1). This transition imposed multiple novel challenges to vertebrates, especially at their mucosal surfaces. As a consequence, drastic physiological, histological, and molecular adaptations took place at vertebrate mucosal barriers for successful colonization of land.

The skin is the outermost organ of the vertebrate body. In aquatic vertebrates, such as teleost fish, the skin is a mucosal epithelium composed of layers of living cells coated by a mucus layer that is in direct contact with the environment. Teleost skin mucus contains many immune factors including innate and adaptive immune molecules that protect the host from invading microorganisms (2). In terrestrial vertebrates, the skin does not contain mucus-secreting cells and is cornified (3). This configuration is thought to help terrestrial vertebrates cope with desiccation stress and UV radiation.

African lungfish (*Protopterus sp.*) are a subclass of Sarcopterygian fish that are obligate air-breathers, and are the extant relative to all tetrapods (4, 5). Lungfish are evolutionarily unique organisms that have the ability to undergo conditional aestivation. Aestivation is a state of metabolic torpor, which is an adaptation for survival in areas that are subject to extreme environmental conditions (6–10). During droughts, as water evaporates from the rivers and food becomes scarce, lungfish detect environmental cues and turn them into internal signals that induce behavioral, physiological, and biochemical changes in preparation of aestivation.

There are four extant species of African lungfish: *P. aethiopicus, P. annectens, P. amphibious*, and *P. dolloi*, which implement different aestivation strategies to survive prolonged dry periods. The best-known method of aestivation is that of *P. annectens*. As water recedes, *P.*

annectens will start to burrow into the mud while simultaneously secreting large quantities of mucus through its gills. This is the induction phase of aestivation. Once it has burrowed deep enough into the mud, it curls back on itself, leaving its head facing the opening of the burrow. As the water dissipates completely, the mucus/mud mixture coating around the lungfish body hardens forming a cocoon that protects the animal for months. Once encased, the lungfish ceases feeding and locomotive activities, has to prevent cell death, and sustain a slow rate of waste production until conditions become favorable (11), this is the maintenance phase of aestivation, where the lungfish can lay dormant for years. Upon the introduction of water, the lungfish instantly awakens from dormancy, leaves the mucus cocoon, and slowly swims toward the surface of the water for air (5). This is the final phase of aestivation, known as arousal, which is completed a week after water is again available and marks the return to a normal metabolic rate. *P. dolloi*, however, uses a different aestivation strategy as they do not burrow into the mud and do not appear to completely reduce their metabolic rate (12). During the induction phase, *P. dolloi* coil up on the surface of the mud while secreting mucus which, over time, turns into a dried mucus cocoon (13). Thus, *P. dolloi's* mode of aestivation has been coined as "terrestrialization," which is different from the complete aestivation and the full metabolic torpor observed in *P. annectens* (14, 15). Both *P. dolloi* and *P. annectens* can be terrestrialized in the laboratory setting making them ideal models to study the effects of air exposure on the vertebrate mucosal immune system (7, 9, 14).

Throughout tetrapod evolution different strategies were coopted to maintain barrier integrity and defend against external aggressors. Antimicrobial compounds are among the most important immune molecules present in the skin of all vertebrates, both aquatic and terrestrial (16, 17). Antimicrobial proteins, lysozyme, histones, S100 proteins, and immunoglobulins (Igs)

have been previously identified to be important players in the vertebrate skin immune system (18–22). Given the importance of immune molecules in skin homeostasis, tissue repair, and responses to environmental insults, we hypothesize that these molecules play a critical role during the process of terrestrialization in lungfish skin and that African lungfish will increase the amount of resources allocated to skin immunity early on in the process of terrestrialization.

The goal of this study is to characterize the African lungfish skin mucus proteome in the freshwater state, as well as the compositional change in the proteome due to terrestrialization. Our results provide a first glance to the skin proteome composition of sarcopterygian fish and its role in adaptation to terrestrial life.

2. Materials and methods

2.1 Animals

Juvenile *P. dolloi* (slender lungfish) were obtained from Tropical Aquatics (FL, USA) and maintained in 10-gallon aquarium tanks with dechlorinated water and a sand/gravel substrate, at a temperature of 27–29°C. Fish were acclimated to laboratory conditions for a minimum of 3 weeks before being used in experiments. During this acclimation period, they were fed frozen earthworms every third day. Feeding was terminated 48 h before the start of the experiment. All animal studies were reviewed and approved by the Office of Animal Care Compliance at the University of New Mexico (protocol number 11-100744-MCC).

2.2 Experimental Aestivation and Mucus Collection

After 3 weeks of acclimation to laboratory conditions, water in the tanks were lowered to 20 cm at 27–29°C and allowed to naturally evaporate (7). As the water level lowered, the fish entered the induction phase of aestivation and began to hyperventilate and profusely secrete mucus from their gills. This mucus combined with the substrate from the bottom of the tank

encased the fish in a cocoon, which hardened after 10 days in the induction phase. In order to avoid severe dehydration due to the dry climate of New Mexico, 1–2 mL of water was sprayed on the surface of the cocoon every third day (12). Mucus was collected from the skin of one P. dolloi individual before the beginning of the terrestrialization experiment (named free-swimming skin mucus) and from the same individual 10 days after the start of the induction phase. At this time point, the liquid mucus actively secreted from the gills (named terrestrialized gill mucus) was aspirated with a sterile plastic Pasteur pipette. Additionally, the hardened mucus cocoon surrounding the lungfish body (named terrestrialized skin mucus) was collected by peeling it off with sterile forceps. All samples were immediately frozen at −80°C until needed for protein solubilization.

2.3 Protein Solubilization

Mucus samples were solubilized in a protein extraction buffer (pH 7.6) made of 60 mM DTT, 2% SDS, and 40 mM Tris–HCl as previously described (23). The proteins were extracted by adding 4× the sample volume of cold (−20°C) acetone and incubating overnight at −20°C. The proteins were pelleted out and dissolved in a solution of 6 M Urea and 200 mM of ammonium bicarbonate. Protein concentrations were measured using the Pierce 660 nm protein assay (Thermo Fisher Scientific, San Jose, CA, USA).

2.4 One-Dimensional Electrophoresis

Proteins extracted from the mucus samples were analyzed by one-dimensional electrophoresis. 12 µL of each sample was loaded into a Mini-PROTEAN TGX precast Gel at a 1:1 ratio with 2× Laemmli Sample Buffer (Bio-Rad, Hercules, CA, USA) for a final volume of 24 µL in each well. A total of 4.56 µg of protein for terrestrialized skin mucus, 3.94 µg for free-swimming skin mucus, and 1.05 µg for terrestrialized gill mucus were loaded. The proteins were

separated out by the sodium dodecyl sulfate polyacrylamide gel electrophoresis (SDS-PAGE) in 1× Tris buffer, run at 120 V for 55 min, then incubated for 1 h with mild agitation in Coomassie Brilliant Blue R-250 (Bio-Rad, Hercules, CA, USA). Each lane of the gel was cut to perform proteomics analyses. Due to the presence of high-intensity band in the free-swimming skin mucus sample and a high-intensity band in the terrestrialized skin mucus sample, these two bands were first excised from their corresponding lanes and solubilized separately from the rest of the lane.

2.5 LC-MS/MS

LC-MS/MS analysis of in-gel trypsin-digested excised protein bands or whole protein mixture-separated gel lanes (24) was carried out using an LTQ Orbitrap Velos mass spectrometer (Thermo Fisher Scientific, San Jose, CA, USA) equipped with an Advion nanomate ESI source (Advion, Ithaca, NY, USA), following ZipTip (Millipore, Billerica, MA, USA) C18 sample clean-up according to the manufacturer's instructions. Peptides were eluted from a C18 pre-column (100 μm id × 2 cm, Thermo Fisher Scientific) onto an analytical column (75 μm id × 10 cm, C18, Thermo Fisher Scientific) using (1) a 2% hold of solvent B (acetonitrile, 0.1% formic acid) for 5 min, followed by a 2–10% gradient of solvent B over 5 min, 10–35% gradient of solvent B over 35 min, 35–50% gradient of solvent B over 20 min, 50–95% gradient of solvent B over 5 min, 95% hold of solvent B for 5 min, and finally a return to 2% in 0.1 min and another 9.9 min hold of 2% solvent B (single protein gel band analysis) or (2) a 2% hold of solvent B (acetonitrile, 0.1% formic acid) for 5 min, followed by a 2–7% gradient of solvent B over 5 min, 7–15% gradient of solvent B over 50 min, 15–35% gradient of solvent B over 60 min, 35–40% gradient of solvent B over 28 min, 40–85% gradient of solvent B over 5 min, 85% hold of solvent B for 10 min and finally a return to 2% in 1 min and another 16 min hold of 2% solvent

B (whole gel lane analysis). All flow rates were 400 nL/min. Solvent A consisted of water and 0.1% formic acid. Data-dependent scanning was performed by the Xcalibur v 2.1.0 software (25) using a survey mass scan at 60,000 resolution in the Orbitrap analyzer scanning mass/charge (m/z) 400–1,600, followed by collision- induced dissociation tandem mass spectrometry (MS/MS) of the 14 most intense ions in the linear ion trap analyzer. Precursor ions were selected by the monoisotopic precursor selection setting with selection or rejection of ions held to a ±10 ppm window. Dynamic exclusion was set to place any selected m/z on an exclusion list for 45 s after a single MS/MS.

2.6 RNA-Sequencing and Assembly

Three different transcriptomes were used to analyze the proteomic data generated in the present study. First, the pre-pyloric spleen from an experimentally infected *P. dolloi* individual was used to generate 454 pyrosequencing (Roche) transcriptome as explained elsewhere (26). Data were assembled using Roche's GS De Novo Assembler. A second database was a *P. annectens* Illumina database kindly shared by Dr. Chris Amemiya and was sequenced and assembled as described in Ref. (4). The third transcriptome consisted of sequence read archive (SRA) databases from P. *annectens*, which were downloaded from the National Center for Biotechnology Information (NCBI). Sratoolkit.2.9.0 fastq-dump was used to convert the SRAs into forward and reverse paired read fastq files (27). The paired-end reads were then assembled into de novo transcriptomes using Trinity assembler at default parameters (28). These new transcriptomes were concatenated together into one large transcriptome, and any redundant sequences were removed using cd-hit-est at a 99% confidence level (29). The resulting transcriptome was translated into a protein database using Transdecoder-5.0.0 (28).

2.7 Protein Identification

The protein and peptide identification results were visualized with Scaffold v 3.6.1 (Proteome Software Inc., Portland, OR, USA), a program that relies on various search engine results (i.e., Sequest, X!Tandem, and MASCOT) and which uses Bayesian statistics to reliably identify more spectra (30). Proteins were accepted that passed a minimum of two peptides identified at 0.1% peptide FDR and 90–99.9% protein confidence by the Protein Profit algorithm, within Scaffold. Tandem mass spectra were searched against the three Protopterus sp. transcriptomes obtained as described above. A translated protein database to which common contaminant proteins (e.g., human keratins obtained at ftp://ftp.thegpm.org/ fasta/cRAP) were appended to each database. All MS/MS spectra were searched using Thermo Proteome Discoverer 1.3 (Thermo Fisher Scientific, San Jose, CA, USA) considering fully Lys C peptides with up to two missed cleavage sites. Variable modifications considered during the search included methionine oxidation (15.995 Da) and cysteine carbamidomethylation (57.021 Da). Proteins were identified at 99% confidence interval with XCorr score cutoffs as determined by a reversed database search (31).

2.8 Proteomic Data Analysis

Transcriptome IDs for each sample were taken from Proteome Discoverer. The proteins retrieved from the excised lanes were first merged with their corresponding whole band resulting in one protein list for free-swimming skin mucus, one for terrestrialized gill mucus, and one for terrestrialized skin mucus. Tblastn searches were performed against each of the three transcriptomic data sets and resulting nucleotide sequences were then used as queries for blastx searches in NCBI (32). Human orthologous genes were assigned using AmiGO2 (33, 34), and gene ontology (GO) analysis was performed using DAVID bioinformatics database (35, 36). GO analysis of the proteome was used to identify the percentage of immune-related proteins in each

sample. Venn diagrams were created in R identifying unique and common protein composition between samples (37). In order to identify proteins with known antimicrobial function, we analyzed our protein results using the list of mammalian skin antimicrobial compounds provided in the review paper by Schauber and Gallo (38).

2.9 Histology

For light microscopy, skin samples from free-swimming and terrestrialized fish were fixed in 4% paraformaldehyde overnight, transferred to 70% ethanol, and embedded in paraffin. Samples were sectioned at a thickness of 5 μm, dewaxed in xylene, and stained using hematoxylin and eosin for general morphological analysis. Images were acquired and analyzed with a Nikon Eclipse Ti-S inverted microscope and NIS-Elements Advanced Research Software (Version 4.20.02).

2.10 Quantitative Real-Time PCR

Skin tissue from free-swimming P. dolloi and terrestrialized P. dolloi (N = 3) was collected using sterile dissecting tools and placed in 1 mL of Trizol (Ambion, Life Technologies, Carlsbad, CA, USA). Total RNA was extracted from each sample, and 1 μg of RNA was synthesized into cDNA as described in Ref. (26). The resulting cDNA was stored at −20°C. The expression levels of IgM1, IgM2, IgW1, H2A, S100-A11, and neutrophil elastase (ELANE) were measured by quantitative real-time PCR (RT-qPCR) using the specific primers shown in Table 1. Phosphoglycerate kinase 1 PGK1F was used as the house-keeping gene. The RT-qPCR and statistical analysis were performed as described in Ref. (26). Data were expressed as mean ± standard error, and qPCR results were analyzed by unpaired t-test ($p < 0.05$).

3. Results

3.1 Histological Changes in the Lungfish Skin in Response to Terrestrialization

Histological examination of freshwater and terrestrialized P. dolloi skin revealed that mucus-secreting goblet cells become exhausted from the process of terrestrialization. The epidermis becomes more compact with flattened keratinocytes on the surface creating a new barrier. We observed eosinophilic granulocytes in the dermis of both samples, but they were more abundant in the terrestrialized skin (Figure 1). These results are in agreement with previously reported changes in African lungfish skin in response to aestivation (7).

3.2 SDS-PAGE Analysis of Lungfish Mucus Proteins

The overall protein composition of the three mucus samples was visualized by SDS-PAGE. The protein band patterns of each sample were unique. There was a distinct band of high intensity at ~52 kDa in the free-swimming skin mucus, while there was an intense band ~15 kDa in the terrestrialized skin mucus sample not found in the other two samples. The gill mucus sample did not contain any predominant band (Figure 2). The two bands with high intensity (arrows) were excised and analyzed separately from the rest of the lane.

3.3 LC/MS-MS Proteomic Analysis, GO, and KEGG Pathway Analyses

Free-swimming, terrestrialized gill mucus, and terrestrialized skin mucus proteins from LC/MS-MS were analyzed against three RNA-seq transcriptomes, two sequenced on an Illumina platform and one sequenced using a 454 pyrosequencing platform. These translated transcriptomes resulted in a total of 53,184 protein sequences in the translated Illumina database, 269,746 protein sequences in the SRA database, and 41,351 protein sequences in the translated 454 database. The analysis returned a total of 974 proteins from the Illumina, 1,256 proteins from the SRA, and 880 proteins from the 454 database. Unique proteins were then identified using human orthologs and multiple copies of proteins were consolidated into single occurrences. As a result, 494 unique proteins were found in Illumina database, 636 unique

proteins were in the SRA database, and 434 from in the 454 database. Comparing the outputted proteins from each database revealed that 298 proteins were shared when using all three databases, 213 proteins were unique proteins to the SRA database, 68 were unique to the Illumina database, and 50 were unique to the 454 database (Figure 3A). When analyzing the protein composition of each of the three mucus samples using the Illumina translated transcriptome we found 50 shared proteins among all three samples, 144 unique proteins in the free- swimming skin mucus, 113 unique proteins in the terrestrialized skin mucus, and 10 unique proteins in the terrestrialized gill mucus (Figure 3B). Analysis of the protein composition using the SRA- translated transcriptome resulted in 44 common proteins among all three samples, 190 unique proteins in the free-swimming skin mucus, 171 unique proteins in the terrestrialized skin mucus, and 11 unique proteins in the terrestrialized gill mucus (Figure 3C). A similar trend was observed when using the 454 translated transcriptome with 33 shared proteins among all three mucus samples, 130 proteins unique to the free-swimming skin mucus, 101 proteins unique to the terrestrialized skin mucus, and only 14 proteins unique to the terrestrialized gill mucus (Figure 3D). These results suggest that the composition of the gill mucus secretion produced during the induction phase of terrestrialization resembles both the free-swimming skin mucus and the terrestrialized skin mucus proteome. Specifically, ~72.9% of the terrestrialized gill mucus proteome was also present in the free-swimming skin mucus proteome and ~71.7% of the terrestrialized gill mucus proteome were found in the terrestrialized skin mucus. As a result, only ~16.4% of all proteins present in the terrestrialized gill mucus were unique to this sample.

Gene ontology analyses using the three data sets revealed that biological processes (BPs) were enriched in free-swimming and terrestrialized skin mucus samples, but no unique GO for the terrestrialized gill mucus (Table S4 in Supplementary Material; Figures 4A–F). Based on the

Illumina analysis, the top five most significant BPs enriched in free-swimming skin mucus were "small GTPase mediated signal transduction," "carbohydrate metabolic process," "UDP-N-acetylglucosamine biosynthetic process," "cell-cell adhesion," and "galactose metabolic process." In terrestrialized skin mucus, in turn, we observed an enrichment in BPs such as "SRP-dependent co-translational protein targeting to membrane," "viral transcription," "nuclear-transcribed mRNA catabolic process, nonsense-mediated decay," "translational initiation," and "translation" (Figures 4A, B). Interestingly, all data sets also contained significant BPs related to immune function that were different in the free-swimming and terrestrialized skin mucus. For instance, free-swimming skin mucus had unique proteins involved in "positive regulation of phagocytosis" and "antigen processing and presentation," whereas the terrestrialized skin mucus proteome included proteins with predicted functions in "platelet degranulation," "antigen processing and presentation of exogenous peptide antigen via MHC class I, TAP-dependent," "viral process," "tumor necrosis factor-mediated signaling pathway," "defense response to Gram-negative bacterium," and "cellular response to hydrogen peroxide" (Table S4 in Supplementary Material). Overall, these data suggest that the immunological processes that govern the skin immune system in lungfish differ in free-swimming and terrestrialized phases. Additionally, non-immune BPs that were enriched in the control skin mucus included "epithelial cell differentiation" and "membrane organization," while in terrestrialized skin mucus they included "translational initiation" and "platelet aggregation." These results may indicate that cellular organization and maintenance functions are enriched in the skin of free-swimming animals, while cell survival is enriched during terrestrialization.

KEGG pathway analyses showed that, overall, in free-swimming lungfish skin mucus, enriched pathways are mostly related to metabolic pathways such as "Histidine metabolism,"

"Amino sugar and nucleotide sugar metabolism," "Galactose metabolism," and "beta- Alanine metabolism." The proteome of the terrestrialized lungfish skin mucus was predicted to be enriched in "Ribosome" and "Biosynthesis of antibiotics" pathways (Figure S1 in Supplementary Material). KEGG pathway analyses using the Illumina and SRA data sets (Figures S1A–D in Supplementary Material) were more similar to each other compared to the 454-derived KEGG pathway analysis (Figures S1E, F in Supplementary Material). These results support previous studies that demonstrated that terrestrialization has profound effects on lungfish skin metabolism with an overall decrease in metabolic activity.

3.4 Changes in Lungfish Skin Immunoproteome in Response to Terrestrialization

In order to examine the allocation of immune resources in lungfish skin in response to terrestrialization, we performed manual counts within our protein lists using previously reported proteins with immune function. We observed an increase in the percentage of immune-related proteins present in the terrestrialized gill and skin mucus compared to the free-swimming skin mucus when using lists generated by the Illumina and SRA data sets but not the 454 data set (Figure 5A). It is worth noting that the SRA-based analysis revealed a higher percentage of immune-related proteins in the gill mucus (~25%) compared to the Illumina and 454 data sets (20% in both). Similarly, when we counted the number of immune proteins that were present in each sample we found a trend toward greater number of immune proteins in the terrestrialized skin mucus compared to free-swimming skin mucus when using the Illumina and SRA data sets but not the 454 data set (Figure 5B). Among the immune-related proteins, we observed a higher number of proteins with known antimicrobial activity in the terrestrialized skin mucus compared to the free-swimming skin mucus in all three data sets (Figure 5C). The greater number of proteins with antimicrobial activity in the terrestrialized skin mucus sample was due to a greater

abundance of histones and S100 proteins (Tables S1–S3 in Supplementary Material). In support, we observed increased levels of expression of H2A and S100A11 in terrestrialized compared to free-swimming skin by RT-qPCR (Figures 6A, B). Moreover, gene expression analysis of neutrophil elastase (ELANE) showed a significant increase (150- fold) in the expression of this gene in terrestrialized compared to free-swimming lungfish skin (Figure 6C). This result supports our histological observations as well as the proteomic results (Tables S1 and S2 in Supplementary Material). Combined, our results suggest that lungfish increase immune resource allocation and undergo inflammation in the skin early on during the aestivation process.

Apart from differences in antimicrobial compound abundance, we also observed changes in the Ig proteins present in each sample. Where no Igs were detected in the gill mucus sample, we detected IgW1 long form (IgW1L) and IgM1 in the free- swimming skin mucus sample and IgW1L, IgM1, and IgM2 in the terrestrialized skin mucus sample using the Illumina and 454 but not the SRA data sets (Tables S1–S3 in Supplementary Material). In support, RT-qPCR analysis showed no significant changes in IgW1 or IgM1 expression as a result of terrestrialization but a significant increase in IgM2 expression (~3-fold) was observed in terrestrialized compared to free-swimming skin (Figures 6D–F). Both sigma and lambda-like light chains were found in both mucus samples (Tables S1 and S2 in Supplementary Material). These results indicate a switch in Ig expression and secretion in the lungfish skin during the induction phase of aestivation.

4. Discussion

The skin of all animals provides a first line of defense against pathogen invasion. Apart from being a physical barrier, the skin has its own unique suite of immune cells and molecules that constitute the skin-associated lymphoid tissue (39–40). As the major interface between the environment and the host, the skin is subject to several external stressors, and these stressors

shifted dramatically during the vertebrate transition from water to land. Hence, we took advantage of the ability to terrestrialize lungfish in the laboratory setting as a model to study the water-to-land transition. We hypothesized that terrestrialization results in changes in the skin proteome composition and specifically, in an increased investment in production of immune molecules that will help prevent pathogen invasion and land stressors.

Previous studies have shown changes in the skin proteome com- position of teleost fish (aquatic vertebrates) in response to infection (41, 42), stress (43–45), wounding (46), or dietary administration of immunostimulants (44, 45, 47). However, most of these studies adopted a two-dimensional (2-D) gel electrophoresis approach where selected spots were then analyzed by peptide fragment fingerprinting and LC-MS/MS. 2-D gel electrophoresis presents a number of drawbacks such as low reproducibility, the need for large sample sizes, and the difficulty to separate proteins with low abundance as well as very hydrophobic proteins (48). Thus, our results constitute a unique and unbiased report of all proteins present in the skin proteome of lungfish. We used three different RNA-seq databases from two different lungfish species (*P. dolloi* and *P. annectens*) generated in three different platforms (named Illumina, SRA, and 454) in our analyses. As expected, we obtained different results depending on the database and tissue origin. We found greater number of proteins in every sample when the SRA database was used, an expected result given the coverage of protein- coding sequences in each data base (636 unique sequences for the lungfish SRA database but only 494 for the Illumina database and 435 for the 454 database according to Swissprot).

As previously reported, we observed dramatic remodeling of the lungfish skin histological organization upon terrestrialization. This tissue remodeling involves multiple processes such as flattening of the epithelial cells, decreases in the overall epidermal thickness,

and loss of goblet cells. In support, our proteomic study showed enriched BPs and KEGG pathways present in the skin mucus before and during terrestrialization highlighting the ability of this vertebrate to respond to environmental stimuli and reshape the cellular and molecular composition of the skin. One potential caveat to our study is that increased amounts of cell debris may be present in the skin mucus samples of terrestrialized animals than in free-swimming lungfish, affecting the overall proteomic composition of the two samples. In any case, tissue remodeling and changes in the external microbial environment likely occur concomitantly in our model and teasing apart the immunoproteome changes that respond to one or the other stimulus is a challenging question.

Transition from water to land also imposes drastic changes in the microbial composition of the external environment. Thus, we observed that lungfish secrete unique suites of innate and adaptive immune molecules into the skin mucus as a response to air exposure. With respect to innate immune molecules, we identified greater number of proteins with known antimicrobial functions in the skin, particularly histones (HIST1H1D and HIST1H3C) and S100 proteins (S100A, S100P, and S100A6). In this study, we confirmed changes at the protein level with gene expression data for six selected genes. Overall, gene expression data supported the findings of the proteomics approach, but it is worth noting that we did not include biological replicates in the proteomics study. Previous work has shown a lack of correlation between proteomics and mRNA transcript levels (49) and therefore future studies should expand our current data sets to multiple biological replicates. GO analyses of the unique proteins present in the terrestrialized skin mucus revealed enrichment in BPs such as defense response to Gram-negative bacterium, antigen processing, and presentation of exogenous peptide antigen via MHC class I, TAP-dependent, tumor necrosis factor- mediated signaling pathway, and cellular response to hydrogen peroxide.

Thus, these data suggest a requirement for the lungfish skin to increase antimicrobial defenses during the process of terrestrialization. Future studies should address the function of antimicrobial compounds triggered by air exposure.

Protopterus sp. express four different immunoglobulin heavy (IgH) chain classes: IgW, IgM, IgN, and IgQ. Additionally, there is extensive intraclass IgH diversification in lungfish, with IgM including three IgM genes (IgM1, IgM2, and IgM3), IgW including two genes (IgW1 and IgW2) as well as short and long forms, and IgN including also three genes (IgN1, IgN2, and IgN3) (50). So far, the immunological functions of different IgM subclasses have not been investigated. This study identified the presence of Igs in the skin mucus proteome of both freshwater and terrestrialized lungfish. Specifically, the freshwater lungfish skin proteome contained IgW1L as well as IgM1 secretory form. Secreted IgW(D) antibodies have not been previously characterized in sarcopterygian fish, but it is known that teleost secrete IgD into their mucosal secretions (51). Our findings support that secretion of IgW into the skin mucus occurs in sarcopterygian fish and that IgW1L may have specialized mucosal immune functions compared to other IgW forms in lungfish. In the terrestrialized skin mucus proteome, apart from IgW1L, we observed both IgM1 and IgM2 expression, suggesting the IgM1 expression occurs constitutively in the skin of lungfish but IgM2 expression is switched on in response to external stressors. We were not able to detect any Ig in the terrestrialized gill mucus sample, but this finding may be a result of the lower protein amounts in this sample compared to the skin mucus samples. Further studies should address the specific immunological function of IgM2 at lungfish mucosal surfaces.

5. Conclusion

This study provides the first characterization of the skin mucus proteome of a sarcopterygian fish, the African lungfish. We report important shifts in both innate and adaptive immune molecules in the skin mucus of lungfish in response to terrestrialization. Our results suggest that the transition from water to land in vertebrates imposed a need for increased investment in immune function in the cutaneous mucosal secretions.

6. Data Availability

Proteomic data sets were submitted to ProteomeXchange (http:// www.proteomexchange.org/) via the PRIDE database, accession: PXD008981 and PXD008982.SRA used in this study can be found at NCBI (accession numbers SRR2027914, SRR2027978, SRR2027979, SRR2028000, SRR2028017, SRR2028020, SRR2028021, SRR2027980, SRR6291329, and SRR6291330). 454 pyrosequencing reads were deposited at NCBI (accession number SRP141470). Output tables from Scaffold containing all peptide table reports are given in Table S5 in Supplementary Material.

7. Ethics Statement

All animal studies were reviewed and approved by the Office of Animal Care Compliance at the University of New Mexico (protocol number 11-100744-MCC).

8. Acknowledgments

The authors would like the thank Dr. Chris Amemiya for sharing his lungfish transcriptome and George Tsaprailis and Cynthia L. David for help with proteomics analysis.

9. Funding

This work was supported by The National Science Foundation (IOS #1456940) and The National Institute of Health (COBRE grant P20GM103452).

10. FIGURES AND TABLES

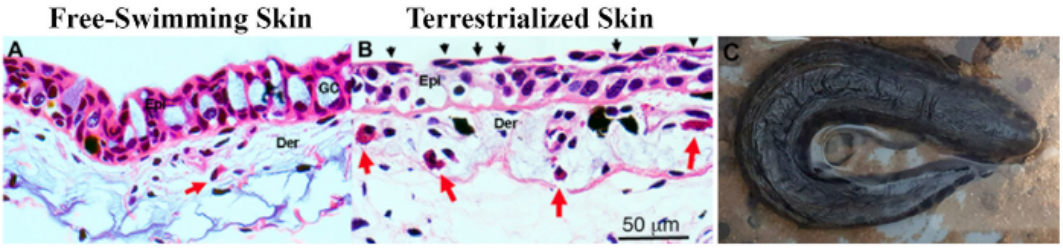

FIGURE 1 | **(A)** Hematoxylin and eosin staining of free-swimming and **(B)** terrestrialized *Protopterus dolloi* skin paraffin sections. Skin sections show significant infiltration of granulocytes (red arrows) in the dermis (Der); epidermis (Epi), and goblet cells (GO). The black arrows indicate flattened keratinocytes after terrestrialization. **(C)** Image of a *P. dolloi* 4 days after the initiation of the induction phase actively secreting mucus from its gills.

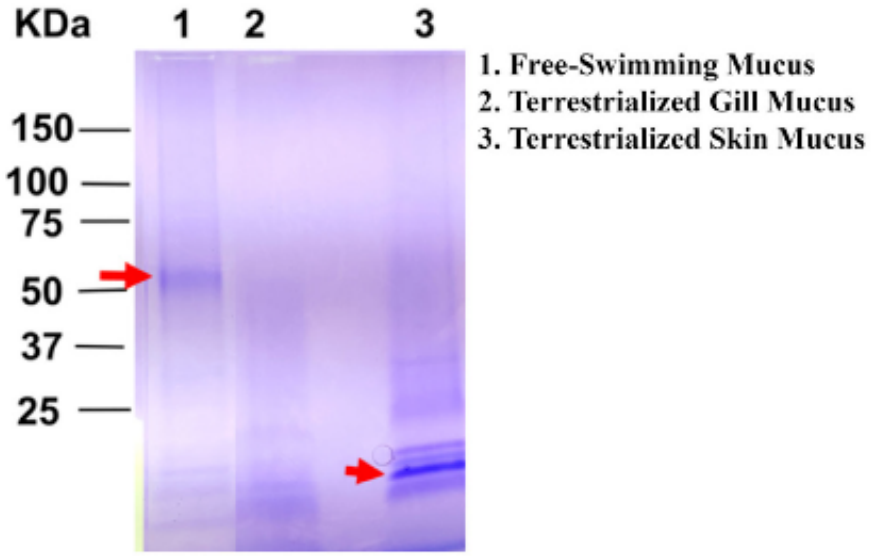

FIGURE 2 | Sodium dodecyl sulfate polyacrylamide gel electrophoresis showing unique protein compositions between free-swimming (lane 1), terrestrialized gill mucus (lane 2), and terrestrialized skin mucus samples (lane 3) used for LC/MS-MS proteomic analysis. Red arrows point to high-intensity bands that were excised and analyzed by LC/MS-MS.

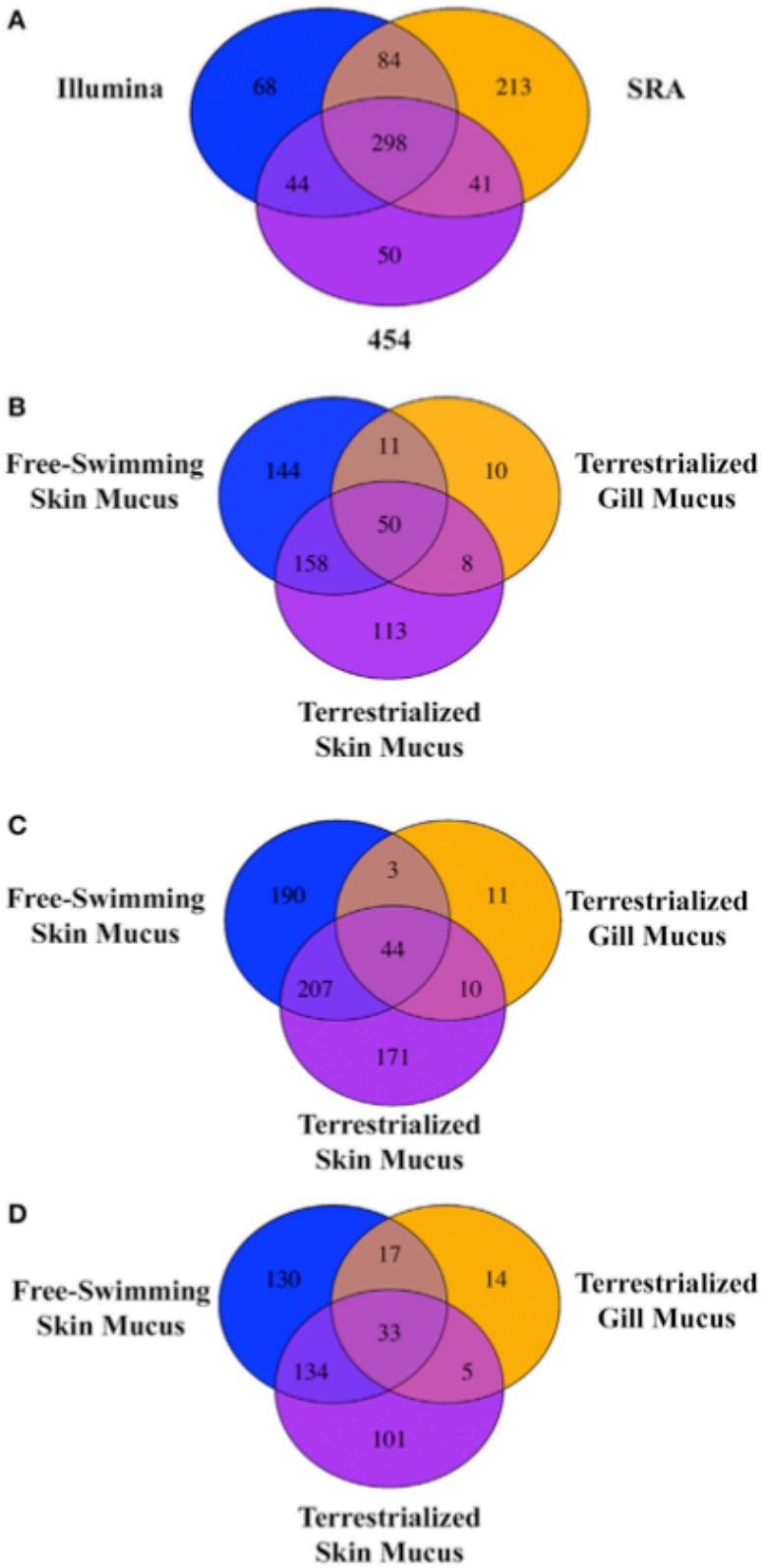

FIGURE 3 | **(A)** Venn diagram showing the unique and shared proteins between the Illumina database, SRA database, and the 454 pyrosequencing database present in all three *Protopterus dolloi* mucus samples. Comparison of shared and unique proteins present in each mucus sample using the **(B)** Illumina database, **(C)** SRA database, and **(D)** 454 database.

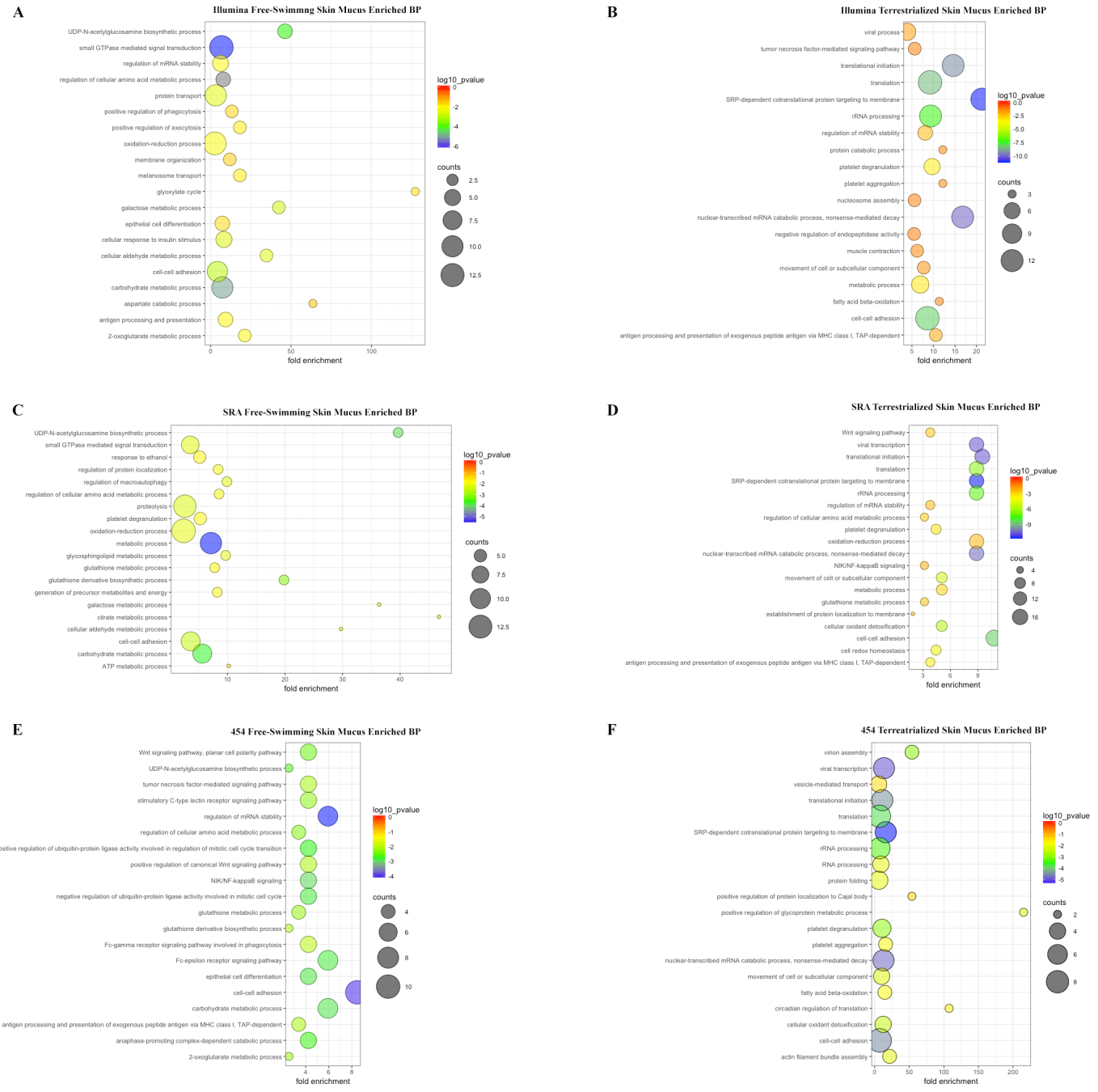

Figure 4. Scatter plots of enriched gene ontology biological process (BP) terms for (a) free-swimming skin mucus and (b) terrestrialized skin mucus using the Illumina database; for (c) free-swimming skin mucus and (D) terrestrialized skin mucus using the sequence read archive (SRA) database; and for (e) free-swimming skin mucus and (F) terrestrialized skin mucus using

the 454 database. The fold enrichment indicates the ratio of the expressed gene number to the total gene number in a pathway. Only the top 20 BPs according to p-value are shown. The size and color of the points represent the gene number and the log10 p-value of each pathway, respectively.

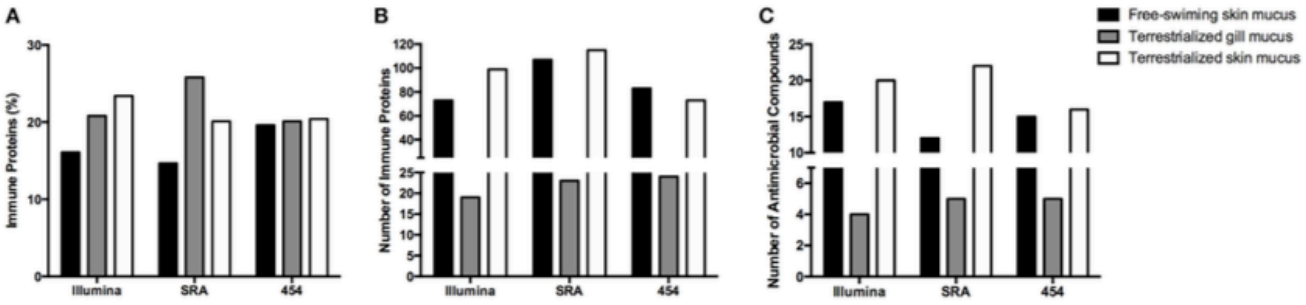

FIGURE 5 | **(A)** Percentage of proteins and **(B)** total number of proteins with known immunological function in the three mucus samples obtained in this study using the Illumina transcriptome, the sequence read archive (SRA) transcriptome, or the 454 transcriptome databases. **(C)** Total number of proteins with known antimicrobial function in the skin identified in the three mucus samples using the Illumina transcriptome, SRA transcriptome, or the 454 transcriptome databases.

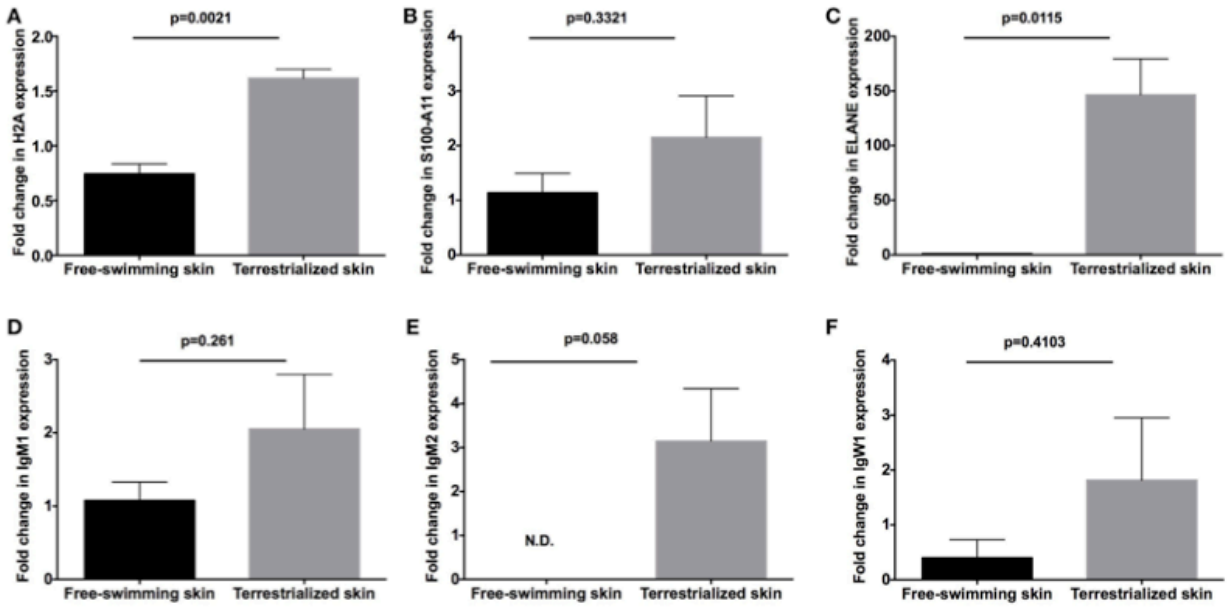

FIGURE 6 | Quantitative real-time PCR analysis of the expression of **(A)** H2A, **(B)** S100-A11, **(C)** neutrophil elastase (ELANE), **(D)** IgM1, **(E)** IgM2, and **(F)** IgW1 in free-swimming and terrestrialized *Protopterus dolloi* skin tissue (N = 3). *p*-Values were calculated by unpaired *t*-test.

11. References

1. Takei Y. From aquatic to terrestrial life: evolution of the mechanisms for water acquisition. Zoolog Sci (2015) 32(1):1–7. doi:10.2108/zs140142.

2. Xu Z, Parra D, Gómez D, Salinas I, Zhang Y, von Gersdorff Jørgensen L, et al. Teleost skin, an ancient mucosal surface that elicits gut-like immune responses. Proc Natl Acad Sci U S A (2013) 110(32):13097–102. doi:10.1073/ pnas.1304319110.

3. Schempp C, Emde M, Wölfle U. Dermatology in the Darwin anniversary. Part 1: evolution of integument. J Dtsch Dermatol Ges (2009) 7(9):750–7. doi:10.1111/j.1610-0387.2009.07193_supp.x.

4. Amemiya CT, Alföldi J, Lee AP, Fan S, Philippe H, MacCallum I, et al. The African coelacanth genome provides insights into tetrapod evolution. Nature (2013) 496(7445):311–6. doi:10.1038/nature12027.

5. Garofalo F, Amelio D, Icardo JM, Chew SF, Tota B, Cerrea MC, et al. Signal molecule changes in the gills and lungs of the African lungfish Protopterus annectens, during the maintenance and arousal phases of aestivation. Nitric Oxide (2015) 44:71–80. doi:10.1016/j.niox.2014.11.017.

6. Fishman AP, Pack AI, Delaney RG, Galante RJ. Estivation in Protopterus. J Morphol (1986) 190:237–48. doi:10.1002/jmor.1051900416.

7. Strula M, Paola P, Carlo G, Angela MM, Maria UV. Effects of induced aestivation in Protopterus annectens: a histomorphological study. J Exp Zool (2002) 292(1):26–31. doi:10.1002/jez.1139.

8. Ojeda JL, Wong WP, Ip YK, Icardo JM. Renal corpuscle of the African lungfish Protopterus dolloi: structural and histochemical modifications during aestivation. Anat Rec (2008) 291(9):1156–72. doi:10.1002/ar.20729

9. Perry SF, Euverman R, Wang T, Loong AM, Chew SF, Ip WK, et al. Control of breathing in African lungfish (Protopterus dolloi): a comparison of aquatic and cocooned (terrestrialized) animals. Respir Physiol Neurobiol (2008) 160(1):8–17. doi:10.1016/j.resp.2007.06.015.

10. Icardo JM, Loong AM, Colvee E, Wong WP, Ip YK. The alimentary canal of the African lungfish Protopterus annectens during aestivation and after arousal. Anat Rec (2012) 295(1):60–72. doi:10.1002/ar.21476.

11. Chng YR, Ong JLY, Ching B, Chen XL, Hiong KC, Wong WP, et al. Aestivation induces changes in the mRNA expression levels and protein abundances of two isoforms of urea transporters in the gills of African lungfish, Protopterus annectens. Front Physiol (2017) 8:71. doi:10.3389/fphys.2017.00071.

12. Chew SF, Chan NKY, Loong AM, Hoing KC, Tam WL, Ip WK. Nitrogen metabolism in the African lungfish (Protopterus dolloi) aestivating in a mucus cocoon on land. J Exp Biol (2004) 207:777–86. doi:10.1242/jeb.00813.

13. Chew SF, Hiong K. Aestivation and brain of the African lungfish Protopterus annectens. Temperature (Austin) (2014) 1(2):82–3. doi:10.4161/temp.29650.

14. Wood CM, Walsh PJ, Chew SF, Ip YK. Greatly elevated urea excretion after air exposure appears to be carrier mediated in the slender lungfish (Protopterus dolloi). Physiol Biochem Zool (2005) 78(6):893–907. doi:10.1086/432919.

15. Wilkie MP, Morgan TP, Galvez F, Smith RW, Kamjimura M, Ip YK, et al. The African lungfish (Protopterus dolloi): ionoregulation and osmoregulation in a fish out of water. Physiol Biochem Zool (2007) 80(1):99–112. doi:10.1086/508837.

16. Casadei E, Wang T, Zou J, Vecino JLG, Wadsworth S, Secombes CJ. Characterization of three novel β-defensin antimicrobial peptides in rain- bow trout (Oncorhynchus mykiss). Mol Immunol (2009) 46(16):3358–66. doi:10.1016/j.molimm.2009.07.018.

17. Gallo RL, Hoopwer LV. Epithelial antimicrobial defence of the skin and intestine. Nat Rev Immunol (2012) 12(7):503–16. doi:10.1038/nri3228.

18. Diamond G, Beckloff N, Weinberg A, Kisich KO. The roles of antimicrobial peptides in innate host defense. Curr Pharm Des (2009) 15(21):2377–92. doi:10.2174/138161209788682325.

19. Dorschner RA, Pestonjamasp VK, Tamakuwala S, Ohtake T, Rudisill J, Nizet V, et al. Cutaneous injury induces the release of cathelicidin antimicro- bial peptides active against group A Streptococcus. J Invest Dermatol (2001) 117(1):91–7. doi:10.1046/j.1523-1747.2001.01340.x.

20. Thorey IS, Roth J, Regenbogen J, Halle JP, Bittner M, Vogl T, et al. The Ca2+- binding proteins S100A8 and S100A9 are encoded by novel injury-regulated genes. J Biol Chem (2001) 276(38):35818–25. doi:10.1074/jbc.M104871200.

21. Büchau AS, Hassan M, Kukova G, Lewerenz V, Kellermann S, Würthner JU, et al. S100A15, an antimicrobial protein of the skin: regulation by E. coli through toll-like receptor 4. J Invest Dermatol (2007) 127(11):2595–604. doi:10.1038/sj.jid.5700946.

22. Kawasaki H, Iwamuro S. Potential roles of histones in host defense as antimi- crobial agents. Infect Disord Drug Targets (2008) 8(3):195–205. doi:10.2174/1871526510808030195.

23. Jurado J, Fuentes-Almargo CA, Guardiola FA, Cuesta A, Esteban MÁ, Prieto- Álamo MJ. Proteomic profile of the skin mucus of farmed gilthead seabream (Sparus aurata). Proteomics (2015) 120:21–34. doi:10.1016/j.jprot.2015.02.019.

24. Shevchenko A, Wilm M, Vorm O, Mann M. Mass spectrometric sequencing of proteins from silver-stained polyacrylamide gels. Anal Chem (1996) 68(5):850–8. doi:10.1021/ac950914h.

25. Andon NL, Hollingworth S, Koller A, Greenland AJ, Yates JR III, Haynes PA. Proteomic characterization of wheat amyloplasts using identification of proteins by tandem mass spectrometry. Proteomics (2002) 2(9):1156–68. doi:10.1002/1615-9861(200209)2:9<1156::AID-PROT1156>3.0.CO;2-4.

26. Tacchi L, Larragoite E, Salinas I. Discovery of J chain in African lungfish (Protopterus dolloi, Sarcopterygii) using high throughput transcriptome sequencing: implications in mucosal immunity. PLoS One (2013) 8(8):e70650. doi:10.1371/journal.pone.0070650.

27. Sequence Read Archive Submissions Staff. Using the SRA Toolkit to convert sra files into other formats. SRA Knowledge Base. Bethesda, MD: National Center for Biotechnology Information (US) (2011). Available from: https:// www.ncbi.nlm.nih.gov/books/NBK158900/ (Accessed: January 10, 2018).

28. Hass BJ, Papanicolaou A, Yassour M, Grabherr M, Blood PD, Bowden J, et al. De novo transcript sequence reconstruction from RNA-Seq: reference generation and analysis with Trinity. Nat Protoc (2014) 8(8):1494–512. doi:10.1038/ nprot.2013.084.

29. Fu L, Niu B, Zhu Z, Wu S, Li W. CD-HIT: accelerated for clustering the next generation sequencing data. Bioinformatics (2012) 28(23):3150–2. doi:10.1093/bioinformatics/bts565.

30. Keller A, Nesvizhskii AI, Kolker E, Aebersold R. Empirical statistical model to estimate the accuracy of peptide identifications made by MS/MS and database search. Anal Chem (2002) 74(20):5383–92. doi:10.1021/ac025747h.

31. Qian WJ, Liu T, Monroe ME, Strittmatter EF, Jacobs JM, Kangas LJ, et al. Probability-based evaluation of peptide and protein identifications from tandem mass spectrometry and SEQUEST analysis: the human proteome. J Proteome Res (2005) 4(1):53–62. doi:10.1021/pr0498638.

32. Altschul SF, Gish W, Miller W, Myers EW, Lipman DJ. Basic local alignment search tool. JMol Biol (1990) 215(3):403–10. doi:10.1016/S0022- 2836(05)80360-2.

33. Carbon S, Ireland A, Mungall CJ, Shu S, Marshall B, Lewis S, et al. AmiGO: online access to ontology and annotation data. Bioinformatics (2009) 25(2):288–9. doi:10.1093/bioinformatics/btn615.

34. Ashburner M, Ball CA, Blake JA, Botstein D, Butler H, Cherry JM, et al. Gene ontology: tool for the unification of biology. The Gene Ontology Consortium. Nat Genet (2017) 25(1):25–9. doi:10.1038/75556.

35. Huang DW, Sherman BT, Lempicki RA. Systematic and integrative analysis of large gene lists using DAVID bioinformatics resources. Nat Protoc (2009) 4(1):44–57. doi:10.1038/nprot.2008.211.

36. Huang DW, Sherman BT, Lempicki RA. Bioinformatics enrichment tools: paths toward the comprehensive functional analysis of large gene lists. Nucleic Acids Res (2009) 37(1):1–13. doi:10.1093/nar/gkn923.

37. R Core Team. R: A Language and Environment for Statistical Computing. Vienna, Austria: R Foundation for Statistical Computing (2017). Available from: https://www.R-project.org/ (Accessed: January 10, 2018).

38. Schauber J, Gallo RL. Antimicrobial peptides and the skin immune defense system. J Allergy Clin Immunol (2008) 122(2):261–6. doi:10.1016/j.jaci.2008.03.027.

39. Streilein JW. Skin-associated lymphoid tissues (SALT): origins and functions. J Invest Dermatol (1983) 80:12–6. doi:10.1111/1523-1747.ep12536743.

40. Egawa G, Kabashima K. Skin as a peripheral lymphoid organ: revisiting the concept of skin-associated lymphoid tissue. J Invest Dermatol (2011) 131:2178–85. doi:10.1038/jid.2011.198.

41. Rajan B, Lokesh J, Kiron V, Brinchmann MF. Differentially expressed proteins in the skin mucus of Atlantic cod (Gadus morhua) upon natural infection with Vibrio anguillarum. BMC Vet Res (2013) 9:103. doi:10.1186/1746- 6148-9-103.

42. Provan F, Jensen LB, Uleberg KE, Larssen E, Rajalahti T, Mullins J, et al. Proteomic analysis of epidermal mucus from sea lice-infected Atlantic salmon, Salmo salar L. J Fish Dis (2013) 36(3):311–21. doi:10.1111/jfd.12064.

43. Pérez-Sánchez J, Terova G, Simó-Mirabet P, Rimoldi S, Folkedal O, Calduch- Giner JA, et al. Skin mucus of gilthead sea bream (Sparus aurata L.). Protein mapping and regulation in chronically stressed fish. Front Phys (2017) 8:34. doi:10.3389/fphys.2017.00034.

44. Cordero H, Guzmán-Villanueva LT, Chaves-Pozo E, Arizcun M, Ascencio- Valle F, Cuesta A, et al. Comparative ontogenetic development of two marine teleosts, gilthead seabream and European sea bass: new insights into nutrition and immunity. Dev Comp Immunol (2016) 65:1–7. doi:10.1016/j.dci. 2016.06.011.

45. Cordero H, Morcillo P, Cuesta A, Brinchmann MF, Esteban MA. Differential proteome profile of skin mucus of gilthead seabream (Sparus aurata) after probiotic intake and/or overcrowding stress. J Proteomics (2016) 132:41–50. doi:10.1016/j.jprot.2015.11.017.

46. Cordero H, Brinchmann MF, Cuesta A, Esteban MA. Chronic wounds alter the proteome profile in skin mucus of farmed gilthead seabream. BMC Genomics (2017) 18(1):939. doi:10.1186/s12864-017-4349-3.

47. Micallef G, Cash P, Fernandes JMO, Rajan B, Tinsley JW, Bickerdike R, et al. Dietary yeast cell wall extract alters the proteome of the skin mucous barrier in Atlantic Salmon (Salmo salar): increased abundance and expression of a calreticulin-like protein. PLoS One (2017) 12(1):e0169075. doi:10.1371/journal.pone.0169075.

48. Gautier V, Mouton-Barbosa E, Bouyssie D, Delcourt N, Beau M, Girard J-P, et al. Label-free quantification and shotgun analysis of complex proteomes by one-dimensional SDS-PAGE/NanoLC-MS. Mol Cell Proteomics (2012) 11(8):527–39. doi:10.1074/mcp.M111.015230.

49. Haider S, Pal R. Integrated analysis of transcriptomic and proteomic data. Curr Genomics (2015) 14(2):91–110. doi:10.2174/1389202911314020003.

50. Zhang T, Tacchi L, Wei Z, Zhao Y, Salinas I. Intraclass diversification of immunoglobulin heavy chain genes in the African lungfish. Immunogenetics (2014) 66(5):335–51. doi:10.1007/s00251-014-0769-2.

51. Xu Z, Takizawa F, Parra D, Gómez D, Jørgensen L, LaPatra SE, et al. Mucosal immunoglobulins at respiratory surfaces mark an ancient association that predates the emergence of tetrapods. Nat Commun (2016) 7:10728. doi:10.1038/ncomms10728.

Chapter 4. THE COCOON OF AFRICAN LUNGFISH IS A LIVING CELLULAR STRUCTURE WITH ANTIMICROBIAL FUNCTIONS

Heimroth, R. D., Casadei, E., Amemiya, C. T., Muñoz, P., and I. Salinas. The cocoon of African lungfish is a living cellular structure with antimicrobial functions. *In prep.*

1. Abstract:

Terrestrialization is an extreme physiological adaptation by which African lungfish (Dipnoi) survive dry seasons. For months and up to several years, lungfish live inside a dry mucus cocoon that protects them from desiccation. Light and electron microscopy show that the lungfish cocoon is a living tissue with a well-defined structure that traps bacteria. Transcriptomics identify a global state of inflammation in the terrestrialized lungfish skin that recruits granulocytes which release potent extracellular traps. *In vivo* DNase I surface spraying during lungfish terrestrialization results in dysbiosis, septicemia and skin wounds and hemorrhages. Thus, lungfish have evolved unique immunological adaptations to protect their bodies from infection for extended periods of time while living on land. Trapping bacteria outside their bodies may benefit aestivating vertebrates that undergo metabolic torpor.

One Sentence Summary: The mucus cocoon of terrestrialized African lungfish is a living tissue with potent antimicrobial functions.

2. Introduction:

African lungfish (*Protopterus sp.*), are extant relatives to all tetrapods, have a dual mode of living, surviving in both aquatic and terrestrial environments (Amemiya et al., 2013; Garofalo et al., 2015). Every year, the dry season in Africa limits the access to food or water to animals like lungfish. Environmental cues such as drought, signal lungfish to begin the aestivation process by which they curl up, reduce their metabolic activity, and produce copious amounts of mucus that will ultimately cover their bodies forming a hardened cocoon (Sturla et al., 2002). Drastic tissue remodeling is observed in terrestrialized animals; the gut disintegrates to allow free diffusion of

nutrients during the aestivation period (Icardo et al., 2012). The lungfish cocoon has thus far been viewed as an inert outer layer that provides physical protection and prevents desiccation, but recent proteomic analyses indicated that the African lungfish cocoon has a unique immunoproteome that is distinct from that of the skin mucus of freshwater animals (Heimroth et al., 2018).

Almost a century ago, the investigation of the African lungfish immune system revealed unusually large deposits of granulocytes located in the gut, gonads and kidneys of these animals and it was proposed that these granulocytes may play a role in aestivation (Jordan and Speidel, 1931). Here we show that granulocyte deposits in the tissue reservoirs of freshwater lungfish become mobilized to the skin, where they release extracellular traps (ETs) upon stimulation. Importantly, the cocoon of lungfish is not just a physical barrier that protects them from desiccation but a living tissue with potent antimicrobial properties that provides lungfish with prolonged protection during the vulnerable terrestrial phase.

3. Tissue reservoirs supply granulocytes to the integument during terrestrialization

The lungfish lymphoid system has a very unique anatomy compared to other jawed vertebrates. The presence of large deposits of granulocytes associated with the gut, kidney and gonads of free-swimming lungfish was noted decades ago (Jordan and Speidel, 1931). Granulocyte migration to epithelial tissues is an established hallmark of mucosal inflammation (Sumagin et al., 2014). Furthermore, recruited granulocytes can then transmigrate across epithelia and reach the lumen (Parkos, 2005; Chin and Parkos, 2006; Sumagin et al., 2014). To understand the role of these large granulocyte reservoirs during terrestrialization, we performed histological analysis on freshwater and terrestrialized lungfish gut and kidney. Hematoxylin and eosin staining confirmed that the gut wall and the kidney are granulocyte-rich structures in freshwater lungfish (Fig. 1, A and C). In terrestrialized animals, reservoir tissues contained lower granulocyte numbers,

increased pigment deposition and increased number of lymphatic pumps (Fig. 1, B and D). Granulocytes entered circulation as result of terrestrialization, as evidenced in the Giemsa stained blood smears (Fig. 1, E-G). In support, and as previously reported (Heimroth et al., 2018), abundant granulocytes were observed in the epidermis and dermis of terrestrialized animals compared to freshwater controls (Fig. 1, I and J and fig. S1A). Granulocyte recruitment to the skin was paralleled to increased expression of granulocyte markers *cxcr2* and *elane* (Baugher and Richmond, 2008; Korkmaz et al., 2010) in the lungfish skin, whereas in reservoir tissues only *elane* expression was down-regulated (4-fold) in the kidney (Fig. 1H and fig. S1B). *Mpo* expression, in turn, was highly up-regulated in both skin (7-fold) and gut and kidney reservoir tissues (68-fold and 120-fold, respectively) in terrestrialized lungfish compared to freshwater controls perhaps as a mechanism to lengthen granulocyte lifespan by preventing apoptosis (Fox et al., 2010) (fig. S1C). As previously reported (Heimroth et al., 2018), terrestrialization involved drastic remodeling of the integument of the lungfish with the thinning of the epidermis, exhaustion of goblet cells and presence of flattened keratinocytes resembling the mammalian skin (Fig. 1, I to J). Thus, free swimming lungfish invest in large deposits of granulocytes which are subsequently mobilized to barrier tissues such as the skin upon adaptation to land.

4. The mucus cocoon of terrestrialized lungfish is a living tissue with a well-defined structure

Aestivating animals such as lungfish and amphibians form cocoon structures to reduce evaporative water loss in the dry season (Chew and Hiong, 2014; Glass et al., 2009). African lungfish live inside their mucus cocoon for months or even years (Smith, 1930). Previous studies described the cocoon of anuran and urodele amphibians as shed epithelial layers whereas the

lungfish cocoon was described as a translucent brownish dried mucus structure (Smith, 1930; Withers, 1995; Withers, 1998).

Histological observations revealed that the lungfish cocoon is not a dead, dry mucus layer, but instead, it is a living tissue with a well-defined cellular structure. The cocoon is composed of different cell types including goblet cells, epithelial cells, endothelial cells and immune cells. Abundant nests of cells were observed surrounded by long channels lined by double layered squamous cells. Series of monolayered vessels running parallel and perpendicular to the main channel were identified. These nests of cells contained endothelium-lined vessels that could potentially serve to transport cells into and within the cocoon (Fig. 2, A and B). Some of these immune cells were identified as granulocytes based on MPO enzymatic staining, indicating transmigration (fig. S2A). The channels were not filled with mucosal secretions based on periodic acid-Schiff (PAS) staining (Fig. 2C). Serial coronal sectioning of paraffin-embedded cocoon samples indicated that the thickness of the cocoon is approximately 350 μm, although this may vary from body site to body site. This cocoon structure is notably different from that of amphibians, which consists of a lamellated structure with several dozens of flattened epidermal cells (MacCanahan et al., 1976; Ruibal, R. and S. Hillman, 1981; Withers, 1995; Withers, 1998; Withers and Thompson, 2000).

Scanning electron microscopy (SEM) and transmission electron microscopy (TEM) analysis showed that during terrestrialization the flattened smooth epidermis of freshwater fish (Fig. 2D) is remodeled to a disrupted surface covered by the cocoon where cells could be seen (Fig. 2, E and F). Clusters of bacterial cells were also visible in the mucus cocoon by SEM and TEM (fig. S2, B and D). Staining with anti-PCNA antibody revealed active proliferation of cells with flattened morphology located in the outer edge of the cocoon (Fig. 2G). Single cell

suspensions of mucus cocoon samples stained with propidium iodide (PI) or activated caspase-3 confirmed that the cocoon is composed of viable cells with only 7% cells being PI-positive and 2% being activated caspase-3-positive (Fig. 2H).

Previous studies on amphibian cocoons noted the presence of bacteria both on the outer surface as well as the deeper layers of the cocoon (MacCanahan et al, 1976). Thus, we hypothesized that the lungfish cocoon serves as a protective barrier against bacteria to protect lungfish during aestivation. Relative quantification of bacterial loads by qPCR showed that the cocoon contained approximately 3 orders of magnitude higher bacterial loads than the control and terrestrialized skin samples (Fig. 2I). In support, fluorescence *in situ* hybridization (FISH) using universal eubacterial oligoprobes (EUB338) revealed few bacterial cells in the skin of freshwater lungfish or in the skin of terrestrialized animals (Fig. 2J and K). In contrast, large clumps of bacteria were present in the cocoon (Fig. 2L). In support of the idea that the cocoon is a living tissue, in all cocoon samples examined we found active transcription of epithelial cell markers (*ck8*, used as house-keeping gene), antimicrobial peptide genes (*defb1-4*), proinflammatory cytokines (*il1b* and *il8*), goblet cell markers (*muc2*, *muc4*, and *csta*), and granulocyte markers (*cxcr2*, *elane, h2a,* and *mpo)* (Fig. 2M). Expression levels of the antimicrobial peptide genes *defb1* and *defb2* (6-fold and 9-fold, respectively, compared to *ck8*) were the highest of all genes examined. Combined, these results reveal that lungfish terrestrialization involves the production of living cellular cocoon that traps bacteria and actively transcribes genes to provide prolonged antimicrobial protection.

5. Terrestrialization induces a proinflammatory environment in the lungfish skin

The drastic tissue remodeling observed during physiological terrestrialization suggested profound changes in the skin transcriptional program of lungfish. Transcriptomic analysis on the

skin of freshwater and terrestrialized fish (n = 4) showed unique transcriptional profiles in each group, with a total of 1560 genes differentially expressed in the skin of terrestrialized lungfish compared to freshwater animals using DESeq and 713 genes using EdgeR analyses (Fig. 3, A and B). Gene ontology analysis identified 13 significantly regulated biological processes in lungfish skin due to terrestrialization using both DESeq and EdgeR pipelines. The identified biological processes included immune response, response to hypoxia, signal transduction, and negative regulation of apoptotic process (Fig. 3C). Among the up-regulated immune genes, a canonical pro-inflammatory signature characterized by *il8*, *il1β*, *mif, mpo*, *ccl20*, and *cd209* expression was associated with terrestrialization. Conversely, down-regulation of the neutrophil elastase inhibitor *serpinb1*, mucin 16 (*muc16*) a marker for goblet cells, anticoagulant molecule annexin A5 (*anxa5*) and genes related to antigen presentation such as *b2m*, *hla-drb1*, *hla-a*, *gp2*, and immunoglobulin K light chain (*igk*) was associated with terrestrialization (Fig. 3, D and E). Together these results show that terrestrialization leads to dramatic skin tissue remodeling in lungfish creating a pro-inflammatory environment which favors granulocyte recruitment from circulation into the integument.

6. Lungfish granulocytes produce extracellular traps (ETs)

From plants to mammals, extracellular trap formation is one of the most ancient and conserved mechanisms of innate immunity (Abi Abdallah et al. 2012; Guimarães-Costa et al. 2012; Biermann et al. 2016; Lázaro-Díez et al. 2017). ETs are DNA structures released due to chromatin decondensation and decorated by histones and up to 30 different globular proteins (Brinkmann et al, 2004; Clark et al. 2007; Delgado-Rizo et al, 2017; de Bont et al. 2019). ETs play critical roles in infection, inflammation, injury, tissue remodeling, and autoimmunity (Saitoh et al, 2012; Kruger et al. 2015; Daniel et al, 2019, Binet et al, 2020). In humans, presence of ETs in the skin has been

described in several pathological states including delayed wound healing in diabetes (Wong, 2015), psoriasis (Lin et al, 2011; Hu et al, 2016; Shao et al, 2019), and systemic and cutaneous lupus erythematosus (Hoffmann and Enk, 2016; Safi et al., 2019). Using immunofluorescence staining with anti-ELANE and anti-MPO antibodies, we found that PMA-stimulated gut cell suspensions of freshwater lungfish form ETs that were inhibited upon treatment with the ETosis inhibitors diphenyliodonium chloride (DC) or cytochalasin A (Cyto) (fig. S4, A to C). In terrestrialized animals, skin cell suspensions stimulated with PMA contained 40-60% of the cells undergoing ETosis. Lungfish ETs in skin cell suspensions stimulated with PMA had cloud-like or spike-like morphologies. Treatment with the inhibitors DC and Cyto prior to PMA stimulation resulted in similar percentages of cells undergoing ETosis as in the unstimulated controls (Fig. 4, A to C). TEM examination of terrestrialized skin revealed the presence of dying granulocytes with extracellular DNA and bacterial cells in very close proximity (fig. S4D). Interestingly, we could not observe any ETosis events in cocoon single cell suspensions, suggesting that granulocytes that have transmigrated into the cocoon likely produce ETs and die in a short period of time and therefore they are unresponsive to further PMA stimulation (data not shown). Combined, these experiments suggest that during terrestrialization, the skin of lungfish recruits granulocytes with potent antimicrobial functions that, along with the cocoon, protect lungfish from microbial invasion for prolonged periods of time.

7. Removal of eDNA leads to skin hemorrhages, dysbiosis and systemic bacterial dissemination

In plants, roots exposed to a root-rotting fungal pathogen and treated with DNase I suffer from severe root necrosis (Wen et al. 2009). To determine the impact of skin ETosis on lungfish terrestrialization, DNase I treatment was performed *in vivo* by surface spraying the lungfish once

a day to deplete eDNA. Spraying treatment effectively eliminated the ability of terrestrialized lungfish skin cell suspensions to form ETs following PMA stimulation (Fig. 4D). DNase I treatment during terrestrialization lead to deleterious effects on lungfish including skin lesions, reddening, head edema, and a prolapsed anus (Fig. 4, E and F). Upon closer investigation of blood smears, we found that DNase I treatment was associated with presence of large numbers of bacterial cocci in circulation, a sign of septicemia (Fig. 4G). These pathologies occurred despite the fact that granulocytes of DNase I treated terrestrialized animals still entered systemic circulation (Fig. 4H). EUB338 FISH staining of DNase I treated skin and cocoon cryosections showed large numbers of bacteria that were able to penetrate through the cocoon and reach the skin (fig. S4, E and F). Elimination of eDNA also caused drastic morphological changes in the terrestrialized skin and cocoon, with severe signs of skin necrosis and disorganized structures (Fig. 4, I and J). Terrestrialization causes a significant increase in the gene expression of antimicrobial peptides, granulocyte marker genes, and proinflammatory markers in the skin. Importantly, *in vivo* DNase I treatment did not significantly impact the expression of *il1β, il8, elane* and *defb2-4*, but resulted in increased mRNA expression levels of *defb1* and *h2a* (Fig. 4, K to N and fig. S4, G to K). Antimicrobial peptides such as LL37 and α-defensin play active roles in NETosis formation, stabilization and function (Neumann et al, 2014a and 2014b; Chu-Sung Hu, S. et al 2016; Hosoda et al, 2017). Thus, lungfish ETs appear to resemble mammalian NETs, where decondensed DNA is associated with elane, mpo and histones. Whether β-defensins are part of the ET complex in lungfish requires further investigation but our data point towards a potential role of β-defensins in skin ETosis in lungfish. Collectively, these results show that eDNA in lungfish skin is essential for microbial control and successful terrestrialization.

ETs trap and inactivate bacteria (Brinkmann et al. 2004). We hypothesized that confining bacteria to the outer cocoon layer may be beneficial to aestivating lungfish in order to conserve energy reserves. Microbiome analysis showed that the mucus cocoon has a distinct microbial community compared to that of control and terrestrialized skin. Shannon diversity index indicated that the control and terrestrialized skin have a higher microbial diversity than the rest of the samples including the cocoon, DNase I treated skin and DNase I treated cocoon (Fig. 5A and fig. S5A). At the phylum level, the microbial communities of all were largely dominated by Proteobacteria which accounted for 75.4% and 65.5% of all diversity in the control and terrestrialized skin, and 82.5% of the total diversity in the cocoon (Fig. 5B, Supplementary Table 2). Importantly, no significant changes at the phylum level were detected between the freshwater skin and the terrestrialized skin bacterial communities (Fig. 5B and Supplementary Table 2), suggesting that the cocoon effectively confines bacteria outside the lungfish body during terrestrialization. In support, the cocoon microbial community was enriched in members of the families *Comamonadaceae*, *Methylophilaceae*, and *Xanthomonadaceae* compared to the skin samples (Fig. 5C and Supplementary Table 3). A total of 37 different operational taxonomic units (OTUs) were identified to be significantly different among all treatment groups (Fig. 5D). DNase I treatment resulted in profound changes in the microbial community composition of the cocoon, particularly in the phyla Actinobacteria, Bacteroidetes and Firmicutes. Specifically, significant increases in abundance of Actinobacteria ($p = 0.021$) and Firmicutes ($p = 0.046$) were observed in the DNase I treated cocoon compared to the untreated cocoon. The abundance of Tenericutes decreased from 1% in the untreated cocoon to 0% in the DNase I treated cocoon ($p = 0.007$) whereas Bacteroidetes abundance decreased from 7% of the untreated cocoon to 1.2% in the DNase I treated cocoon ($p = 0.231$). In terrestrialized skin, DNase I treatment resulted in several

changes that were not significant due to high interindividual variability. This may be due to the fact that each lungfish was maintained in an individual tank to avoid physical attack. Yet, a trend to increased Proteobacteria abundance (65.5% in control terrestrialized skin vs 88.9% in DNase I treated terrestrialized skin, p = 0.43) and decreased Acinobacteria abundance (10.5% in control terrestrialized animals vs 1.3% in DNase I treated animals, p=0.08) and Firmicutes abundances (7% in terrestrialized skin to 3.9% in the DNase I treated terrestrialized skin) (p = 0.78) was observed (Supplementary Table 2). The dysbiosis caused by DNase I treatment was evident at the family and genus levels (Fig. 5, C to E and fig S5, B and C, Supplementary Table 3 and 4). Increased abundances of pathogenic taxa such as*, Stenotrophomonas sp.* and *Aeromonas sp.* were observed in the skin and cocoon treated with DNase I (Fig. 5E). The relative abundances of *Variovorax sp., Methylophilus sp.* and *Limnobacter sp.* overall decreased as a result of DNase I treatment in both the skin and the cocoon (Fig. 5E, Supplementary Tables 3 and 4). These results indicate that eDNA is critical for the maintenance and control of the cocoon and skin microbial communities of lungfish during terrestrialization.

8. Conclusions

Our study unravels striking adaptations of the lungfish immune system to support the physiological process of terrestrialization. In many ways, the tissue remodeling and inflammation that takes place in the lungfish skin recapitulate mucosal inflammatory disorders and dermatological diseases described in mammals characterized by granulocyte infiltration of epithelia, granulocyte transmigration and production of ETs (Sumagin et al., 2014; Hoffmann and Enk, 2016). Yet, lungfishes are able to physiologically induce this inflammatory process every dry season; their mucosal barriers restoring once water returns. Thus, our findings may reveal new mechanisms by which barrier tissues are remodeled and restored following inflammatory damage.

Finally, our study reveals a remarkable new form of antimicrobial defense consisting of an outer living tissue that envelopes the lungfish body and traps bacteria. Since lungfish can survive on land inside their cocoons for years and our study was limited to the first two weeks of aestivation, we cannot conclude for how long this outer layer effectively protects lungfish against infection. It appears, however, that this extracorporeal bacterial trapping device is likely advantageous in aestivating animals during metabolic torpor.

9. Materials and Methods

Animals

Juvenile *Protopterus dolloi* (slender lungfish) (0.3-1 kg) were obtained from ExoticFishShop.com (https://exoticfishshop.net/) and maintained in individual 10 gallon aquarium tanks with dechlorinated water and a mixture of sand/gravel substrate, at a temperature of 27-29 °C. Fish were acclimated to laboratory conditions for 4 weeks before being used in experiments. During this acclimation, fish were fed one earth worm every third day, with feeding terminated 48 h before the start of terrestrialization experiments. All animals used in this study were sampled between 8AM and 11AM. All animal studies were reviewed and approved by the Office of Animal Care Compliance at the University of New Mexico (protocol number 11-100744-MCC).

Terrestrialization

After acclimating to laboratory settings, feeding was stopped and the water level in tanks were lowered to 20 cm and allowed to naturally evaporate (Sturla et al. 2002). With the cessation of food and the lowering of water, the fish entered the induction phase of terrestrialization and began to hyperventilate and profusely secrete mucus from their gills. Secreted mucus combined with the substrate in the tank formed a mucus cocoon that hardened 10 days after the start of the

induction phase. Due to the extreme dry climate of New Mexico, the protocol was modified, and the fish tanks were sprayed with 1-2 mL of water every third day to avoid severe dehydration.

DNase I Treatment

In order to eliminate extracellular DNA, 1U of DNase I in PBS (Worthington, Lakewood, NJ) was administered to the terrestrializing fish (n = 3) by spraying 1-2 mL per day, starting at the beginning of the induction phase until sampling 10 days later. Control terrestrialized fish were sprayed once a day with 1-2 mL of PBS.

Tissue Sampling

Lungfish mucus cocoon was peeled off with sterile forceps and divided into six pieces. One piece was fresh-frozen, the second embedded in Tissue-Tek OCT compound (Sakura Finetek), a third fixed in 4% paraformaldehyde (PFA) for histology, a fourth piece was placed in 1 mL of sucrose lysis buffer (SLB) for microbiome analysis, the firth piece was preserved in RNAlater (ThermoScientific) for molecular analysis and the last piece was subject to cell isolation in Dispase I as explained below. Once the mucus cocoon was removed, the animals were euthanized with blunt force to their second cervical vertebra and then bled through their caudal vein for blood smears. Skin, gut, kidneys and gonads were dissected and fixed in 4% PFA for histology. A piece of each organ was also placed in 1 mL of RNAlater for gene expression analyses. Additionally, a 2 cm x 2 cm piece of the skin and gut were used for cell isolation and a final 0.5 cm x 0.5 cm piece was placed in sucrose lysis buffer (SLB) for DNA extraction and microbiome sequencing.

Cell Isolation

Cells from the skin and mucus cocoon were isolated by enzymatic treatment as explained elsewhere (Xu et al, 2013). Briefly, samples were excised in small pieces with sterile scissors and placed in 10 mL of DMEM containing 5% fetal bovine serum (FBS, Peak Serum, Wellington, CO), penicillin/streptomycin (P/S, Gibco) and 5 mg/mL Dispase I (Worthington Biochemical Corporation) and incubated at 4 °C on a shaker for 3 h. Supernatants were collected and filtered through a 100-µm nylon cell strainer into a new 50 mL Falcon tube and kept on ice. Ten mL of fresh dispase I solution were then added to the tubes containing the tissue pieces and incubated for another 3 h at 4 °C on a shaker. Supernatants were filtered and combined and the remaining tissue pieces were grounded through the cell strainer with a sterile syringe plunger. Cells were spun down at 400g at 4 °C for 10 min, supernatants discarded, and the cell pellets were washed twice in DMEM containing 5% FBS and P/S. For isolation of gut granulocytes in freshwater lungfish, a 1 cm-long piece of the gut was dissected, placed in DMEM containing 5% FBS and P/S, minced into small pieces and filtered through 100-µm nylon cell strainer while mashing the tissue with a sterile syringe plunger. Cells were washed twice in DMEM containing 5% FBS and P/S. Cells were counted under a hematocytometer and adjusted to 10^6 cells/mL. Cell suspensions were then used for cell viability and active caspase-3 staining by flow cytometry or seeded onto slides for ETosis assays.

Flow Cytometry

The viability of the cells isolated from either skin or cocoon samples was quantified by staining 10^5 cells with 1:500 dilution of propidium iodide (PI) solution (1 mg/ml, Sigma). A total of 30,000 events per sample were recorded in an Attune NxT Flow Cytometer (Life Technologies). Cell death was quantified as the percentage of PI^+ cells. To determine apoptosis in skin and cocoon cell suspensions, 10^5 cells of each cell suspension were fixed in 2% PFA for

15 min at room temperature and then permeabilized and blocked using the Perm/Wash Buffer (BioRad). Next, cells were stained with rabbit anti-human caspase-3 antibody (ab13847, Abcam) (1:200 dilution), washed three times in Perm/Wash Buffer and labeled with secondary antibody FITC donkey anti-rabbit IgG (711-095-152, Jackson ImmunoResearch) (1:200 dilution). After three washes, cells were resuspended in Perm/Wash and 30,000 events were recorded in the Attune NxT Flow Cytometer.

ETosis assays

Cell suspensions (50,000 cells/slide) isolated from gut, skin and mucus cocoon were seeded onto slides for 30 min at 27 °C in 5% CO_2. Positive controls consisted of cells treated with phorbol 12-myristate 13-acetate (0.1 μM, PMA) for 3 h at 27 °C in 5% CO_2 without inhibitors. Additionally, cells were treated with PMA and either the inhibitor cytochalasin (10 μM, Cyto) or diphenyleneiodium chloride (2 μM, DC) diluted in culture medium (DMEM + 5% FBS + P/S). Negative controls received culture medium only. All slides were fixed in 4% PFA for 30 min at room temperature and stained for ETosis markers visualization as explained below.

Histology and light microscopy

Skin, gonads, and gut samples from free-swimming and terrestrialized fish (n = 3) were fixed in 4% PFA overnight, transferred to 70% ethanol, and embedded in paraffin. Sections were stained using hematoxylin and eosin or Periodic acid-Schiff stain for general morphological analyses. Serial coronal sections of one control cocoon and one DNase I treated cocoon were performed to estimate thickness of the cocoon. Large field images for cocoon samples stained for hematoxylin and eosin were acquired on a Brightfield Images were captured on a Keyence BZ-X700 digital microscope. Multiple images were taken across the entire cross section using a 20X objective, and compiled into a single image using proprietary stitching software from the

manufacturer. Blood smears were fixed in 100% methanol for 60 s and stained in 1:10 dilution of Giemsa solution (Sigma Aldrich) in tap water for 50 min. Quantification of granulocytes in Giemsa stained blood smears was performed in 10 fields of view per animal with 3 animals per treatment by two different persons in a blind fashion. For myeloperoxidase staining, skin and cocoon cryosections were fixed for 1 min in 10% formal-ethanol and washed in tap water for 30 s. Slides were stained in myeloperoxidase stain mixture (Kaplow, 1965) for 30 s, washed briefly for 15 s and mounted in DPX (Sigma Aldrich). Images were acquired and analyzed with a Nikon Eclipse Ti-S inverted microscope and NIS-Elements Advanced Research Software (Version 4.20.02).

Immunofluorescence microscopy

Cryoblocks were sectioned (5 µm thick) and stored at -80°C until processing. Cryosections were post-fixed with 4% PFA for 3 min followed by 5 min rinse in tap water. Slides were blocked in StartingBlock T20 buffer (Pierce) for 15 min at room temperature and incubated in each of the corresponding primary antibodies (see Table 1) diluted in PBT (PBS containing 0.5% Triton X-100 and 0.1% bovine serum albumin) overnight at 4 °C. For detection of ETs, slides containing treated and untreated cell suspensions were stained with anti H2A antibody labeled with Mix-n-Stain™ CF™ 555 Antibody Labeling Kit (Milipore Sigma), anti-MPO antibody or anti-ELANE antibody. After three washes in PBS, slides were incubated with secondary antibody Alexa Fluor 647-conjugated donkey anti rabbit IgG (Abcam, ab150075) for 2 h at room temperature in the dark. Slides were washed twice in PBS and stained with DAPI (4,6-diamidino-2-phenylindole; 1 µg/mL in water; Invitrogen) for 60 s. After rinsing in water, slides were mounted in KPL fluorescent mounting media (Sera Care) and observed under a Zeiss LSM 780 laser scanning confocal microscope.

Primary Antibody	Dilution
Proliferating cell nuclear antigen (PCNA)	1:500
Myeloperoxidase (MPO)	1:200
Histone 2Az (H2A)	1:200
Neutrophil Elastase (ELANE)	1:200
CF555 labeled H2A	1:100

Table S1: Primary antibodies used for immunofluorescence staining.

16S Fluorescence In Situ Hybridization

Cryosections (10 sections/animal, n=3) were fixed in 10% formaldehyde for 20 min, washed twice in PBS and permeabilized in 70% ethanol overnight at 4 °C. Slides were hybridized with 5'-end-Cy5-labelled EUB338 (anti-sense probe) and 5'-end-Cy5-labelled NONEUB (control sense probe complementary to EUB338) oligonucleotide probes (Eurofins Genomics). Hybridizations were performed at 37 °C for 8 h in hybridization buffer (2 × SSC/10% formamide) containing 1 μg/mL of the labeled probes. Slides were then washed with hybridization buffer without probes followed by two more washes in washing buffer (2 × SSC) and two washes in PBS at 37 °C. Nuclei were stained with DAPI (2.5 μg/mL, Invitrogen) for 30 min at 37 °C, washed twice in PBS at 37 °C and mounted in KPL fluorescent mounting media (Sera Care). Sections were observed under a Zeiss LSM 780 laser scanning confocal microscope. Images are shown as maximum projections of the Z-stacks (5 stacks, of 5 microns each).

Scanning and Transmission Electron Microscopy

Skin from control and skin and cocoon samples from terrestrialized fish were fixed in formaldehyde/glutaraldehyde, 2.5% in 0.1M sodium cacodylate buffer, pH 7.4 (Electron Microscopy Sciences, Hatfield PA) overnight at 4°C. Samples were then washed three times in

sodium cacodylate buffer and post-fixed using 1% osmium tetroxide for 1 h and washed in sodium cacodylate buffer. Samples were then dehydrated through a graded ethanol series, for 1 h and coated in gold-palladium. Samples were analyzed on a JSM-IT100 InTouchScope scanning electron microscope. For transmission electron microscopy, control and infected skin *P. dolloi* (n = 2) were fixed overnight at 4 °C in 2.5 % (v/v) glutaraldehyde in PBS, then transferred to 1% osmium tetroxide (w/v) in PBS for 2 h, at 4 °C. Samples were washed in PBS three times for 10 min, then dehydrated in a graded series of ethanol (10–100 %) through changes of propylene oxide. Samples were then embedded in Epon resin, sectioned and stained with uranyl acetate and lead citrate before being examined in a PHILIPS ECNAI 12 transmission-electron microscope.

RT-qPCR

Tissue from free-swimming and terrestrialized lungfish (n = 3-4) was collected using sterile dissecting tools and preserved in 1mL of RNAlater. Total RNA was extracted from each sample using TRIzol reagent (Invitrogen) and following the manufacturer's instruction and 1µg of RNA was synthesized into cDNA as described in (Tacchi et al. 2013). The final cDNA was stored at -20 °C. Expression levels of granulocyte markers *h2a, csta, cxcr2, mpo*; proinflammatory cytokines *il1b, il8*; mucins *muc2* and *muc4*; and antimicrobial peptides *defb1-4* were measured by quantitative real-time PCR (RT-qPCR) using primers shown in Table 2. Beta actin *(β-actin*), phosphoglycerate kinase 1 (*pgk-1*) and cytokeratin-8 (*ck8*) were used as the house-keeping genes.

Genes	**Sequences (5'-3')**
*β-actin*_F0	GCCTCTGGTCGAACAACTGG
*β-actin*_R1	GGAGGATGCAGCAGTAGCCA

*h2a*_F1	CGGACATGATTATTGCAGCTAT
h2a _R1	GCTTTTGGCTTGGATGTCTTT
*csta*_F1	GGTACTTCTGAAGTCAAGCCTG
*csta*_R1	GGATGTTATGCAAACTTACTTCTT
*cxcr2*_F1	GCAAAGACAGTAATATTGTTTGG
*cxcr2*_R1	GCATCAGTAACAGACAAATGG
*il1b*_F0	CCACCTGTCTATGTACAAATCACG
il1b _R0	GCAGACTCAAACCTGGAGGAG
*il8*_F0	CCTCCTGTGCTGTGTGACTGT
*il8*_R0	GGAACTTTCCAACATTCTGTCG
*mpo*_F1	GCCCAACTGCAGATCATAACG
*mpo*_R1	GGTGCTCTTGGAAGGCTTCA
*defb1*_F1	GGAGTTATTGGTGAAAAAGATGG
*defb1*_R1	GCAGATCTTCTACGTACACAACACC
*defb2*_F1	GGAATAATCAGTGAACAAGATGGAG
*defb2*_R1	GGAATCATTTAGGTGTGCAGCA
*defb3*_F1	GGTGCATTTCAAAAGTATCGAGACAC
*defb3*_R1	GTTTTGGTGTGCAGCATCTCC
*defb4*_F1	GGAGTTAATGTGGAGGCTCATT
*defb4*_R1	CCAAGTTCTTCATGTTAGACAGC
muc2_F0	GCTGTTTCCATTACGAATGTGAAG
*muc2*_R0	CCTCTGTGTGGTACAAATCCTTC
*muc4*_F0	GGAAATGGGACTCCTTTTATGAC

*muc4*_R0	CCTGAGCTAGTGGAGATTCCTTG
ck8_F1	GCTGAACTAACCAGGTACATC
ck8_R1	GGTGGCAATTTCAATGTCTAGG
pgk-1_F1	GCAAAACAGATTGTATGGAATGGA
pgk-1_R1	GGCACAGCATGTGGCTGTATC

Table S2: Primers used in this study for RT-qPCR.

RNA Sequencing and Assembly

Extracted RNA was cleaned of genomic DNA contamination using Turbo DNase (Invitrogen, Thermo Fisher Scientific, Waltham MA). Illumina libraries were constructed using Kapa mRNA HyperPrep Kits (Roche Sequencing, Pleasanton, CA) and sequenced on an Illumina NextSeq 500 at the University of New Mexico Biology Molecular Core Facility. Quality of fastq files were assessed using FastQC (Andrews 2010), poor quality reads were trimmed by Trimmomattic using default parameters (Bolger et al. 2014). The trimmed ends were assembled into *de novo* transcriptomes using Trinity (Grabherr et al. 2011; Haas et al., 2013). The success of the assembly was determined by realigning the raw fastq reads to the corresponding assembled transcriptome using BWA (Li and Durbin, 2009) and samtools (Li et al. 2009). Differential gene analysis was assessed through DESeq and EdgeR in R. Gene ontology analysis was performed using the bioinformatic database DAVID (Huang et al., 2009) and scatterplots were made in R.

Microbiome Sequencing and Analysis

Whole genomic DNA was extracted using the cetyltrimethylammonium bromide method previously described by Mitchell et al. (Mitchell et al., 2008) and DNA concentration and purity were assessed by a Nanodrop ND 1000 (Thermo Scientific). Skin and cocoon microbial

communities were determined via PCR, where bacterial DNA was amplified using 5'PRIME HotMasterMix (Quantabio, Beverly, MA, USA) and primers 28f (5'-GAGTTTGATCNTGGCTCAG-3') and 519r (5'-GTNTTACNGCGGCKGCTG-3'), targeting the variable V1-V3 regions of the prokaryotic 16S rDNA gene. All DNA samples were amplified with three independent reactions and pooled before the clean-up.

Amplicons were purified using Axygen AxyPrep Mag PCR clean-up kit (Thermo Scientific) and eluted in nuclease free water to a final volume of 30 μL. Unique barcodes were ligated to the Illumina adapters via PCR using the Nextera XT Index Kit v2 Set A (Illumina). All DNA sample concentrations were quantified using the dsDNA HS assay kit and Qubit fluorometer (Invitrogen), then DNA were normalized to 200 ng/μL for DNA library pooling. Pooled samples were cleaned again using the Axygen PCR clean-up kit. Sequencing was performed on the Illumina MiSeq platform using MiSeq Reagent Kit v3 (600cycles) at the Clinical and Translational Sciences Center at the University of New Mexico Health Sciences Center. Sequence data was analyzed using Quantitative Insights Into Microbial Ecology (QIIME 1.9) pipeline (Caporaso et al., 2010) within the web-based platform Galaxy at the University of New Mexico. Operational Taxonomic Units (OTUs) were selected by open reference picking using the sumaclust method. OTUs were aligned in the SILVA 16S/18S database with a 97% identity. Rarefaction analysis was performed in QIIME using several alpha diversity metrics (PD_whole_tree, chao1, and observed_otus). Core diversity analysis was run with a normalized sampling depth of 10525 sequences. Alpha diversity metrics, non-phylogenetic and phylogenetic beta-diversity analyses were performed in QIIME using the Bray Curtis metric or the unweighted and weighted UniFrac, respectively. Principal coordinate analysis and taxonomic summaries were produced in QIIME to compare the bacterial communities in all tissue samples/groups.

Statistical Analysis

Data were expressed as mean ± standard error. Statistical analysis was performed by unpaired Student's t-test. Differences were considered statistically significant when $P < 0.05$. Statistical analyses were performed in Prism GraphPad version 6. For RT-qPCR assays, relative gene expressions were determined using the Pfaffl method (Pfaffl 2001).

10. Figures and Tables:

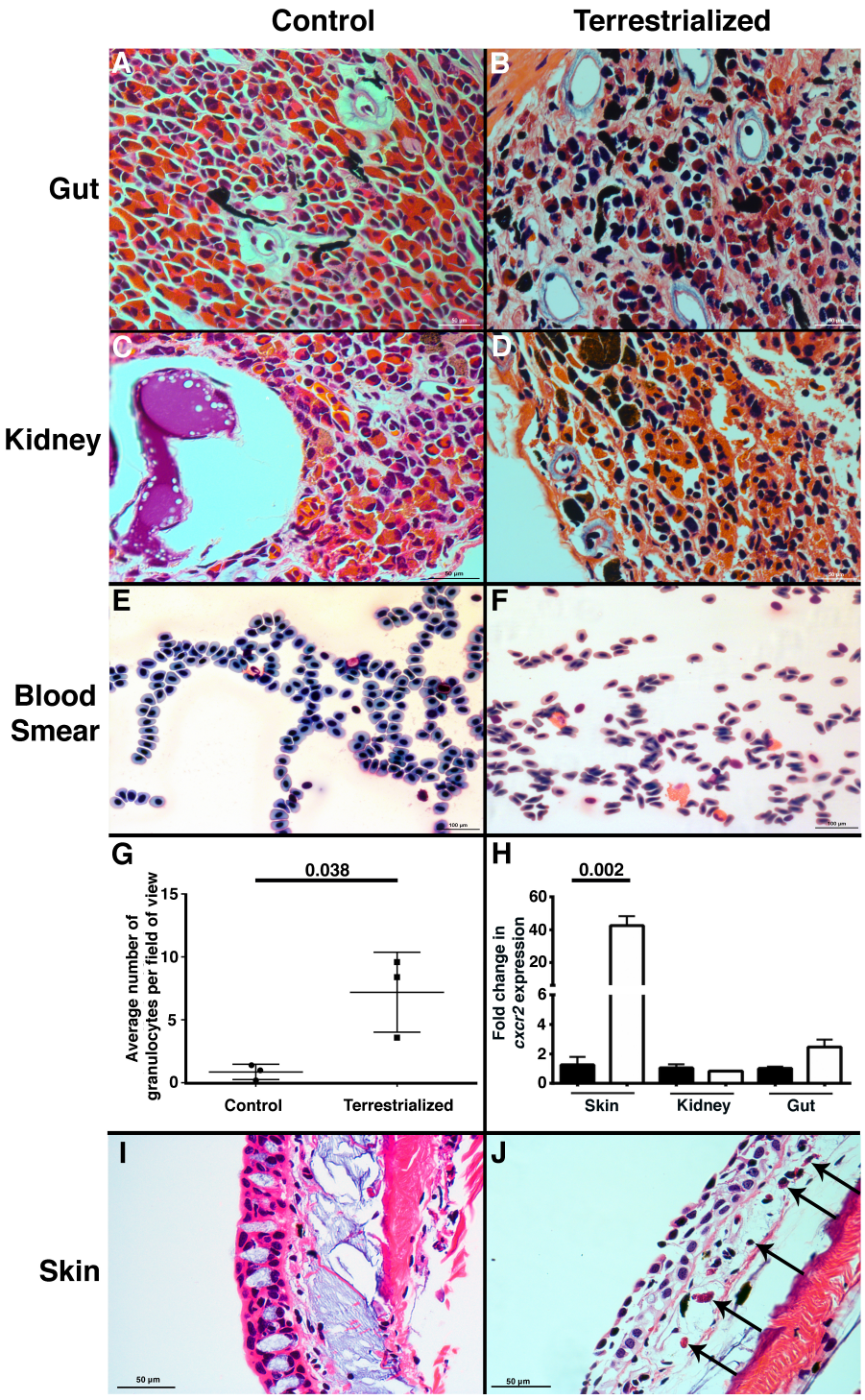

u

Figure 1: Lungfish terrestrialization results in the mobilization of granulocytes from reservoir tissues into the integument. H&E staining of control gut (**A**) and terrestrialized gut (**B**) and control kidney (**C**) and terrestrialized kidney (**D**) tissues of African lungfish (n = 3/group). Giemsa stain of control (**E**) and terrestrialized (**F**) lungfish blood smears. (**G**) Quantification of granulocyte counts in control and terrestrialized lungfish blood (n = 3 animals/group, 10 fields

were scored by two independent researchers). (**H**) Quantification of *cxcr2* mRNA levels by RT-qPCR in the skin, gut and kidney of control and terrestrialized lungfish (n = 3). H&E stain of control (**I**) and terrestrialized (**J**) skin of African lungfish showing infiltration of granulocytes (black arrows). (n = 3). Data were analyzed by unpaired Student's *t*-test.

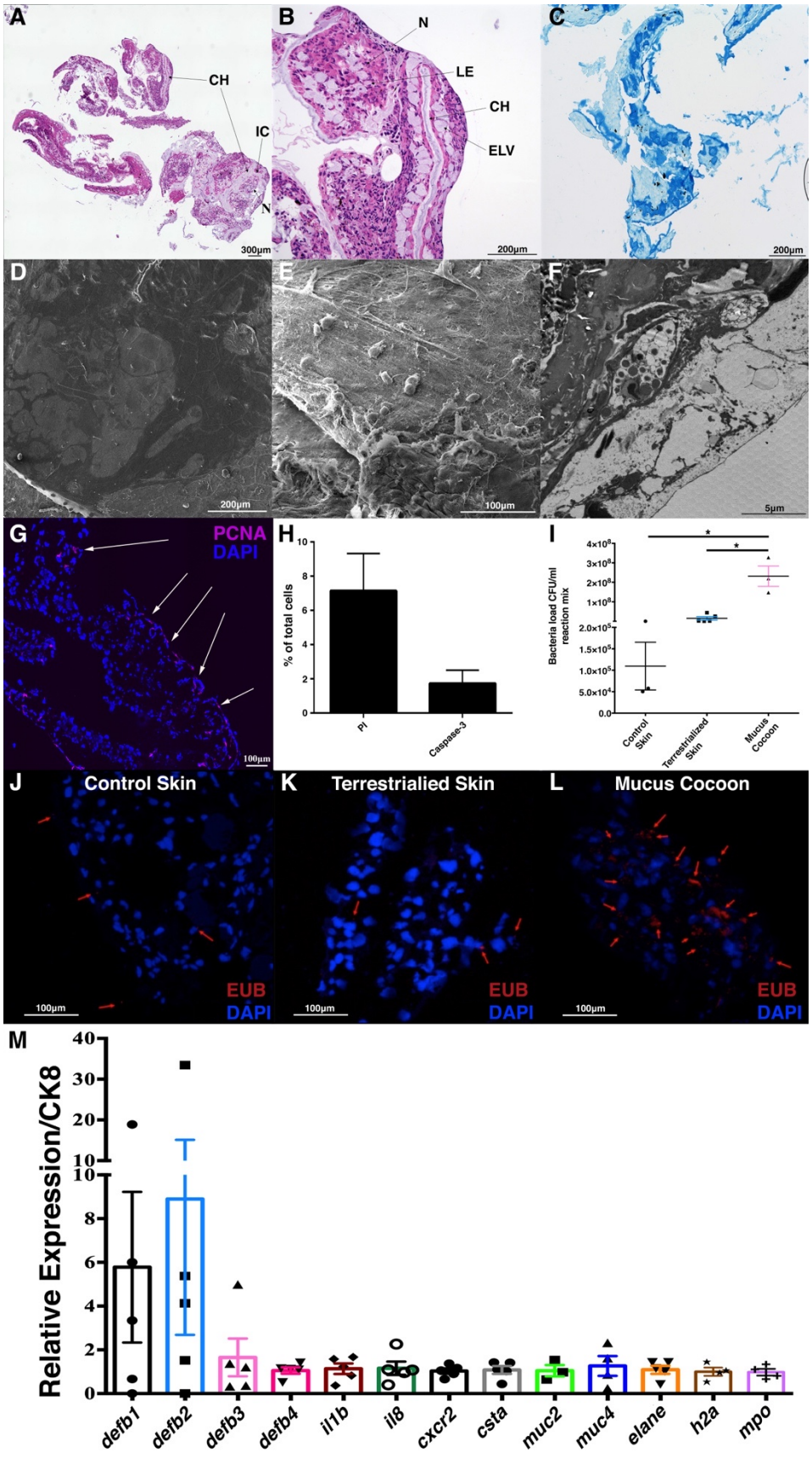
A
CH
IC
N
300μm
B
N
LE
CH
ELV
200μm
C
200μm
D
200μm
E
100μm
F
5μm
G
PCNA
DAPI
100μm
H
% of total cells
PI
Caspase-3
I
Bacteria load CFU/ml reaction mix
Control Skin
Terrestrialized Skin
Mucus Cocoon
J
Control Skin
EUB
DAPI
100μm
K
Terrestrialied Skin
EUB
DAPI
100μm
L
Mucus Cocoon
EUB
DAPI
100μm
M
Relative Expression/CK8
defb1
defb2
defb3
defb4
il1b
il8
cxcr2
csta
muc2
muc4
elane
h2a
mpo

Figure 2: The lungfish mucus cocoon is a living cellular structure that traps bacteria. (**A**) H&E staining of terrestrialized mucus cocoon (large image composite). (**B**) magnified view of composite in (A). N: Nest of cells; CH: channels; IC: intercommunicating channels; LE: loss of eosinophilia of nest cells; ELV: endothelium lined vessels. (**C**) Periodic Acid Schiff stain of lungfish mucus cocoon showing presence of goblet cell (dark blue) and mucus but no positive staining in the channels. Images are representative of n = 3 cocoons. (**D**) Coronal scanning electron microscopy image of control lungfish skin showing polygonal epithelial cells and the openings of goblet cells. (**E**) Coronal scanning electron microscopy image of terrestrialized lungfish skin with the intact cocoon showing presence of lungfish cells and bacterial cells. (**F**) Transmission electron micrograph of a terrestrialized mucus cocoon sample showing presence of a goblet cell with many secretory mucus granules with dense core. (**G**) Proliferating cell nuclear antigen (PCNA) staining (magenta) of the lungfish mucus cocoon showing the presence of proliferating cells at the edge of the cocoon (white arrows). Cell nuclei were stained with DAPI (blue). (**H**) Percent of propidium iodide $(PI)^+$ and activated caspase-3^+ cells in total cocoon cell suspensions. (**I**) Relative quantification of total bacterial loads by qPCR in control skin, terrestrialized skin and mucus cocoon (n = 3-4). Asterisk denotes statistically significant differences ($P<0.05$) by unpaired Student's *t*-test. (**J-L**) Maximum projection (1 μm-thick Z-stacks, 5 stacks) of confocal fluorescence images of FISH using EUB338 oligoprobe (red) showing presence of bacteria in control skin, terrestrialized skin, and mucus cocoon of lungfish. Images are representative of 10 fields/sample, n = 3 animals. (**M**) Gene expression of antimicrobial peptide genes (*defb1-4*), proinflammatory cytokines (*il1b, il8*), the anti-apoptotic cysteine proteinase inhibitor *csta* usually expressed by epithelial cells, keratinocytes or granulocytes, the goblet cell markers (*muc2*, *muc4*) and granulocyte markers (*cxcr2*, *mpo*, *elane*), and *h2a* in the lungfish mucus cocoon by RT-qPCR. mRNA expression levels were normalized to cytokeratin 8 (*ck8*).

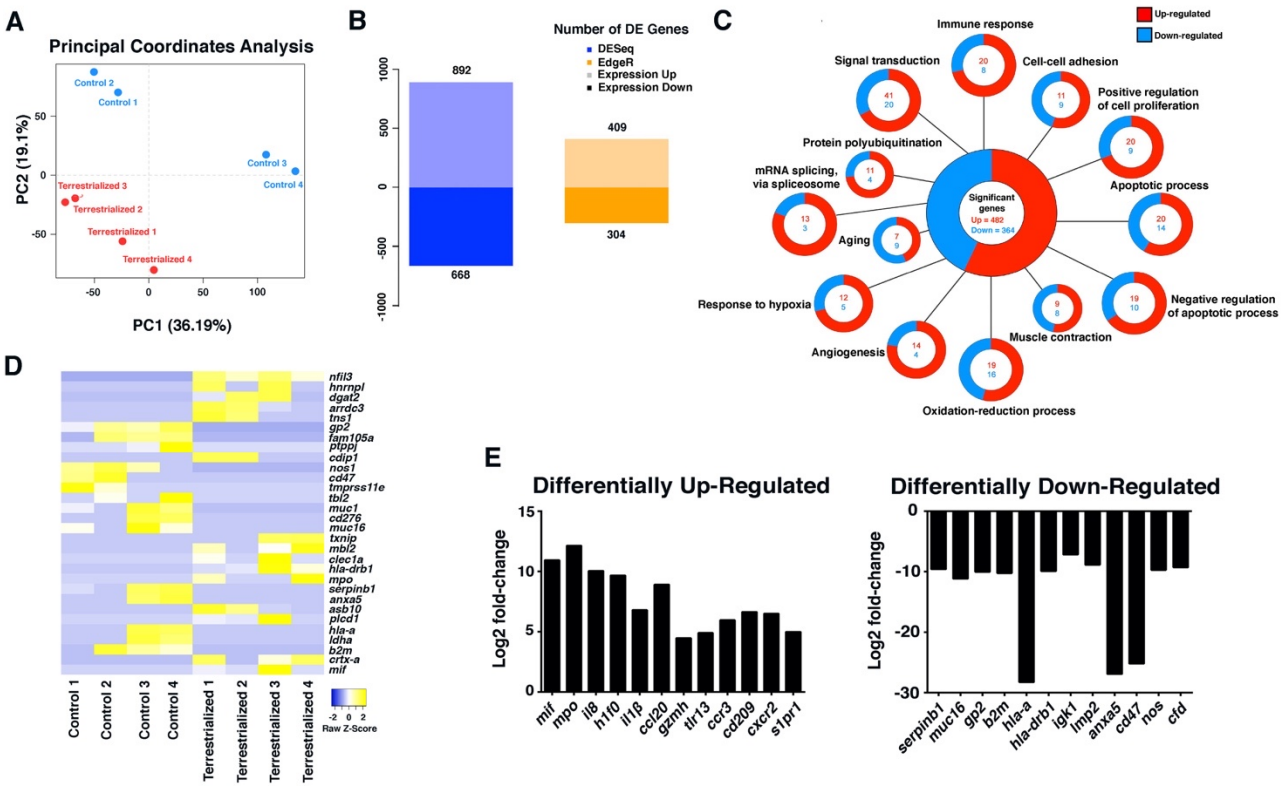

Figure 3: Terrestrialization results in a global pro-inflammatory state of the lungfish skin. (**A**) Principal component analysis of control and terrestrialized lungfish skin samples used in RNA-Seq analyses. (**B**) Number of differentially up- and down- regulated genes in control and terrestrialized lungfish skin using DESeq and EdgeR. (**C**) Gene ontology analyses of RNA-Seq results showing the top 13 significantly regulated biological processes in lungfish skin due to terrestrialization using both DESeq and EdgeR pipelines. (**D**) Heatmap of the top 30 significantly regulated genes in terrestrialized lungfish skin compared to controls. (**E**) Changes in gene expression (log2-fold) of the top 12 up and down regulated immune genes in terrestrialized lungfish skin compared to control free-swimming skin.

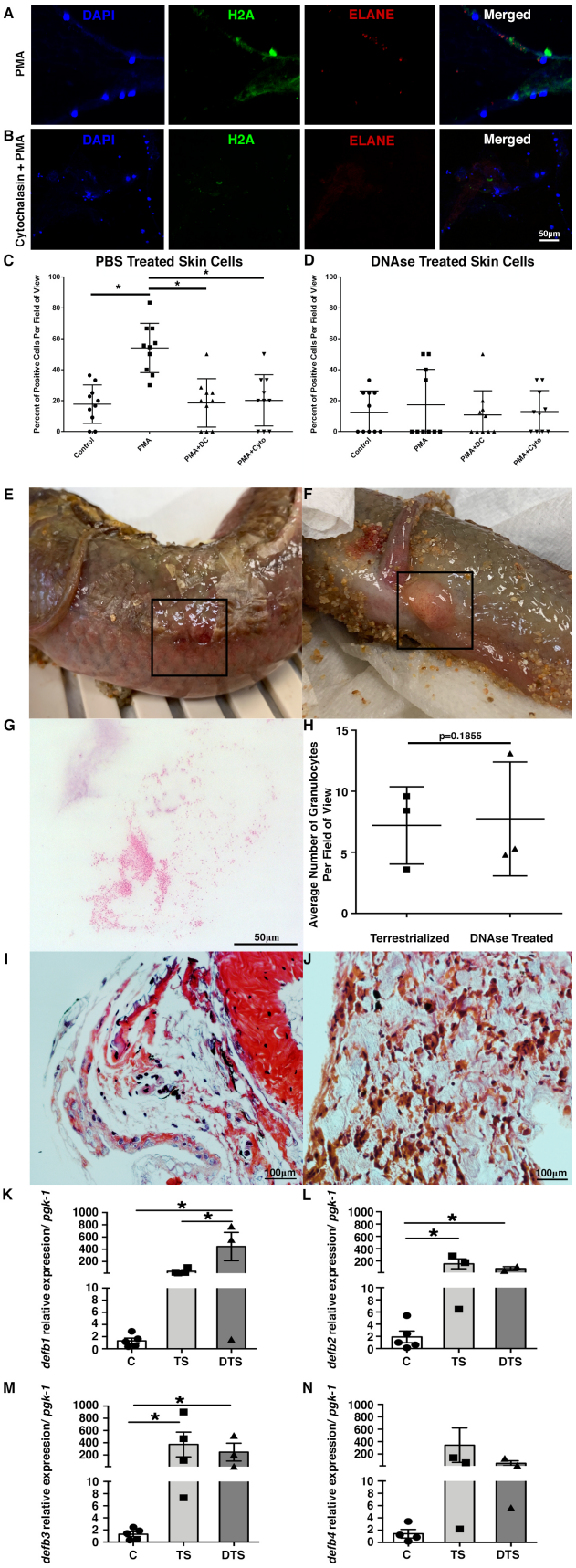
A
DAPI
H2A
ELANE
Merged
PMA
B
Cytochalasin + PMA
50μm
C
PBS Treated Skin Cells
D
DNAse Treated Skin Cells
Percent of Positive Cells Per Field of View
Control
PMA
PMA+DC
PMA+Cyto
E
F
G
50μm
H
p=0.1855
Average Number of Granulocytes Per Field of View
Terrestrialized
DNAse Treated
I
100μm
J
100μm
K
defb1 relative expression/ pgk-1
L
defb2 relative expression/ pgk-1
M
defb3 relative expression/ pgk-1
N
defb4 relative expression/ pgk-1
C
TS
DTS

Figure 4: Skin ETosis is essential for successful terrestrialization in lungfish. Terrestrialized lungfish skin cell suspensions (50,000 cells/treatment) were either not stimulated (control), stimulated with PMA, or stimulated with PMA and treated with the ETosis inhibitors diphenyliodonium chloride (PMA+DC), or cytochalasin A (PMA+Cyto). Cells were stained with DNA stain DAPI (blue), anti-histone 2A antibody (H2A) (green), anti-human neutrophil elastase antibody (ELANE) (red), and merged. (**A**) Representative confocal microscopy images of terrestrialized lungfish skin stimulated with PMA. (**B**) Representative confocal microscopy images of terrestrialized lungfish skin stimulated with PMA+Cyto. (**C**) Quantification of the percentage of cells undergoing ETosis in control terrestrialized lungfish skin (n = 2 fish). Asterisk denotes statistically significant differences ($P<0.05$) by unpaired Student's *t*-test. (**D**) Quantification of the percentage of cells undergoing ETosis in *in vivo* DNase I treated terrestrialized lungfish skin (n = 2 fish). Counts were performed in n = 10 fields per fish and treatment. Asterisk denotes statistically significant differences ($P<0.05$) by unpaired Student's *t*-test. (**E**) Skin lesion and (**F**) prolapsed anus in DNase I treated terrestrialized lungfish. (**G**) Giemsa stained blood smear of terrestrialized lungfish treated with DNase I showing large numbers of bacteria in circulation. (**H**) Quantification of average number of granulocytes in blood smears of control terrestrialized and DNAse I treated terrestrialized lungfish (n = 3). (**I**) Representative H&E stain of skin and (**J**) mucus cocoon of DNase I treated terrestrialized lungfish (n = 3). (**K-N**) Quantification of gene expression levels of antimicrobial peptide genes (*defb1-4*) in control free-swimming lungfish skin (C), terrestrialized lungfish skin (TS), and DNase I treated terrestrialized lungfish skin (DTS) (n = 3-5/group). Gene expression levels were normalized to the house-keeping gene *pgk-1*. Asterisks denote statistically significant differences ($p<0.05$) by unpaired Student's *t*-test.

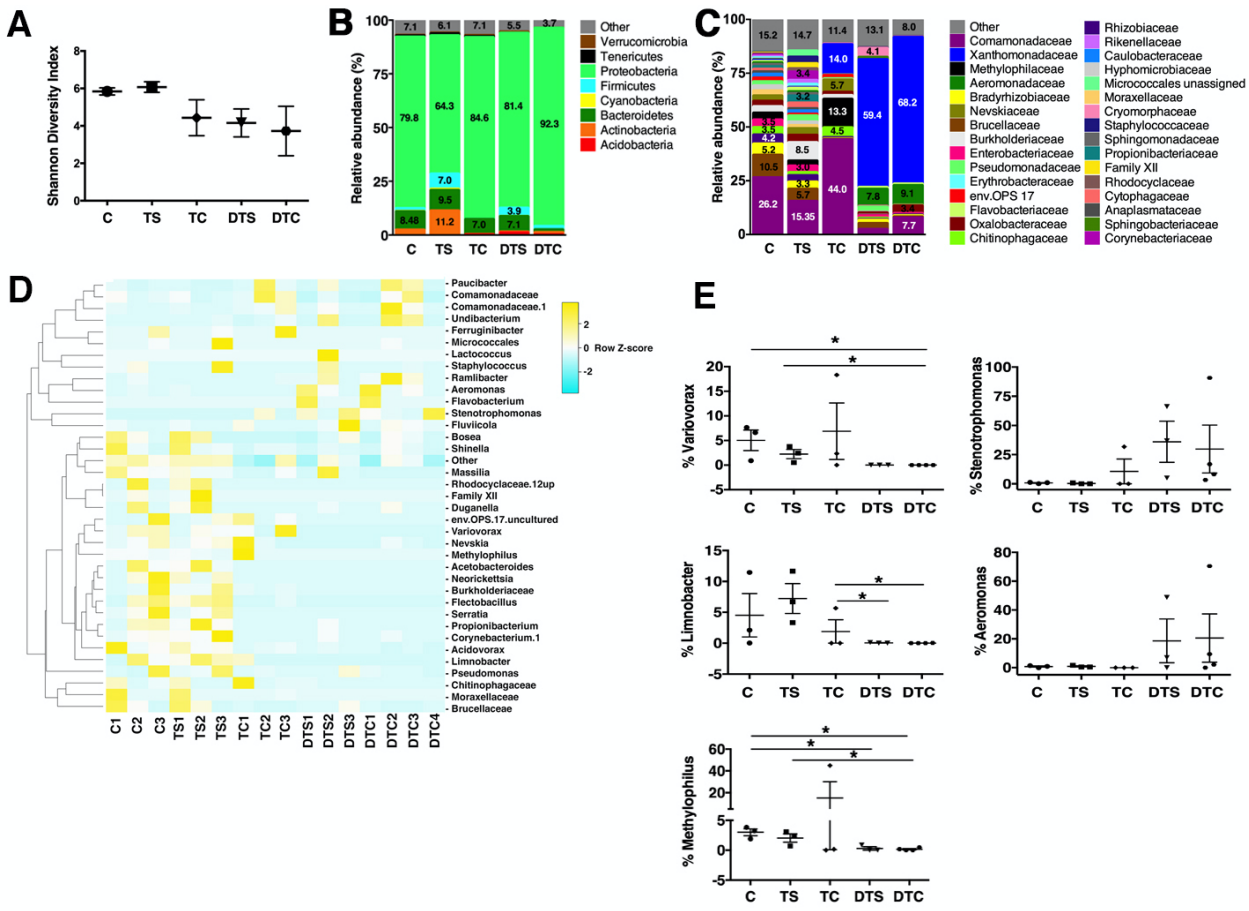

Figure 5: Lungfish cocoon harbors a unique microbial community and removal of extracellular DNA results in dysbiosis. (**A**) Shannon Diversity Index of the microbial communities of control free-swimming lungfish skin (C), terrestrialized lungfish skin (TS), terrestrialized cocoon (TC), DNase I treated terrestrialized lungfish skin (DTS), DNase I treated terrestrialized lungfish cocoon (DTC) (n = 3). (**B**) Microbial community composition at the phylum level of the microbial communities of control free-swimming lungfish skin (C), terrestrialized lungfish skin (TS), terrestrialized cocoon (TC), DNase I treated terrestrialized lungfish skin (DTS), DNase I treated terrestrialized lungfish cocoon (DTC). (**C**) Microbial community composition at the family level of the microbial communities of control free-swimming lungfish skin (C), terrestrialized lungfish skin (TS), terrestrialized cocoon (TC), DNase I treated terrestrialized lungfish skin (DTS), DNase I treated terrestrialized lungfish cocoon (DTC). (**D**) Heatmap of the top 36 bacterial genera with differential abundances in the bacterial communities of control free-swimming lungfish skin (C), terrestrialized lungfish skin (TS), terrestrialized cocoon (TC), DNase I treated terrestrialized lungfish skin (DTS), DNase I treated terrestrialized lungfish cocoon (DTC) ($P < 0.05$). The heatmap was generated using the online free tool Heatmapper using average linkage as a clustering method followed by the Spearman rank correlation for distance measurement. (**E**) Mean relative abundance at the genus level of *Variovorax sp.*; *Stenotrophomonas sp.*; *Limnobacter sp.*; and *Aeromonas sp.* in the microbial communities of control free-swimming lungfish skin (C), terrestrialized lungfish skin (TS), terrestrialized cocoon (TC), DNase I treated terrestrialized lungfish skin (DTS), DNase I treated terrestrialized lungfish

cocoon (DTC). Data were analyzed in Qiime 1.8. Differential abundances were determined by unpaired Student's *t*-test. *$P < 0.05$.

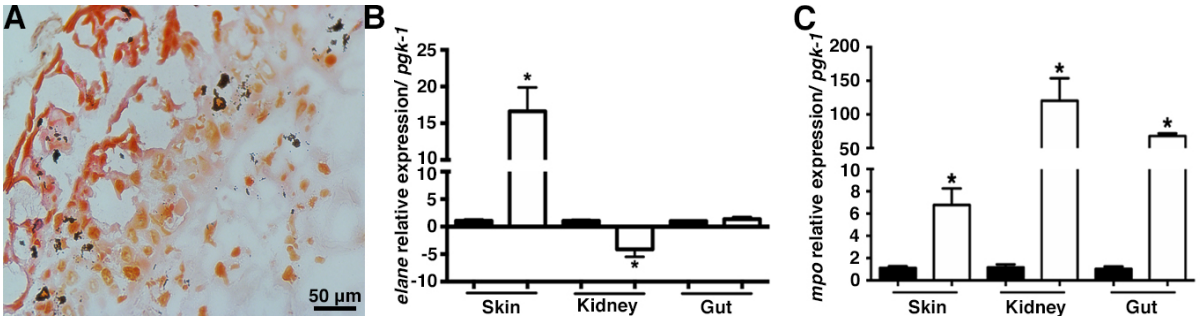

Supplementary Figure 1: (A) Myeloperoxidase (mpo) staining of a terrestrialized lungfish skin cryosection showing infiltration of mpo^+ cells in brown (arrows). (B) Quantification of *elane* mRNA levels by RT-qPCR in the skin, gut and kidney of control and terrestrialized lungfish (n = 3). Quantification of *mpo* mRNA levels by RT-qPCR in the skin, gut and kidney of control and terrestrialized lungfish (n = 3). Data were analyzed by unpaired Student's *t*-test. $*P < 0.05$.

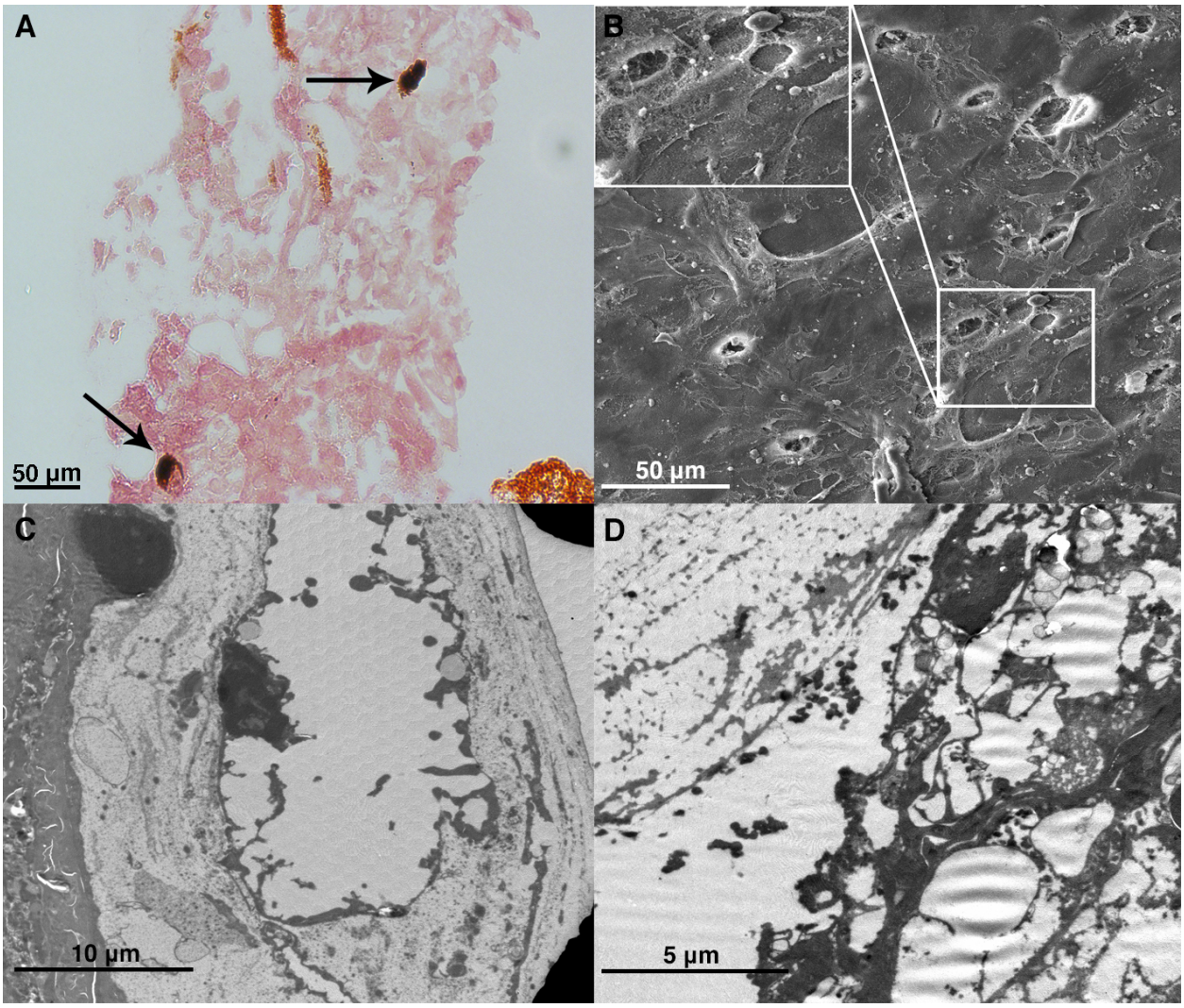

Supplementary Figure 2: (A) Myeloperoxidase staining of a lungfish cocoon cryosection showing presence of mpo^{+} cells in brown (arrows). (B) Scanning electron micrograph (coronal view) of the lungfish cocoon showing abundant bacterial cells trapped in it. (C) Transmission electron micrograph of the lungfish cocoon showing a channel with a cell in the lumen. (D) Transmission electron micrograph of the lungfish cocoon showing large groups of bacteria. Images are representative of n = 2-3 fish.

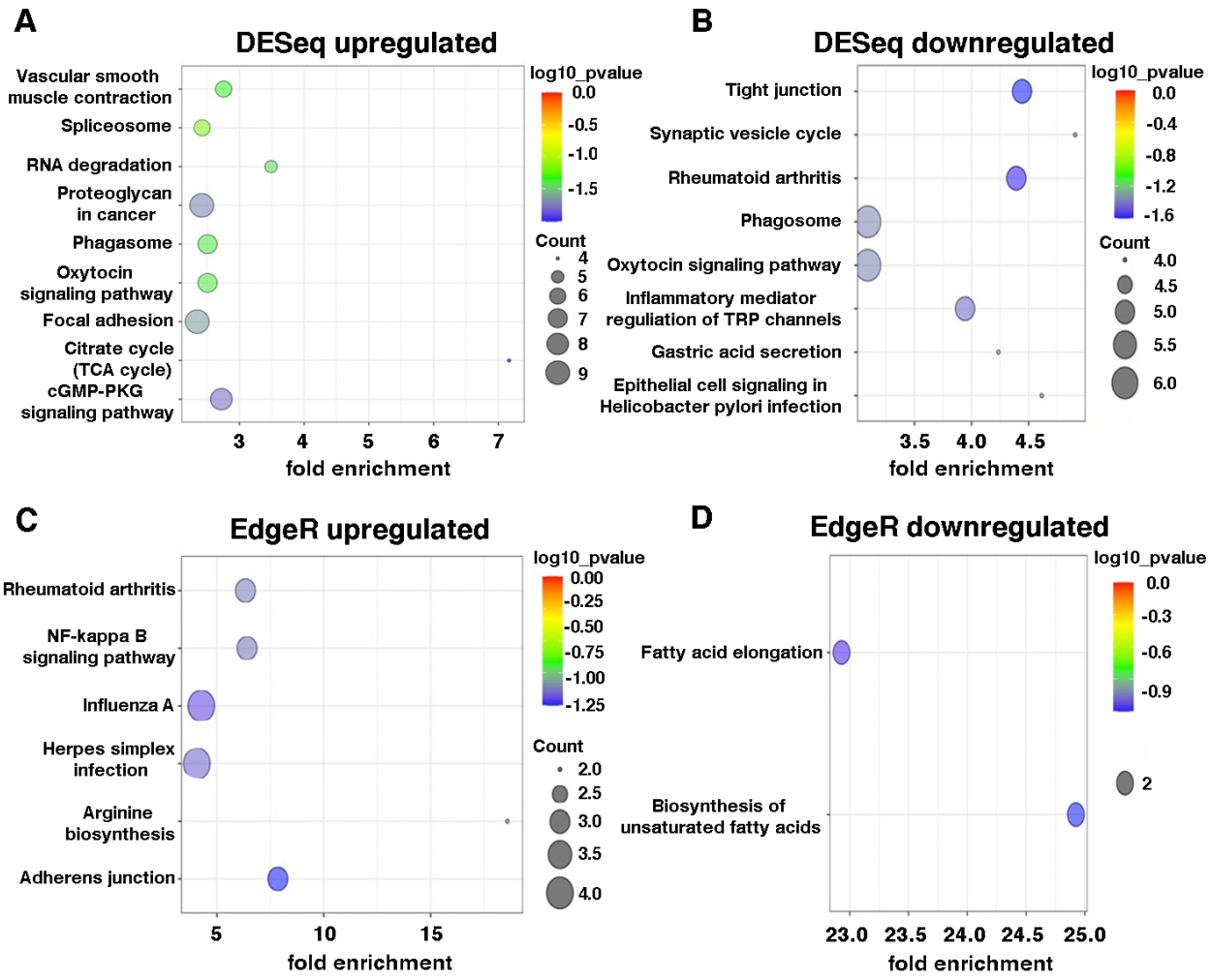

Supplementary Figure 3: Scatter plots of enriched KEGG pathway for (A) Up-regulated genes in the skin of terrestrialized lungfish compared to free-swimming lungfish based on DESeq analysis. (B) Down-regulated genes in the skin of terrestrialized lungfish compared to free-swimming lungfish based on DESeq analysis. (C) Up-regulated genes in the skin of terrestrialized lungfish compared to free-swimming lungfish based on EdgeR analysis. (D) Down-regulated genes in the skin of terrestrialized lungfish compared to free-swimming lungfish based on EdgeR analysis. The fold enrichment indicates the ratio of the expressed gene number to the total gene number in a pathway. The size and color of the points represent the gene number and the log10 p-value of each pathway, respectively. Note that no significant KEGG pathways were found in the down-regulated gene list using EdgeR (D).

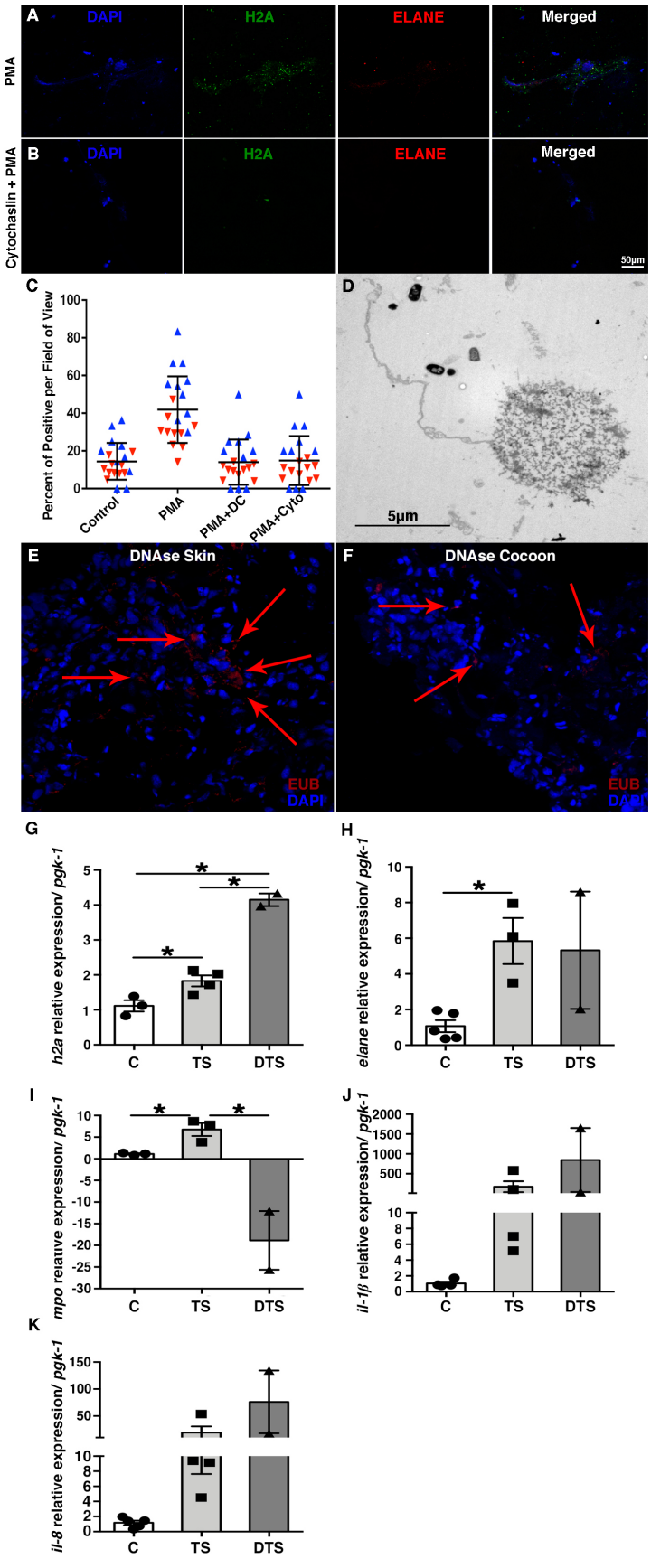
A
DAPI
H2A
ELANE
Merged
PMA
B
DAPI
H2A
ELANE
Merged
Cytochasiln + PMA
50µm
C
Percent of Positive per Field of View
100
80
60
40
20
0
Control
PMA
PMA+DC
PMA+Cyto
D
5µm
E
DNAse Skin
EUB
DAPI
F
DNAse Cocoon
EUB
DAPI
G
h2a relative expression/ pgk-1
5
4
3
2
1
0
C
TS
DTS
H
elane relative expression/ pgk-1
10
8
6
4
2
0
C
TS
DTS
I
mpo relative expression/ pgk-1
10
5
0
-5
-10
-15
-20
-25
-30
C
TS
DTS
J
il-1β relative expression/ pgk-1
2000
1500
1000
500
10
8
6
4
2
0
C
TS
DTS
K
il-8 relative expression/ pgk-1
150
100
50
10
8
6
4
2
0
C
TS
DTS

Supplementary Figure 4: Gut cell suspensions (50,000 cells/treatment) of a free-swimming lungfish were either not stimulated (control), stimulated with PMA, or stimulated with PMA and treated with the ETosis inhibitors diphenyliodonium chloride (PMA+DC), or cytochalasin A (PMA+Cyto). Cells were stained with DNA staining (DAPI), anti-histone 2A antibody (H2A) (green), anti-human neutrophil elastase antibody (ELANE) (red), and merged. (A) Representative confocal microscopy images of gut cell suspensions from free-swimming lungfish stimulated with PMA. (B) Representative confocal microscopy images of gut cell suspensions from free-swimming lungfish stimulated with PMA+Cyto. (C) Quantification of the percentage of cells in gut cell suspensions from free-swimming lungfish undergoing ETosis. (D) Transmission electron micrograph of a terrestrialized lungfish skin sample showing a granulocyte undergoing ETosis with a bacterial cell in the proximity of the extracellular DNA. Maximum projection (1 μm-thick Z-stacks, 5 stacks) of confocal fluorescence images of FISH using EUB338 oligoprobe (red) of the skin (E) and cocoon (F) of a DNAse I treated terrestrialized lungfish showing high numbers of bacteria in the skin of DNAse I treated animals (n = 3). Cell nuclei were stained with DAPI (blue). Red arrows indicate bacterial cells. (G-K) Quantification of gene expression levels of *h2a*, *elane*, *mpo*, *il1b* and *il8* in control free-swimming lungfish skin (C), terrestrialized lungfish skin (TS), and DNase I treated terrestrialized lungfish skin (DTS) (N = 3-5/group). Gene expression levels were normalized to the house-keeping gene *pgk-1*. Asterisks denote statistically significant differences (*$P < 0.05$) by unpaired t-test.

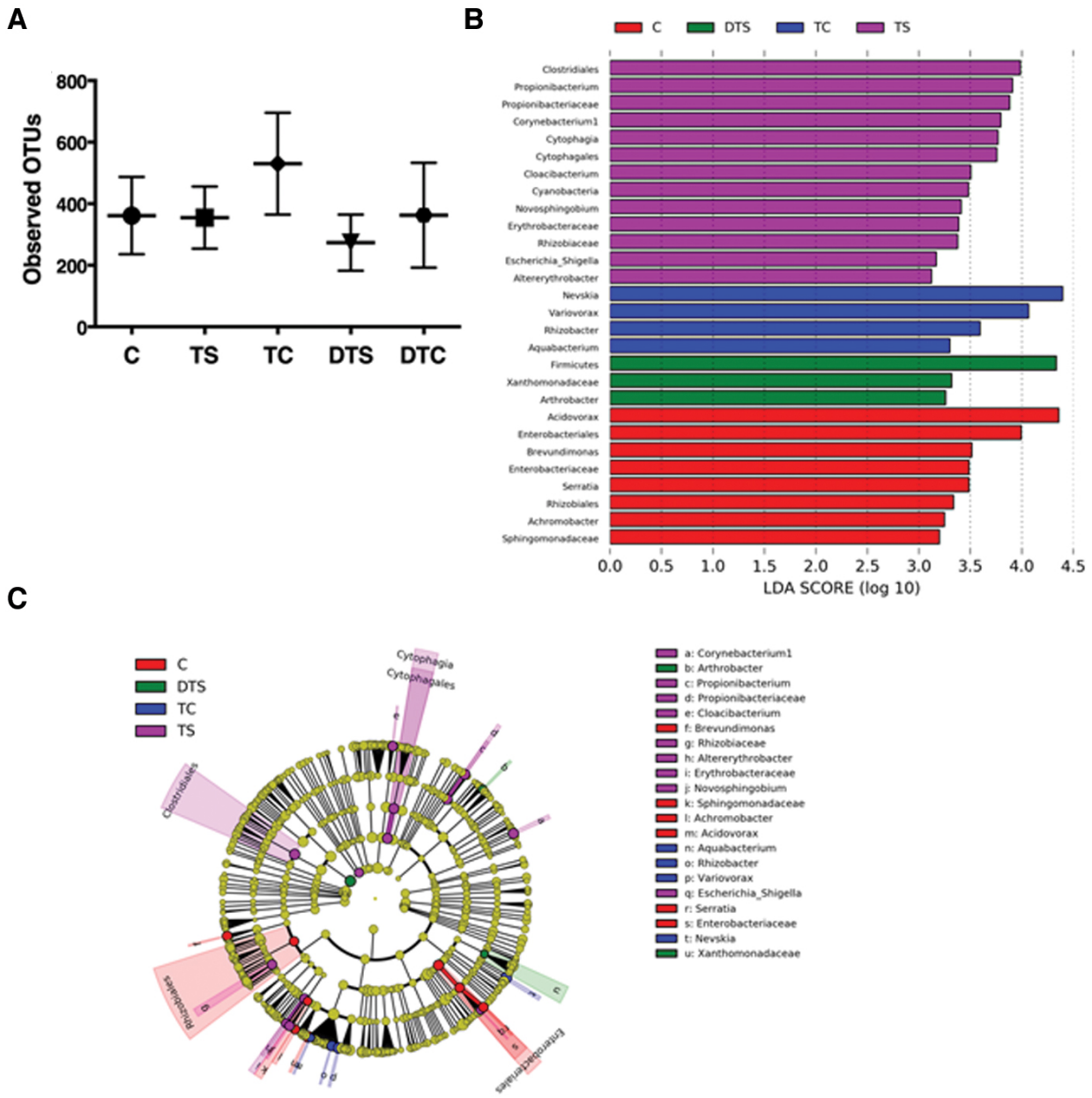

Supplementary Figure 5: Microbiome analyses of lungfish control skin (CS), terrestrialized skin (TS), cocoon (TC), DNase I treated skin (DTS) and DNase I treated cocoon (DTC). (A) Mean number of observed OTUs in each sample. (B) Bar chart of the log-transformed linear discrimination analysis (LDA) score of bacterial taxa found to be significantly associated with CS, TS, TC and DTS by LEfSe ($P < 0.05$). No taxa were uniquely associated with DTC. (C) Cladogram representation of LEfSe analysis showing bacterial taxa that were significantly associated with each of the tissue samples ($P < 0.05$).

References:

1. Abi Abdallah, D. S, and E. Y. Denkers. 2012. Neutrophils cast extracellular traps in response to protozoan parasites. *Front. Immunol.* 3(382): 1-6.

2. Amemiya, C.T., Alföldi, J., Lee, A.P., Fan, S., Philippe, H., MacCallum, I., Braasch, I., Manousaki, T., Schneider, I., and N. Rohner. 2013. The African coelacanth genome provides insights into tetrapod evolution. *Nature*. 496: 311–316.

3. Andrews, S. 2010. FastQC: a quality control tool for high throughput sequence data. Available at: http://www.bioinformatics.babraham.ac.uk/projects/fastqc.

4. Baugher, P. J., and A. Richmond. 2008. The carboxyl-terminal PDZ ligand motif of chemokine receptor CXCR2 modulates post-endocytic sorting and cellular chemotaxis. *J. Biol. Chem.* 283(45): 30868-30878.

5. Biermann, M. H. C., Podolska, M. J., Knopf, J., Reinwald, C., Weidner, D., Maueröder, C., Hahn, J., Kienhöfer, D., Barras, A., Boukerroub, R., Szunerits, S., Bilyy, R., Hoffmann, M., Zhao, Y., Schett, G., Herrmann, M., and L. E. Munoz. 2016. Oxidative burst-dependent NETosis is implicated in the resolution of necrosis-associated sterile inflammation. *Front. Immunol.* 7(557): 1-13.

6. Binet, F., Cagnone, G., Crespo-Garcia, S., Hata, M., Neault, M., Dejda, A., Wilson, A. M., Buscarlet, M., Mawambo, G. T., Howard, J. P., Diaz-Marin, R., Parinot, C., Guber, V., Pilon, F., Juneau, R., Laflamme, R., Sawchyn, C., Boulay, K., Leclerc, S., Abu-Thuraia, A., Côté, J., Andelfinger, G., Rezende, F. A., Sennlaub, F., Joyal, J., Mallette, F. A., and P. Sapieha. 2020. Neutrophil extracellular traps target senescent vasculature for tissue remodeling in retinopathy. *Science*. 369(6506): eaay5356.

7. Bolger, A. M., Lohse, M., and B. Usadel. 2014. Trimmomatic: a flexible trimmer for Illumina sequence data. *Bioinformatics* 30: 2114–2120.

8. Brinkmann, V., Reichard, U., Goosmann, C., Fauler, B., Uhlemann, Y., Weiss, D. S., Weinrauch, Y., and A. Zychlinsky. 2004. Neutrophil extracellular traps kill bacteria. *Science.* 303(5663): 1532-1535.

9. Brinkmann, H., Venkatesh, B., Brenner, S., and A. Meyer. 2004. Nuclear protein-coding genes support lungfish and not the coelacanth as the closest living relatives of land vertebrates. Proc Natl Acad Sci. 101: 4900–4905.

10. Caporaso, J. G., Kuczynski, J., Stombaugh, J., Bittinger, K., Bushman, F. D., Costello, E. K., Fierer, N., Peña, A. G., Goodrich, J. K., Gordon, J. I., Huttley, G. A., Kelley, S. T., Knights, D., Koenig, J. E., Ley, R. E., Lozupone, C. A., McDonald, D., Muegge, B. D., Pirrung, M., Reeder, J., Sevinsky, J. R., Turnbaugh, P. J., Walters, W. A., Widmann, J., Yatsunenko, T., Zaneveld, J., and R. Knight. 2010. QIIME allows analysis of high-throughput community sequencing data. *Nat. Meth.* 7(5): 335–336.

11. Chew, S. F., and K. Hiong. 2014. Aestivation and brain of the African lungfish *Protopterus annectens. Temperature.* 1(2): 82-83.

12. Chin, A. C., and C. A. Parkos. 2006. Neutrophil transepithelial migration and epithelial barrier function in IBD: potential targets for inhibiting neutrophil trafficking. *Ann. N.Y. Acad. Sci*. 1072: 276–287.

13. Clark, S. R., Ma, A. C., Tavener, S. A., McDonald, B., Goodarzi, Z., Kelly, M. M., Patel, K. D., Chakrabarti, S., McAvoy, E., Sinclair, G. D., Keys, E. M., Allen-Vercoe, E., DeVinney, R., Doig, C. J., Green, F. H. Y., and P. Kubes. 2007. Platelet TLR4 activates neutrophil extracellular traps to ensnare bacteria in septic blood. *Nat. Med.* 13: 463-469.

14. Daniel, C., Leppkes, M., Muñoz, L.E. Schley, G., Schett, G., and M. Herrmann. 2019. Extracellular DNA traps in inflammation, injury and healing. *Nat. Rev. Nephrol.* 15: 559–575.

15. de Bont, C. M., Boelens, W. C., and G. J. M. Pruijn. 2019. NETosis, complement, and coagulation: a triangular relationship. *Cell. Mol. Immunol.* 16: 19-27.

16. Delgado-Rizo, V., Martinez-Guzman, M. A., Inguez-Gutierrez, L., Garcia-Orozco, A., Alvarado-Navarro, A., and M.Fafutis-Morris. 2017. Neutrophil extracellular traps and its implications in inflammation and overview. *Front. Immunol.* 8(81): 1-20.

17. Fox, S., Leitch, A. E., Duffin, R., Haslett, C., and A. G. Rossi. 2010. Neutrophil apoptosis: relevance to the innate immune response and inflammatory disease. *J. Innate. Immun.* 2(3): 216-227.

18. Garofalo, F., Amelio, D., Icardo, J. M., Chew, S. F., Tota, B., Cerra, M. C., and Y. K. Ip. 2015. Signal molecule changes in the gills and lungs of the African lungfish Protopterus annectens, during the maintenance and arousal phases of aestivation. *Nitric Oxide.* 44:71-80.

19. Glass, M. L., Amin-Naves, J., and G. S. F. da Silva. 2009. Aestivation in amphibians, reptiles, and lungfish. Cardio-Respiratory Control in Vertebrates. Springer, Berlin, Heidelberg.

20. Grabherr, M. G., Haas, B. J., Yassour, M., Levin, J. Z., Thompson, D. A., Amit, I., Adiconis, X., Fan, L., Raychowdhury, R., Zeng, Q., Chen, Z., Mauceli, E., Hacohen, N., Gnorke, A., Rhind, N., di Palma, F., Birren, B. W., Nusbaum, C., Lindblad-Toh, K., Friendman, N., and A. Regev. 2011. Full-length transcriptome assembly from RNA-seq data without a reference genome. *Nat. Biotechnol.* 29: 644–652.

21. Guimarães-Costa, A. B., Nascimento, M. T. C., Wardini, A. B., Pinto-da-Silva, L. H., and E. M. Saraiva. 2012. ETosis: A microbicidal mechanism beyond cell death. *J. Parastol. Res.* Article ID 929743: 1-11.

22. Haas, B. J., Papanicolaou, A., Yassour, M., Grabherr, M., Blood, P. D., Bowden, J., Couger, M. B., Eccles, D., Li, B., Lieber, M., MacManes, M. D., Ott, M., Orvis, J., Pochet, N., Strozzi, F., Weeks, N., Westerman, R., William, T., Dewey, C. N., Henschel, R., LeDuc, R. D., Friedman, F., and A. Regev. 2013. De novo transcript sequence reconstruction from RNA-seq using the Trinity platform for reference generation and analysis. *Nat. Protoc*. 8: 1494–1512.

23. Heimroth, R. D., Casadei, E., and I. Salinas. 2018. Effects of experimental terrestrialization on the skin mucus proteome of African lungfish (Protopterus dolloi). *Front. Immunol.* 9(1259): 1-11.

24. Hoffmann, J. H. O., and A. H. Enk. 2016. Neutrophil extracellular traps in dermatology: Caught in the NET. *J. Derm. Sci.* 84(1): 3-10.

25. Hosoda, H., Nakamura, K., Hu, Z., Tamura, H., Reich, J., Kuwahara-Arai, K., Iba, T., Tabe, Y., and I. Nagaoaka. 2017. Antimicrobial cathelicidin peptide LL-37 induces NET formation and suppresses the inflammatory response in a mouse septic model. *Mol. Med. Rep*. 16(4): 5618-5626.

26. Hu, S. C., Yu, H., Yen, F., Lin, C., Chen, G., and C. E. Lan. 2016. Neutrophil extracellular trap formation is increased in psoriasis and induces human β-defensin-2 production in epidermal keratinocytes. *Sci. Rep.* 6: 31119.

27. Huang, D. W., Sherman, B. T., and R. A. Lempicki. 2009. Systematic and integrative analysis of large gene lists using DAVID Bioinformatics Resources. *Nat. Protoc*. 4(1): 44-57.

28. Icardo, J. M., Loong, A. M., Colvee, E., Wong, W. P., and Y. K. IP. 2012. The alimentary canal of the African lungfish Protopterus annectens during aestivation and after arousal. *Anat. Rec.* 295: 60-72.

29. Jordan, H. E., and C. C. Speidel. 1931. Blood formation in the African lungfish, under normal conditions and under conditions of prolonged estivation and recovery. *J. Morph.*51(2): 319-371.

30. Kaplow, L. S. 1965. Simplified myeloperoxidase stain using benzidine dihydrochloride. *Blood.* 26(2): 215-219.

31. Korkmaz, B., Horwitz, M. S., Jenne, D. E., and F. Gauthier. 2010. Neutrophil elastase, proteinase 3, and cathepsin G as therapeutic targets in human diseases. *Pharmacol. Rev.* 62(4): 726-759.
32. Kruger, P., Saffarzadeh, M., Weber, A. N., Rieber, N., Radsak, M., von Bernuth, H., Benarafa, C., Roos, D., Skokowa, J., and D. Hartl. 2015. Neutrophils: between host defence, immune modulation, and tissue injury. *PLoS Pathog.* 11: e1004651.
33. Lázaro-Díez, M., Chapartegui-González, I., Redondo-Salvo, S., Leigh, C., Merino, D>, Segundo D. S., Fernández A., Navas J., Icardo, J. M., Acosta, F., Ocampo-Sosa, A.,

Martínez- Martínez L., and J. Ramos-Vivas. 2017. Human neutrophils phagocytose and kill *Acinetobacter baumannii* and *A. pittii*. *Sci. Rep.* 7(4571): 1-11.

34. Li, H., and R. Durbin. 2009. Fast and accurate short read alignment with Burrows-Wheeler transform. *Bioinformatics* 25: 1754–1760.

35. Li, H., Handsaker, B., Wysoker, A., Fennell, T., Ruan, J., Homer, N., Marth, N., Abecasis, G., and R. Durbin, 1000 Genome Project Data Processing Subgroup. 2009. The sequence alignment/map format and SAMtools. *Bioinformatics*. 25: 2078–2079.

36. Lin, A. M., Rubin, C. J., Khandpur, R., Wang, J. Y., Riblett, M., Yalavarthi, S., Villanueva, E. C., Shah, P., Kaplan, M. J., and A. T. Bruce. 2011. Mast cells and neutrophils release IL-17 through extracellular trap formation in psoriasis. *J. Immunol.* 187: 490-500.
37. McClanahan, L. L., Shoemaker, V. H., and R. Ruibal. 1976. Structure and function of the cocoon of a Ceratophryd frog. *American Society of Ichthyologists and Herpetologists*. 1976: 179-185.
38. Mitchell, K. R., and C. D. Takacs-Vesbach. 2008. A comparison of methods for total community DNA preservation and extraction from various thermal environments. *J. Ind. Microbiol. Biotechnol.* 35: 1139-1147.

39. Neumann, A., Berends, E. T., Nerlich A, Molhoek, E. M., Gallo, R. L., Meerloo, T., Nizet, V., Naim, H. Y., and M. von Köckritz-Blickwede. 2014. The antimicrobial peptide LL-37 facilitates the formation of neutrophil extracellular traps. *Biochem. J*. 464(1):3-11.

40. Neumann, A., Völlger, L., Berends, E. T., Molhoek, E. M., Stapels, D. A. C., Midon, M., Friães, A., Pingoud, A., Rooijakkers, S. H. M., Gallo, R. L., Mörgelin, M., Nizet, V., Naim, H. Y., and M. von Köckritz-Blickwede. 2014. Novel role of the antimicrobial peptide LL-37 in the protection of neutrophil extracellular traps against degradation by bacterial nucleases. *J Innate Immun*. 6(6): 860-868.

41. Parkos, C. A. 2005. Molecular events in neutrophil transepithelial migration. *BioEssays.* 19(10): 865-873.

42. Pfaffl, M. W. 2001. A new mathematical model for relative quantification in real-time RT-PCR. *Nuc. Acid. Res.* 29(9): e45.

43. Ruibal, R. and S. Hillman. 1981. Cocoon structure and function in the burrowing hylid frog, *Pternohyla fodiens. J. Herp.* 15: 403-407.

44. Safi, R., Al-Hage, J., Abbas, O., Kibbi, A-G., and D. Nassar. 2019. Investigating the presence of neutrophil extracellular traps in cutaneous lesions of different subtypes of lupus erythematosus. *Exp Dermatol*. 28: 1348-1352.

45. Saitoh, T., Komano, J., Saitoh, Y., Misawa, T., Takahama, M., Kozaki, T., Uehata, T., Iwasaki, H., Omori, H., Yamaoka, S., Yamamoto, N., and S. Akira. (2012). Neutrophil

extracellular traps mediate a host defense response to human immunodeficiency virus-1. *Cell Host Microbe.* 12: 109–116.

46. Shao, S., Fang, H., Dang, E., Xue, K., Zhang, J., Li, B., Qiao, H., Cao, T., Zhuang, Y., Shen, S., Zhang, T., Qiao, P., Li, C., Gudjonsson, J. E., and G. Wang. 2019. Neutrophil Extracellular Traps Promote Inflammatory Responses in Psoriasis via Activating Epidermal TLR4/IL-36R Crosstalk. *Front. Immunol*. 10: 746.

47. Smith, H. W 1930. Metabolism of lungfish Protopterus aethiopicus*. J. Biol. Chem*. 88: 97-130.

48. Sturla, M., Paola, P., Carlo, G., Anegla, M. M., and U. B. Maria. 2002. Effects of induced aestivation in *Protopterus annectens*: a histomorphological study. J. Exp. Zool. 292: 26-31.

49. Sumagin, R., Robin, A. Z., Nusrat, A., and C. A. Parkos. 2014. Transmigrated neutrophils in the intestinal lumen engage ICAM-1 to regulate the epithelial barrier and neutrophil recruitment. *Mucosal Immunol*. 7: 905-915.

50. Xu, Z., Parra, D., Gomez, D., Salinas, I., Zhang, Y., von Gersdorff Jorgensen, L., Heinecke, R. D., Buchmann, K., LaPatra, S., and J. O. Sunyer. 2013. Teleost skin, an ancient mucosal surface that elicits gut-like immune responses. *Proc. Nat. Acad. Soc.* 110(32): 13097-13102.

51. Wen, F., White, G. J., VanEtten, H. D., Xiong, Z., and M. C. Hawes. 2009. Extracellular DNA is required for root tip resistance to fungal infection. 151: 820-829.

52. Withers, P. C. 1995. Cocoon formation and structure in the aestivating Australian desert frogs, *Neobatrachus* and *Cyclorana*. *Aus. J. Zool.* 43: 429-441.
53. Withers, P. C. 1998. Evaporative water loss and the role of cocoon formation in Australian frogs. *Aus. J. Zool.* 46: 405-418.
54. Withers, P. C. and G. G. Thompson. 2000. Cocoon formation and metabolic depression by the aestivating hylid frogs *Cyclorana australis* and *Cyclorana cultripes* (Amphibia: Hylidae). *J. R. Soc. West. Aust.* 83: 39-40.

55. Wong, S., Demers, M., Martinod, K., Gallant, M., Wang, Y., Goldfine, A. B., Kahn, C. R., and D. D. Wagner. 2015. Diabetes primes neutrophils to undergo NETosis, which impairs wound healing. *Nat. Med*. 21: 815–819.

Chapter 5

Discussion:

The immune system is a complex, intriguing and mysterious physiological system. There are two main branches of the immune system: the innate and the adaptive immune system. The innate immune system is categorized by a non-specific rapid response to foreign and internal danger that is recognized by pattern recognition receptors (PRRs). This branch of immunity is present in some form throughout evolution going back to the first multicellular organisms. The innate immune system is generally conserved throughout vertebrate evolution including myeloid cells, PRRs and downstream signaling pathways. The adaptive immune system (other than the bacterial CRISPR system) is a vertebrate innovation that emerged about 500 million years ago (Flajnik, 2018).

Studies in non-model organisms continue to reveal the adaptability and malleability of both innate and adaptive immune systems (Criscitiello and Figueiredo, 2013). The present thesis contributes to the notion that immune systems are incredibly diverse and that investigating non-model organisms is key to unveil immunological innovations. In particular, I have described unique adaptations of both the innate and the adaptive immune system of African lungfish that best suit the peculiar lifestyle of this organism. The lungfish immune system has significant peculiarities including large reservoirs of granulocytes that can be mobilized in the aestivating phase to form a cocoon, suites of antimicrobial peptides that are highly expressed in the skin and the cocoon, the presence of lymphoid aggregates at mucosal tissues not found in bony fish and an expansion of Ig isotypes that may be also useful at mucosal tissues during aestivation.

Innate immune systems use PRRs to detect pathogen-associated molecular patterns (PAMPs) found in microorganisms and trigger immediate non-specific immune responses. The

innate immune system of some taxa is known to display unique expansions in specific PRRs. For instance, sea urchins have expanded sets of TLRs, more then 200 Nod-like receptors, and a 10-fold expansion of scavenger receptor cysteine-rich domains (Rast et al., 2006; Buckley and Rast, 2012; Buckley and Rast, 2017). In the case of AMPs, amphibian skin is known expression of diverse AMP repertoire that plays a role in wound healing and prevents pathogen infection. The wide breadth of different AMPs found in amphibians provides them with a broad-spectrum response to Gram-positive, Gram-negative bacteria, fungi, and protozoa (Rinaldi, 2002; Huerta-Cantillo and Navarro-García, 2016). In the cased of jawed vertebrates, the complement system, a critical arm of the innate immune response, is known to be expanded in bony fish such as salmonids with 35 soluble proteins and receptors that function at a wide range of temperatures (Sunyer et al., 2003). Combined, this body of work reveals that specific branches of the innate immune system are preferably utilized by different animal taxa in order to provide protection in their particular environment. In the case of lungfish, investment in granulopoiesis and antimicrobial molecules seems vital for the success of this species and its bimodal lifestyle.

As mentioned earlier, one of the key aspects of this thesis was the discovery that granulocytes are involved in lungfish skin during aestivation. Granulocytes are myeloid cells with many known innate immune functions ranging from phagocytosis, wound healing and cytokine production. Phagocytic cells are present in all multicellular organisms and have been proposed to have emerged in protozoans. In primitive invertebrates without a vascular system, these cells are called amoebocytes or neoblasts and possess some characteristics similar to red blood cells. Granularity in these invertebrate cells shows a high similarity with vertebrate macrophages. As the animal body evolved to be more complex, the diversity of granulocytes increased (Fingerhut et al., 2020). Granulocytes play a role in both the innate and adaptive

immune responses (Mantovani et al., 2011; Rosales, 2020). They migrate to the site of infection and release effector molecules such as cytokines, chemokines, histamine, and extracellular traps (ETs) (Mayadas et al., 2013). These ETs are a net of chromatin fibers made up of DNA and histones that have granule-derived AMPs and enzymes such as myeloperoxidase (MPO), neutrophil elastase (ELANE) and cathepsin G (Korkmaz et al., 2010). ETs play critical roles in infection, inflammation, injury, autoimmunity, and tissue remodeling. There are two proposed methods of ET formation. First, is that ETs are a form of active cell death that is characterized by the release of decondensed chromatin and granular contents. These cells do not display signals saying that they are dying which may prevent them from being cleared by phagocytes. The second form is DNA/serine protease extrusion from intact neutrophils when mitochondrial DNA is release but it is not associated with cell death (von Köckritz-Blickwede et al., 2008; Yousefi et al., 2008). ETs have been described in many organisms, from plants to fish and mammals (Kaplan and Radic, 2013). Yet, their presence in lungfish had not been reported to date.

Amphibians such as salamanders and frogs as well as lungfish are aestivating animals that form a cocoon in order to avoid evaporative water loss and desiccation during drought. Whereas the structure and function of the amphibian cocoon have been extensively studied (MacCanahan et al., 1976; Ruibal, R. and S. Hillman, 1981; Withers, 1995; Withers, 1998; Withers and Thompson, 2000), the function of this structure has thus far been attributed to avoidance of water loss. My work reveals a novel function for the cocoon of aestivating animals in that it has an immunological role. Upon aestivation, we witnessed drastic remodeling of the skin and massive migration of granulocytes to the integument as previously reported (Strula et al., 2002; Icardo et al., 2012; Heimroth et al., 2018). The skin of African lungfish changes from having a thick living epidermis filled with mucus-secreting goblet cells and little to no

granulocytes, to a thin keratinized epidermis with exhausted of goblet cells and a massive influx of granulocytes from circulation. African lungfish possess unusually large granulocyte reservoirs in their gut, kidneys, and gonads which were proposed almost a century ago to play and important role in aestivation (Jordan and Speidel, 1931). In my work, we added new tools to the investigation of lungfish granulocytes including molecular markers such as *cxcr2, elane* and *mpo* whose expression was elevated in the skin in terrestrialized animals. Although we still do not know the exact mechanisms of cocoon formation in vertebrates, histological examination of the skin and cocoon of African lungfish in the present study suggest that epidermal layers slough off of the skin to create a cocoon. This appeared to be promoted by degradation of the basal membrane likely by the action of granulocyte proteases. Further studies will identify the stepwise events that lead to the formation of the African lungfish cocoon.

My work identified the African lungfish cocoon as a living, well-defined structure of approximately 600-900 μm that is composed of different cell types such as epithelial cells, endothelial cells, goblet cells and immune cells. Nests of these cells were observed with long channels around them which may be as means of transporting the cells. Electron microscopy analysis showed the flat smooth epidermis of the free-swimming lungfish gets remodeled to a disrupted surface covered in mucus with clusters of bacteria visible in the cocoon. Immunofluorescence with anti-PCNA revealed active proliferation of cells on the outer edge of the cocoon along with single cell suspension of the cocoon showed that the cells in the cocoon are alive. In support, we found active transcription of epithelial cell markers, antimicrobial peptide genes, goblet cell markers, granulocyte markers and proinflammatory cytokines.

In aestivating amphibians, presence of bacteria in the cocoon was revealed by electron microscopy (MacCanahan et al., 1976) but bacterial loads and analysis of the microbial

community composition of the skin and the cocoon have never been performed. Using qPCR for relative quantification of bacterial loads, we observed that the cocoon contained almost 3 times higher bacterial loads than the free-swimming or terrestrialized skin. This finding led us to conclude that the cocoon acts as a bacterial trapping structure that precludes bacterial invasion into the lungfish body during aestivation. In order to control the high levels of bacteria in the cocoon, lungfish likely use AMPs, as we detected high expression of these molecules in the cocoon by RT-qPCR.

The large influx of granulocytes into the lungfish skin during aestivations appears to have several functions. First, these cells likely contribute to the sloughing of the epidermis as well as the tissue repair necessary for the "new skin" to reach homeostasis. Second, we provide evidence that the granulocytes in the lungfish skin have potent ETosis functions. Immunofluorescence staining with antibodies for ETosis markers ELANE and MPO showed that skin granulocytes in aestivating lungfish are capable of producing ETs. However, we found no evidence of ETosis in cocoon cell suspensions, indicating that the granulocytes that transmigrated to the cocoon had likely been exhausted and/or require other cues (not PMA) to release ETs.

In plants, roots exposed to a fungal pathogen and treated with DNase I suffer from severe root necrosis (Wen et al., 2009). We used *in vivo* DNAse I treatment to eliminate extracellular DNA (eDNA) from the skin of the lungfish to observe the impact that ETs have on the terrestrialized lungfish. This led to detrimental effects on the lungfish such as head edema lesions and a prolapsed anus. The DNAse I treatment caused systemic bacterial infection, with the presence of large cocci in circulation. This treatment also caused drastic morphology changes in the skin and cocoon of terrestrialized fish with severe skin necrosis and thinning of the cocoon. With the cocoon trapping the bacteria during aestivation we observed distinct microbial

communities in the cocoon compared to free-swimming and terrestrialized skin. There is higher microbial diversity in the free-swimming and terrestrialized skin compared to the cocoon, DNAse I treated skin and DNAse I treated cocoon. This shows that eDNA is essential for successful terrestrialization and microbial control in lungfish and that the cocoon of aestivating animals has an important immunological role needed for survival during aestivation, a period of energy conservation.

Adaptive immune systems, even if more recent than innate immune systems, also show a large degree of diversity in different lineages. Early studies in agnathans revealed that lampreys were able to accept skin autographs but reject first-set allografts slowly and second-set allografts at accelerated rates (Finstad and Good, 1964; Perey et al., 1968). Immunization of lampreys and hagfish with a variety of antigens induced the production of circulating antigen-specific agglutinins (Linthicum and Hildemann, 1970; Fujii et al., 1979). Attempts to validate that these agglutinins were actually immunoglobulins failed, until searching for lamprey genes that were upregulated during antigens and mitogen stimulation, led to the discovery of cDNA clones encoding leucine-rich repeats (LRR). Upon further genomic analysis they found that these LRR modules were highly diverse and they were variable in number. The lymphocyte-like cells secreting these agglutinins possessed receptors akin the BCRs and TCRs and were termed variable lymphocyte receptors (VLRs) (Pancer et al., 2004; Alder et al., 2005). These VLRs had three subsets: $VLRA^+$ and $VLRC^+$ which acted in a similar manner to TCRα/β and TCRγ/δ T cells, respectively, and $VLRB^+$ cells that secrete agglutinins similar to antibodies. These recent discoveries have shown the Comparative Immunology community that the conventional mammalian immune system is not used by all vertebrates and that convergent evolution has resulted in analogous types of adaptive immunity.

All gnathostomes (jawed vertebrates) are capable of using what has been termed as the conventional adaptive immune system based in B and T cell receptors. B and T lymphocyte lineages use V(D)J recombination to generate diversity in B cell receptor (BCR) and T cell receptor (TCR) repertoires, along with the presence of recombination adaptive genes (RAG), and major histocompatibility complex (MHC). This response has constantly evolved throughout the jawed vertebrate lineage. The most ancestral jawed vertebrate, cartilaginous fish, possess five TCRs (α, β, δ, γ, and NAR), three immunoglobulin isotypes (IgM, IgW, and IgNAR), RAG genes, and polymorphic MHC genes. Elasmobranchs are unique from other vertebrates because they possess the unique immunoglobulin superclass chain IgNAR and have their Ig loci organized in clusters (Criscitiello et al., 2006). Most teleost fish have all four conventional TCRs (α, β, δ, and γ,) and three Ig isotypes (IgM, IgD, and IgT/Z) (Zhang et al., 2010). However, recent large genomic efforts by several groups have revealed outstanding losses in the conventional adaptive immune system. First, gadoids were found to lack the entire CD4 and MHC-system (Wermenstam and Pilstrom 2001; Star et al., 2011; Star and Jentoft, 2012). Recently, studies in parasitic anglerfishes revealed dramatic losses in functional *aicda* and *rag* genes in attaching males (Dubin et al., 2019; Swan et al., 2020). Although this thesis did not delve deep into lungfish adaptive immune system, we did observe some interesting changes in Ig expression in the cocoon compared to the freshwater skin mucus of lungfish that deserve further investigation.

One of the main features of the mammalian adaptive immune system is the organization of lymphocytes in secondary and tertiary lymphoid structures, where selection of high affinity B cell clones takes place to achieve maturation of the adaptive immune response. However, the evolutionary origins of these organized lymphocyte structure are still under debate. My work

consisted of a comparative analysis of different organized mucosa-associated lymphoid tissues (O-MALT) in different vertebrate taxa with the goal of identifying molecular signatures that govern lymphocyte clustering across all vertebrates. In salmonids, primitive secondary lymphoid organs (SLOs) with no compartmentalization of T cell zones or germinal centers have been described in the gills (Haugarvoll et al., 2008; Dalum et al., 2015; Dalum et al., 2016). They are composed of clusters of lymphocytes that primarily consist of T cells (Aas et al., 2014). Sarcopterygians (lobed-finned fish) and amphibians also show evidence of these primitive O-MALT (Ardavín et al., 1982; Tacchi et al., 2015). These primitive O-MALTs resemble those found in teleosts with no compartmentalization and are largely composed of T lymphocytes (Goldstine et al., 1975; Ardavín et al., 1982; Tacchi et al., 2015). Not much is known about the SLOs in reptiles. Birds lack conventional lymph nodes but have cecal tonsils that show the first compartmentalization of O-MALT in the vertebrate lineage (Crole and Soley, 2012). Mammals such as mice or humans have been studied in extensive detail and our current dogma for SLO formation is merely based on murine studied. Their O-MALT is highly compartmentalized and characterized, with defined T cell zones and germinal centers (Oláh and Glick, 1979; Kajiwara et al., 2003). *Bona fide* mammalian O-MALT include lymph nodes and Peyer's patches and TNFSF members such as TNFSF1, TNFSF3, TNFSF7, TNFSF11, TNFRSF1, TNFRSF3, TNFRSF7, and TNFRSF11 have been proposed to be the molecular drivers of SLO formation based on mouse knock-out models (De Togni et al., 1994; Banks et al., 1995; Pasparakis et al., 1997; Neumann et al., 1996). The findings of this thesis highlight once more that solutions to one problem may be achieved in many different ways by different vertebrate taxa. In the case of lungfish, many TNFSF molecules were expressed in the primitive O-MALT along with enrichment of olfactory related genes, which was also found in mouse PPs and LNs. However, in

other taxa, enrichment in genes related to the neuroactive-ligand pathway was found in O-MALT, suggesting alternative molecular drivers for SLO formation and maintenance that are not dependent on TNFSF molecules.

In conclusion, lungfish hold a unique position in the jawed vertebrate lineage. They are the extant relatives to all tetrapods and can survive in both aquatic and terrestrial environments. Thus, lungfish are able to show the evolution of the immune system not in generations but in days. The African lungfish immune system had barely been investigated. The present thesis brings new life to the study of immunity in non-model organisms and showcases the need for the immune system to be part of the physiological adaptations that have enabled organisms to survive in this planet.

References:

1. Alder, M. N., Rogozin, I. B., Iyer, L. M., Glazko, G. V., Cooper, M. D., and Z. Pancer. 2005. Diversity and function of adaptive immune receptors in a jawless vertebrate. *Science*. 310: 1970–1973.

2. Ardavín, C.F., Zapata, A., Garrido, E., and A. Villena. 1982. Gut-associated lymphoid tissue (GALT) in the amphibian urodele, *Pleurodeles waltlii*. *J. Moprhol.* 173: 35-41.

3. Aas, I. B., Austbø, L., König, M., Syed, M., Falk, K., Hordvik, I., and E. O. Koppang. 2014. Transcriptional characterization of the T cell population within the salmonid interbranchial lymphoid tissue. *J. Immunol.* 193: 3463–3469.

4. Banks, T. A., Rouse, B. T., Kerley, M. K., Blair, P. J., Godfrey, V. L., Kuklin, N. A.,
5. Bouley, D. M., Thomas, J., Kanangat, S., and M. L. Mucenski. 1995. Lymphotoxin- alpha-deficient mice. Effects on secondary lymphoid organ development and humoral immune responsiveness. *J. Immunol*. 155: 1685–1693.

6. Baugher, P. J. and A. Richmond. 2008. The carboxyl-terminal PDZ ligand motif of chemokine receptor CXCR2 modulates post-endocytic sorting and cellular chemotaxis. *J. Biol. Chem.* 283(45): 30868-30878.

7. Buckley, K. M. and J. P. Rast. 2012. Dynamic evolution of toll-like receptor multigene families in echinoderms. *Front. Immunol.* 3(136): 1-16.

8. Buckley, K. M. and J. P. Rast. 2017. An Organismal model for gene regulatory networks in the gut-associated immune response. *Front. Immunol.* 8(1297): 1-8.

9. Criscitiello, M. F., Saltis, M., and M. F. Flajnik. 2006. An evolutionarily mobile antigen receptor variable region gene: doubly rearranging NAR-TcR genes in sharks. *Proc. Natl Acad. Sci.* 103: 5036–5041.

10. Criscitiello, M.F., and P. de Figueiredo. 2013. Fifty shades of immune defense. *PLoS Pathog.* 9(2): e1003110.

11. Crole, M. R., and J. T. Soley. 2012. Evidence of a true pharyngeal tonsil in birds: a novel lymphoid organ in Dromaius novaehollandiae and Struthio camelus (Palaeognathae). *Front. Zool.* 9: 21.

12. Dalum, A.S., Austø, L., Bjørgen, H., Skjødt, K., Hordvik, I., Hansen, T., Fjelldal, P.G., Press, C.M., Griffiths, D.J., and E.O. Koppang. 2015. The interbranchial lymphoid tissue of Atlantic salmon (*Salmo salar* L) extends as a diffuse mucosal lymphoid tissue throughout the trailing edge of the gill filament. *J. Morph.* 276:1075-1088.

13. Dalum, A.S., Griffiths, D.J., Valen, E.C., Amthor, K.S., Austø, L., Koppang, E.O., Press, C.M, and A. Kvellestad. 2016. Morphological and functional development of the interbranchial lymphoid tissue (ILT) in Atlantic salmon (*Salmo slar* L). *Fish Shellfish Immunol.* 58:153-164.

14. De Togni, P., J. Goellner, N. H. Ruddle, P. R. Streeter, A. Fick, S. Mariathasan, S. C. Smith, R. Carlson, L. P. Shornick, J. Strauss-Schoenberger, et al. 1994. Abnormal development of peripheral lymphoid organs in mice deficient in lymphotoxin. *Science.* 264: 703–707.

15. Dubin, A., Jørgensen, T.E., Moum, T., 1, Johansen, S.D., and L.M. Jakt. 2019. Complete loss of the MHC II pathway in an anglerfish, *Lophius piscatorius*. *Biol. Lett.* 15(10): 20190594.

16. Fingerhut, L., Dolz, G., and N. de Buhr. 2020. What is the evolutionary fingerprint in neutrophil granulocytes? *Int. J. Mol. Sci.* 21: 1-37.

17. Finstad, J., and R.A. Good. 1964. The evolution of the immune response. Immunologic responses in the lamprey. *J. Exp. Med*. 120: 1151–68.

18. Flajnik, M.F. 2018. A cold-blooded view of adaptive immunity. *Nat. Rev. Immunol.* 18(7): 438-453.

19. Fox, S., Leitch, A. E., Duffin, R., Haslett, C., and A. G. Rossi. 2010. Neutrophil apoptosis: relevance to the innate immune response and inflammatory disease. *J. Innate. Immun.* 2(3): 216-227.

20. Fujii, T., Nakagawa, H., and S. Murakawa. 1979. Immunity in lamprey. Production of haemolytic and haemagglutinating antibody to sheep red blood cells in Japanese lampreys. *Dev Comp Immunol.* 3: 441–51.

21. Goldstine, S.N., Manickavel, V., and N. Cohen. 1975. Phylogeny of gut-associated lymphoid tissue. *Am. Zool.* 15:107-118.

22. Haugarvoll, E., Bjerka ̊s, I., Nowak, B. F., Hordvik, I., and E. O. Koppang. 2008. Identification and characterization of a novel intraepithelial lymphoid tissue in the gills of Atlantic salmon. *J. Anat.* 213: 202–209.

23. Heimroth, R. D., Casadei, E., and I. Salinas. 2018. Effects of experimental terrestrialization on the skin mucus proteome of African lungfish (*Protopterus dolloi*). *Front. Immunol.* 9(1259): 1-11.

24. Huerta-Cantillo, J. and F. Navarro-García. 2016. Properties and design of antimicrobial
25. peptides as potential tools against pathogens and malignant cells. *Investigación en Discapacidad*. 5(2): 96-115.

26. Icardo, J. M., Loong, A. M., Colvee, E., Wong, W. P., and Y. K. Ip. 2012. The alimentary canal of the African lungfish Protopterus annectens during aestivation and after arousal. *Anat. Rec.* 295(1): 60–72.

27. Jordan, H. E. and C. C. Speidel. 1931. Blood formation in the African lungfish, under normal conditions and under conditions of prolonged estivation and recovery. *J. Morph.* 51(2): 319-371.

28. Kajiwara, E., Shigeta, A., Horiuchi, H., Matsuda, H., and S. Furusawa. 2003. Development of Peyer's patch and cecal tonsil in gut-associated lymphoid tissues in the chicken embryo. *J. Vet. Med. Sci.* 65: 607–614.

29. Kaplan, M. J., and M. Radic. Neutrophil extracellular traps (NETs): Double-edged swords of innate immunity. *J. Immunol.* 189(6): 2689-2695.

30. Korkmaz, B., Horwitz, M. S., Jenne, D. E., and F. Gauthier. 2010. Neutrophil elastase, proteinase 3, and cathepsin G as therapeutic targets in human diseases. *Pharm. Rev.* 62(4): 726-759.

31. Linthicum, D. S. and W. H. Hildemann. 1970. Immunologic responses of Pacific hagfish. III Serum antibodies to cellular antigens. *J. Immunol.* 105: 912–918.

32. Mantovani, A., Cassatella, M. A., Constantini, C., and S. Jaillon. 2011. Neutrophils in the activation and regulation of innate and adaptive immunity. *Nat. Rev. Immonl.* 11: 519-531.

33. Mayadas, T. N., Cullere, X., and C. A. Lowell. 2013. The multifaceted functions of neutrophils. *Annu. Rev. Pathol.* 9: 181-218.

34. McClanahan, L. L., Shoemaker, V. H., and R. Ruibal. 1976. Structure and function of the cocoon of a Ceratophryd frog. *American Society of Ichthyologists and Herpetologists*. 1976: 179-185.
35. Neumann, B., Luz, A., Pfeffer, K., and B. Holzmann. 1996. Defective Peyer's patch organogenesis in mice lacking the 55-kD receptor for tumor necrosis factor. *J. Exp. Med.* 184: 259–264.

36. Oláh, I., and B. Glick. 1979. Structure of the germinal centers in the chicken caecal tonsil: light and electron microscopic and autoradiographic studies. *Poult. Sci.* 58: 195–210.

37. Pancer, Z., Amemiya, C. T., Ehrhardt, G. R. A., Ceitlin, J., Gartland, G. L., and M.D. Cooper. 2004. Somatic diversification of variable lymphocyte receptors in the agnathan sea lamprey. *Nature*. 430: 174–80.

38. Pasparakis, M., Alexopoulou, L., Grell, M., Pfizenmaier, K., Bluethmann, H., and G. Kollias. 1997. Peyer's patch organogenesis is intact yet formation of B lymphocyte follicles is defective in peripheral lymphoid organs of mice deficient for tumor necrosis factor and its 55-kDa receptor. *Proc. Natl. Acad. Sci.* USA 94: 6319–6323.

39. Perey, D.Y., Finstad, J., Pollara, B., and R.A. Good. 1968. Evolution of the immune response. First and second set skin homograft rejections in primitive fishes. *Lab Invest.* 19: 591–597.

40. Rast, J.P., Smith, L.C., Loza-Coll, M., Hibino, T., and G.W. Litman. 2006. Genomic insights into the immune system of the sea urchin. *Science.* 314(5801): 952–956.

41. Rinaldi, A.C. 2002. Antimicrobial peptides from amphibian skin: an expanding scenario. *Curr. Opin. Chem. Eng.* 6: 799–804.

42. Rosales, C. 2020. Neutrophils at the crossroads of innate and adaptive immunity. *J. Leuk. Biol.* 108: 377-396.

43. Ruibal, R. and S. Hillman. 1981. Cocoon structure and function in the burrowing hylid frog, *Pternohyla fodiens. J. Herp.* 15: 403-407.

44. Star, B., Nederbragt, Jentoft, A.J., Grimholt, S., Malmstrøm, U., Gregers, M., Rounge, T.F., Paulsen, T.B., Solbakken, J., Sharma, M.H., Wetten, A., Lanzén, O.F., Winer, A., Knight, R., Vogel, J., Aken, B., Andersen, Ø., Lagesen, K., Tooming-Klunderud, A., Edvardsen, R.B., Tina, K.G., Espelund, M., Nepal, C., Previti, C., Karlsen, B.O., Moum, T., Skage, M., Berg P.R., Gjøen, T., Kuhl, H., Thorsen, J., Malde, K., Reinhardt, R., Du, L., Johansen, S.D., Searle, S., Lien, S., Nilsen, F., Jonassen, I., Omholt, S.W., Stenseth, N.C., and K.S. Jakobsen. 2011. The genome sequence of Atlantic cod reveals a unique immune system. *Nature.* 477: 207-210.

45. Star, B., and S. Jentoft. 2012. Why does the immune system of Atlantic cod lack MHC II? *Bioessays.* 34(8): 648-651.

46. Strula, M., Paola, P., Carlo, G., Angela, M. M., and U. V. Maria. 2002. Effects of induced aestivation in Protopterus annectens: a histomorphological study. *J. Exp. Zool.* 292(1): 26–31.

47. Sunyer, J. O., Boshra, H., Lorenzo, G., Parra, D., Freedman, B., and N. Bosch. 2003. Evolution of the complement as an effector system in innate and adaptive immunity. *Immunol. Research.* 27: 1-16.

48. Swan, J. B., Holland, S. J., Petersen, M., Pietsch, T. W., and T. Boehm. 2020. The immunogenetics of sexual parasitism. *Science.* 369(6511): 1608-1615.

49. Tacchi, L., Larragoite, E. T., Muñoz, P., Amemiya, C. T., and I. Salinas. 2015. African lungfish reveal the evolutionary origins of organized mucosal lymphoid tissue in vertebrates. *Curr. Biol*. 25: 2417–2424.

50. von Köckritz-Blickwede, M., Goldmann, O., Thulin, P., Heinemann, K., Norrby-Teglund, A., Rohde, M., and E. Medina. 2008. Phagocytosis-independent antimicrobial activity of mast cells by means of extracellular trap formation. *Blood.* 111(6): 3070-3080.

51. Wen, F., White, G. H., VanEtten, H. D., Xiong, Z., and M. C. Hawes. 2009. Extracellular DNA is required for root tip resistance to fungal infection. *Plant. Physiol.* 151: 820-829.

52. Wermenstam, N.E. and L. Pilstrom. 2001. T-cell antigen receptors in Atlantic cod (*Gadus morhua L.*): structure, organisation and expression of TCR α and β genes. *Dev. Comp. Immunol*. 25: 117-135.

53. Withers, P. C. 1995. Cocoon formation and structure in the aestivating Australian desert frogs, *Neobatrachus* and *Cyclorana*. *Aus. J. Zool.* 43: 429-441.
54. Withers, P. C. 1998. Evaporative water loss and the role of cocoon formation in Australian frogs. *Aus. J. Zool.* 46: 405-418.
55. Withers, P. C. and G. G. Thompson. 2000. Cocoon formation and metabolic depression by the aestivating hylid frogs *Cyclorana australis* and *Cyclorana cultripes* (Amphibia: Hylidae). *J. R. Soc. West. Aust.* 83: 39-40.

56. Yousefi, S., Gold, J. A., Andina, N., Lee, J. J., Kelly, A. M., Kozlowski, E., Schmid, I., Straumann, A., Reichenbach, J., Gleich, G. J., and H. Simon. 2008. Catapult-like release of mitochondrial DNA by eosinophils contributes to antibacterial defense. *Nat. Med.* 14: 949-953.

57. Zhang, Y. A., Salinas, I., Li, J., Parra, D., Bjork, S., Xu, Z., LaPatra, S. E., Bartholomew, J., and J. O. Sunyer. 2010. IgT, a primitive immunoglobulin class specialized in mucosal immunity. *Nat. Immunol.* 11: 827–835.

Chapter 6.

Summary and Conclusions

Comparative Immunology is a unique field that aims to unveil the diversity of immune systems found on Earth. The outstanding diversity of immunological solutions found across organisms from bacteria to humans has attracted the attention of scientists throughout history. Major technological breakthroughs in the last decade have boosted this field and revealed new paradigms of immunity in species for which traditional tools such as antibodies are not commercially available. Next generation sequencing (NGS) techniques as well as other "omics" tools thus provide scientists with large datasets, and the inherent challenge of analyzing and making biological sense of such big data. This doctoral thesis uses large proteomic and RNA sequencing datasets along with other immunological, molecular and microscopic techniques to investigate the unique aspects of the immune system of a non-model organism that holds a key phylogenetic position, the African lungfish. Prior to this dissertation, the lungfish immune system had barely been studied and therefore, the findings here reported represent major advances to the field of Comparative Immunology.

Chapter 2

The advances in NGS have drastically altered researchers' abilities to investigate the evolution and development of immune systems. NGS techniques bypass the need for species-specific reagents typically available for traditional model organisms, opening up the range of species used to interrogate different aspects of immunity. With these advances I was able to reinvestigate secondary lymphoid organs (SLOs) in non-traditional model organisms such as rainbow trout, African lungfish, and turkeys. In doing so, I revisited the previously proposed tumor necrosis family (TNF) hypothesis that postulated that TNFSF/TNFRSFs are vital for the

formation and organization of SLOs in mammals (Fütterer et al., 1998, van de Pavert and Mebius, 2010). To do this I performed an exhaustive search for all TNFSF/TNFRSF molecules in vertebrates by scanning all publicly available genomes. Additionally, I performed *de novo* assembled transcriptome sequencing from mammalian and non-mammalian SLOs and data mined these new datasets for TNFSF/TNFRSF expression. I discovered the presence of more TNFSFs and TNFRSFs in teleost and lungfish than had previously been reported (Tacchi et al. 2015), but that there was still the absence of lymphotoxins in teleost and bird genomes, which have been previously proposed to be vital for SLO development in mammals. To investigate what other mechanisms besides the TNF hypothesis that might be in play in SLO formation and maintenance, gene ontology (GO) analysis of O-MALT transcriptomes was performed. This analysis showed that there are unique enriched biological processes that are likely driving lymphocyte aggregation at mucosal surfaces for each of the vertebrate groups studied including mammals, Aves, sarcopterygian fish and bony fishes. For instance, neuronal ligand-receptor interactions appear to be enriched in the SLOs of both birds and ectotherms, whereas olfactory genes are enriched in the SLOs of mammals and sarcopterygian fish. These results lead us to believe that, through the vertebrate lineage, SLOs have evolved and formed through processes of convergent evolution. My findings also challenge the previous hypothesis derived from murine literature that TNFSF/TNFRSFs are the main driving molecular mechanism in SLO development and organization and show that SLOs form by diverse molecular mechanisms in different jawed vertebrate taxa.

Chapter 3

In order to survive terrestrialization, lungfish rely heavily on their mucus cocoon to protect them from desiccation, UV radiation and invading pathogens. During cocoon formation,

the internal gills of the lungfish produce copious amount of mucus that combined with the skin mucosal secretions form the cocoon. In this chapter I presented the first proteomic analysis of the terrestrialized mucus cocoon of the African lungfish (*Protopterus sp.*). Here I showed that African lungfish undergo drastic remodeling of the integument that is accompanied by an influx of granulocytes from circulation during the first 10 days of terrestrialization. The overall protein composition from the three mucus samples analyzed (free-swimming skin mucus, terrestrialized gill mucus and terrestrialized skin cocoon) was unique. A total of about 175 proteins were shared between free-swimming skin mucus and terrestrialized skin mucus, whereas free-swimming skin mucus and terrestrialized gill mucus only shared around 11 protein hits. An increased abundance in immune related proteins was detected in both gill and skin mucus of terrestrialized animals compared to free-swimming controls, especially in proteins with known antimicrobial functions. Previous worked had characterized the diversity of Ig heavy chain genes in African lungfish (Zhang et al., 2014). In this study, there were also differences in the types of Igs that were present in each proteomic skin sample. While there was no detectable Igs in the terrestrialized gill mucus, in both the free-swimming mucus and terrestrialized skin mucus IgW1L and IgM1 were found. Interestingly, in the terrestrialized skin mucus I also found the expression of IgM2. These results suggest that IgM1 is constantly expressed in the skin while the expression of IgM2 is turned on in response to external stimuli. Thus, in response to the drastic changes in microbial pressures imposed to the lungfish due to terrestrialization their skin underwent drastic physiological changes in order to survive. This includes the secretion of unique collections of innate and adaptive immune molecules in their integument to prevent the invasion of pathogens. Overall, this chapter reveals drastic immunological and physiological changes in the lungfish skin proteome in response to terrestrialization.

Chapter 4

Based on our findings in chapter 3, this chapter focused on understanding the intricacies of the vertebrate adaptation to terrestrial life. As previously published in 2018, upon terrestrialization, drastic physiological changes take place in the integument of African lungfish. I confirmed these previous findings using light microscopy. Then the question was where were the granulocytes migrating from? In support of Jordan and Speidel's characterization of the white blood cells and their reservoirs in lungfish, I found large numbers of granulocytes in the gonads, gut, and kidneys of free-swimming lungfish. Upon terrestrialization these cells migrated from the reservoirs into the bloodstream and reached the integument, where they were observed to infiltrate the dermis, epidermis and transmigrate into the cocoon. The cocoon was made from mucus as well as a living, well-organized cellular structures. The cocoon retained the ability to express antimicrobial peptide genes and contained a unique microbiome that ensures the underlaying skin remains free of invading pathogens during aestivation. Transcriptomic analysis showed that terrestrialization stimulated a proinflammatory environment in the lungfish skin, likely required for the dramatic tissue remodeling observed in this tissue. Skin granulocytes found in the skin of terrestrialized lungfish were able to form extracellular traps (ETs) upon PMA stimulation. Using DNAse I treatment to deplete extracellular DNA *in vivo*, I found that lungfish had increase morbidity with edema, septicemia, and prolapsed anus. It was also evident that depletion of ETs lead to a decreased diversity in the skin microbial community with expansions of pathogenic taxa. Overall, this study indicates that the lungfish uses a double layer of protection during terrestrialization. First, an outer layer, living cocoon with highly antimicrobial functions and a second modified skin highly rich in granulocytes that undergo ETosis to protect lungfish from invading pathogens. These unique immunological adaptations

suite aestivating vertebrates such as lungfish and reveal previously unknown functions for ETs in physiological tissue remodeling.

References:

1. Fütterer, A., K. Mink, A. Luz, M.H. Kosco-Vilbois, K. Pfeffer. 1998. The lymphotoxin beta receptor controls organogenesis and affinity maturation in peripheral lymphoid tissues. *Immunity.* 9(1):59-70.
2. Tacchi, L., E.T. Larragoite, P. Muñoz., C.T. Amemiya, and I. Salinas. 2015. African lungfish reveal the evolutionary origins of organized mucosal lymphoid tissue in vertebrates. *Curr. Biol.* 25:2417-2424.
3. van de Pavert, S. A., and R. E. Mebius. 2010. New insights into the development of lymphoid tissues. *Nat. Rev. Immunol*. 10: 664–674.
4. Zhang, T., L. Tacchi, Z. Wei, Y. Zhao, and I. Salinas. 2014. Intraclass diversification of immunoglobulin heavy chain genes in the African lungfish. *Immunogenetics.* 66(5):335-351.